James Donnelly

Diketopyrrolopyrrole Derivatives for Bulk Heterojunction and Dye Sensitised Solar Cells

MSc Thesis

Supervisor – Professor Graeme Cooke

Acknowledgements

First and foremost I would like to thank my family and friends that have supported me throughout this process. Most notably my fiancé Caitlin Quinn for her continuing support in all my endeavours, she put up with all the ups and downs that come along with research work without ever having set foot in the lab. Also a massive thank you to my sister (soon to be Dr) Mary-Ellen Donnelly, for all her help, support, random conversations, article acquiring and the fun of the constant ribbing between a chemist and a physicist. A thank you to Hunter Fairley, James Shearer and Kirsten Swinfen, who were always there at the end of a tough week for Jack Daniel's and shenanigans. Antonia Ngama for the times sharing stories of our first years in academia, for enduring Jason Duncan and myself (I know it was tough for her) and for putting up with my jokes about her being the chemistry equivalent of an accountant.

Academically, a great deal of thanks has to go to Professor Graeme Cooke for his guidance and patience during my time at the University of Glasgow. No matter how busy his schedule was, always making time to speak with his group members and promptly responding to any questions. I couldn't have hoped for a better supervisor. Thanks to the Cooke group postdoctoral researchers, Dr Alan Wiles and Dr Brian Fitzpatrick, for their assistance in the lab. A big thank you to Dr Luis Serrano for teaching me the ways of the DPP and my second fumehood-mate (soon to be Dr) Michele Cariello for hours of entertainment. Also to the rest of the Cooke group for their help along the way and for some good times (and many baked potatoes) shared.

My thanks to the various support staff of the school of chemistry, including Mr Jim Tweedie for his help with mass spectrometry, Dr David Adam for his assistance with any NMR issues encountered during my research and Mr Ted Easdon for all his help with anything regarding lab supplies.

I would also like to acknowledge our collaborators at the University of St. Andrews, École Polytechnique Fédérale de Lausanne and the mass spectrometry service at Swansea University for their support during my research.

Finally, I would like to acknowledge the Engineering and Physical Science Research Council for funding my research and for my financial support during my research.

Abstract

This thesis describes the synthesis and characterisation of a series of molecules for use in bulk heterojunction and dye sensitised solar cells. The target molecules were based on a central diketopyrrolopyrrole subunit. Molecules based on diketopyrrolopyrrole have a conjugated structure, allowing for π-π interaction. Diketopyrrolopyrrole molecules also have relatively low lying HOMO and LUMO levels and high absorption coefficients and exhibit efficient charge transport properties. Furthermore, their electron withdrawing properties have warranted their use as promising organic photovoltaic materials. A number of molecules were successfully synthesised and sent to collaborators for testing in organic photovoltaic devices and development of this series of molecules continues to be of interest within the research group.

Table of Contents

Abbreviations

Ac - Acetate

bpy – Bipyridine

dba - Dibenzylideneacetone

DCM – Dichloromethane

DEE – Diethyl Ether

DMF – *N,N*-Dimethylformamide

DPP – Diketopyrrolopyrrole

dppf - 1,1'-Bis(diphenylphosphino)ferrocene

DSSC – Dye-Sensitised Solar Cell(s)

Et - Ethyl

FF – Fill Factor

HOMO – Highest Occupied Molecular Orbital

I_{SC} or J_{SC} – Short-Circuit Current

ICT – Intramolecular Charge Transfer

LDA – Lithium Diisopropylamine

LUMO – Lowest Unoccupied Molecular Orbital

NBS – *N*-Bromosuccinimide

NIR – Near Infra-Red

NMP - *N*-Methyl-2-pyrrolidone

PCBM - [6,6]-Phenyl-C_{61} Butyric Acid Methyl Ester

$PC_{71}BM$ - [6,6]-Phenyl-C_{71} Butyric Acid Methyl Ester

PCE – Power Conversion Efficiency

PEDOT:PSS - Poly(3,4-ethylenedioxythiophene) Polystyrene Sulfonate

P_{in} - Incident Solar Power

PPh_3 – Triphenylphosphine

THF – Tetrahydrofuran

TLC – Thin Layer Chromatography

TTF - Tetrathiafulvalene

V_{OC} – Open Circuit Voltage

Figures, Schemes and Tables

1. Introduction

Meeting the ever increasing global energy demand is undoubtedly one of the biggest challenges facing the scientific community. It is estimated that 81% of global energy in 2011 was provided by ever declining reserves of fossil fuels, the global population is expected to grow to 8 billion people by 2025 and the strain being placed on the environment by the burning of aforementioned fossil fuels is ever increasing[1]. The combination of these factors means that urgent action is required to shift the balance of energy production worldwide.

It is believed that solar energy is the most promising solution amongst renewable energy sources, given that the sun is the most abundant source of energy found on earth. It is estimated that the solar energy that hits the planet in one hour would be sufficient to meet the global requirement for energy for an entire year [2]. Thus solar energy has huge potential to make a massive difference in the issue.

It is predicted that solar energy will be the fastest growing source of renewable energy between 2012 and 2040, expected to increase at a rate of 7.5% per year [3]. Whilst there are predictions that solar power could possibly become the dominant energy source by 2050, much development is required. There are many types of photovoltaic materials, an overview of the development in photovoltaics over the last 30 years can be seen in Figure 1.1.

It can be see that the greatest efficiencies can be achieved with inorganic photovoltaic materials (purple), however these efficiencies are achieved by combining various metals and metalloids; such as arsenic, gallium and indium[5]. Such materials have the disadvantages of raw material scarcity, high cost and acute toxicity. The most common type of solar cells are silicon based (blue and green), with a market share of around 90%[6].

Silicon based photovoltaics have reasonable efficiencies of 20-27%. Unfortunately though, it can be seen that efficiencies have not improved at a great rate over the past 30 years and many will argue that they are not going to improve much further beyond their current efficiencies. However, the cost of silicon based cells has fallen drastically over the same time period, with prices equivalent to $0.74 per watt in 2013[7].

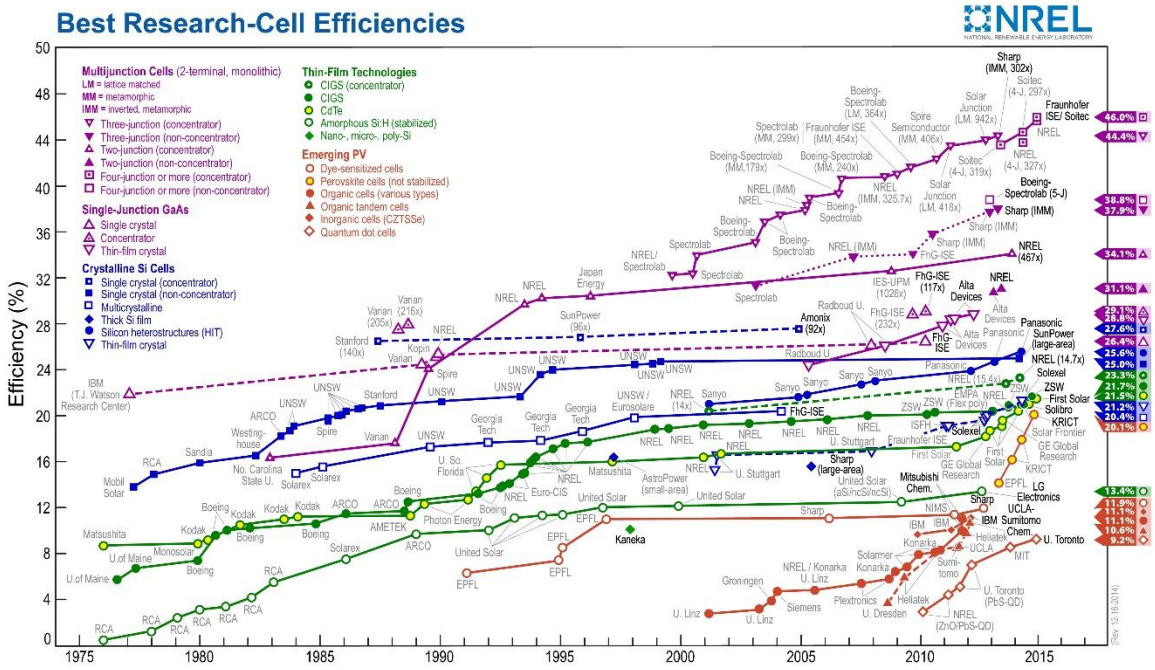

Figure 1.1 - Efficiencies of Photovoltaic Cells Arranged by Type (http://www.nrel.gov/ncpv/)

Since the early 1990's, the development of organic photovoltaics (orange) has been a slow and steady process and although current efficiencies are little over 10%, it can be seen that organic photovoltaics are still trending upwards. Organic photovoltaic technologies have the advantages that they can benefit from low-cost materials, high volume and high throughput manufacturing, flexibility and low energy expenditure; making organic photovoltaics the most promising prospect for solar energy production in the future.

1.1. Heterojunction Cells

1.1.1. Development

A natural starting point in the search for organic photovoltaic materials in the early 1950's was the material that had been harvesting light energy for centuries, chlorophyll. Early studies hypothesised that the primary process for harvesting light energy in photosynthetic tissues was the separation of charges to opposing sides of a lamina followed by the trapping of electrons and holes which led to reduction and oxidation, respectively[8]. From these results magnesium phthalocyanine discs coated with a thin film of air oxidised tetramethyl p-phenylenediamine were developed and were the first organic/organometallic materials to show a photovoltaic effect.

Early organic photovoltaics were limited by the recombination of the separated charges upon excitation. The difference in work functions of the electrodes alone was not high enough to overcome the Coulombic attraction of the opposing charges causing them to recombine[9]. To overcome the problem of charge recombination the first multi-component organic photovoltaic cell was created in

1986. This cell was constructed of indium tin oxide coated glass, onto which a 300 Å thick layer of copper phthalocyanine was deposited, followed by a 500 Å thick layer of a perylene tetracarboxylic derivative and an opaque Ag layer[10]. This new two layer configuration led to a record efficiency at the time of 0.95%, the improved efficiency was attributed to the difference in electron affinities and ionisation potentials of the copper phthalocyanine (donor material) and perylene tetracarboxylic derivative (acceptor material). The heterojunction is born.

1.1.2. Construction and Basic Principles

The limitations of the first heterojunction cells arose from their construction. Because the charge separation takes place at the interface between the donor and acceptor materials, in a planar heterojunction configuration the interaction occurs at the geometrical interface. To circumvent the problem the bulk heterojunction cell was developed. A bulk heterojunction consists of a blended film of both donor and acceptor materials being deposited between the electrodes[9]. The advantage of the bulk heterojunction being that there is a large increase in the interface between the acceptor and donor materials, leading to more efficient charge separation.

The majority of modern bulk heterojunctions are constructed of a modified indium tin oxide (ITO) anode coated on glass, onto the anode a hole transporting layer (usually consisting of poly(3,4-ethylenedioxythiophene) polystyrene sulfonate (PEDOT:PSS)) is deposited. The donor:acceptor blend is then deposited onto PEDOT:PSS layer before an electron transporting layer (TiO_x or Ca typically) and a low work function metal (usually Al) cathode finish the cell[11,12].

The PEDOT:PSS is used as the hole transporting layer so that the donor and acceptor materials are not in direct contact with the anode, which leads to current leakage and the recombination of charge carriers[13]. However PEDOT:PSS is hygroscopic and acidic, which leads to issues with device stability. Replacement hole transporting layers have been investigated leading to promising developments using transition metal oxides, such as NiO, MoO_3, WO_3 and V_2O_5[14].

Typical photovoltaic cells work using the basic principles shown in Figure 1.2

1. Photoinduced generation of excitons,
2. Transfer of electrons from LUMO of the of the donor material to the LUMO of the acceptor material, occurring at the interface,
3. Collection of electrons and holes at the cathode and anode, respectively.

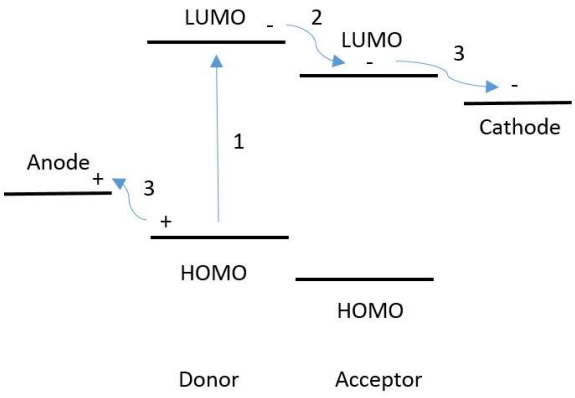

Figure 1.2 - Basic Principles of a Heterojunction Cell

For these processes to take place efficiently, fine-tuning of the HOMO and LUMO levels of both the donor and acceptor materials must take place. Well matched HOMO and LUMO levels allow for more efficient charge separation and collection[15], and studies have been carried out in an attempt to design donor materials for use in bulk heterojunction cells that will maximise their efficiency[16].

1.1.3. Morphology

The morphology of the donor:acceptor blend is an important factor in bulk heterojunction cells, and has been the subject of many studies[17-21]. The main methods of solution processing utilised are dip coating, drop casting and spin coating. Each technique has merits, and is highly dependent on the solvent used during processing[22]. Solvent additives, such as alkanedithiols, have also been shown to increase the control of the morphology, thus increasing efficiency[23]. Thermal annealing is another alternative method for controlling the morphology of bulk heterojunction cells. It is believed that heating the film allows for one component to crystallise and the other to diffuse out to form larger aggregates outside of the crystals[24]. The annealing process leads to more ordered domains and thus better transitions between those domains. The morphology of the film can be changed by the temperature at which annealing occurs and for how long. These solution-processing techniques tend to be used in polymer based heterojunctions.

Small molecule heterojuction cells are more likely to utilise vacuum deposition, which allows for more precise control of the morphology of the active layers by utilising insoluble materials that are very often more stable than their soluble analogues.

Whatever method is used, optimisation is required for all elements affecting the morphology for the successful construction of a heterojunction cell.

1.1.4. Performance

The performance of photovoltaics is measured using three factors:

- The short circuit current (I_{SC} or J_{SC})
- The open current voltage (V_{OC})
- The fill factor (FF)

All of which combine to give the maximum power conversion efficiency (PCE).

The I_{SC} is the current that would flow if there was no external field applied. Thus I_{SC} can be determined by the number of photons absorbed, the quantum efficiency was of the separation of charges and the transport of the separated charges through the materials. It follows that the I_{SC} is very dependent on the absorption spectrum, as a broad spectrum will mean that more photons will be absorbed, increasing the I_{SC}[25].

The V_{OC} can be defined as the maximum voltage that can be delivered by the cell, which occurs when the current is zero. The V_{OC} can be calculated by:

$$V_{OC} \approx E_{acceptor(LUMO)} + E_{donor(HOMO)} + k_B/e\{ln(n_e n_h/N_c^2)\}$$

Where n_e and n_h are the electron and hole densities, respectively, and N_C is the corresponding density of the states. The third term is introduced by the temperature dependence of the quasi-Fermi levels[26].

The FF is determined as by the competition between the recombination of charge carriers and the charge carriers being swept out to the electrodes[27]. The FF can be found by finding the ratio of the green area to the grey area in Figure 1.3[25].

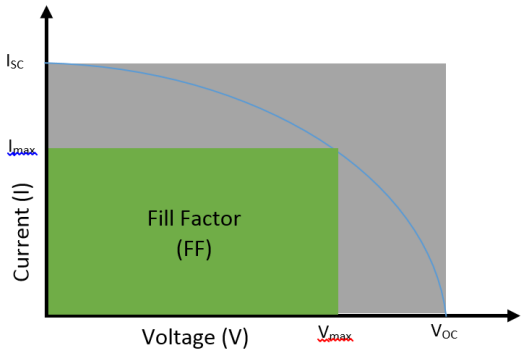

Figure 1.3 – Calculating Fill Factor

The PCE, η, of a cell can be found using the equation:

$$\eta = \frac{I_{SC} V_{OC} FF}{P_{in}}$$

Where P_{in} is the incident solar power[27].

1.1.5. Acceptors in Heterojunctions

Bulk heterojunction cells utilising the donor:acceptor blend of polymers and fullerenes are the most widely used and studied[28]. Fullerenes are ideal for use as an acceptor, due to their high electron affinity, small reorganisation energy and superior ability for electron transport. An additional property that also makes fullerenes ideal for use in heterojunctions is that by attaching organic moieties, their properties can be tuned to suit their usage. Solubility, energy levels, molecular interactions, orientation in the solid state and their surface area can be tuned using this method[29]. The most widely used and best known fullerene derivative is [6,6]-phenyl-C_{61} butyric acid methyl ester (PCBM, Figure 1.4). PCBM has become the benchmark which other acceptor materials are measured against and is almost always the acceptor that new donor materials are tested with[30].

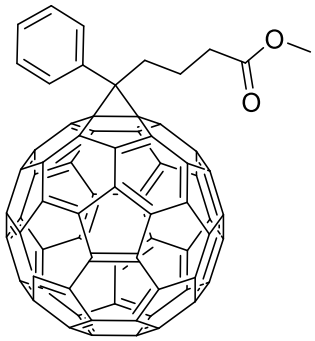

Figure 1.4 - PCBM

Despite the advantages of using PCBM as an acceptor material, there are several drawbacks such as high costs, low air stability and narrow absorption in the visible region. However, the larger fullerene [6,6]-phenyl-C_{71} butyric acid methyl ester ($PC_{71}BM$) has broader absorption in the visible region[31]. The increased absorption of $PC_{71}BM$ is believe to be due to the loss of symmetry that is found in PCBM. $PC_{71}BM$ also has shown an internal quantum efficiency close to 100% in bulk heterojunction cell[32].

Attempts to create alternative acceptor materials had been abundant but unsuccessful until recently; with perylenediimide derivatives **1** and **2** (Figure 1.5), which when combined with donor poly[4,8-bis(5-(2-ethyylhexyl)thiophen-2-yl)benzo[1,2-*b*;4,5-*b'*]dithiophene-2,6-diyl-*alt*-(4-(2-ethylhexyl)-3-fluorothieno[3,4-*b*]thiophene)-2-carboxylate-2,6-diyl] (**5**, Figure 1.7) gave PCE values of 6.05%[33] and 5.90%[34] respectively.

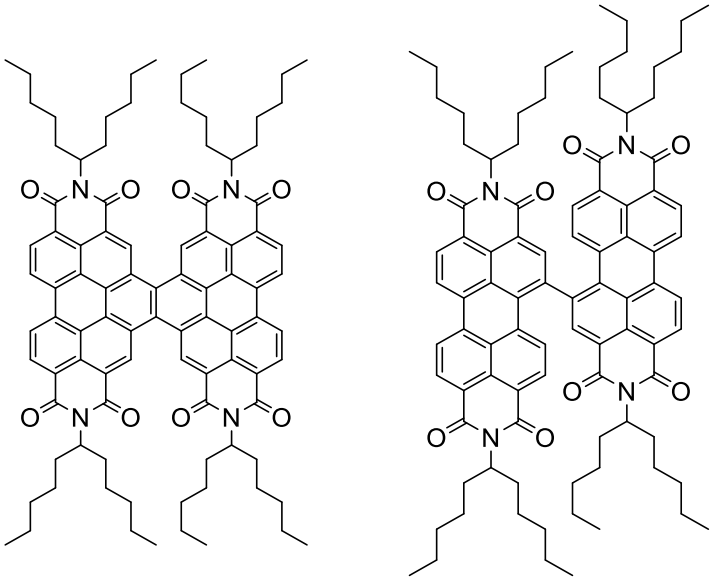

1 **2**

Figure 1.5 - Perylenediimide Acceptor Materials

Another group of successful acceptor materials that has garnered interest are phthalocyanine derivatives, most notably subphthalocyanines. Subphthalocyanines have the advantage over phthalocyanines because of their cone-shaped structure, which makes them less likely to aggregate and thus making them more soluble. This feature, along with the 14-π-electron core leads to strong absorption and fluorescence emission[35]. A three layer device containing boron subphthalocyanine chloride (**3**, Figure 1.6) and boron subnaphthalocyanine chloride (**4**, Figure 1.6) with donor material α-sexithiophene (**11**, Figure 1.9) gave a PCE value of 8.40%[36].

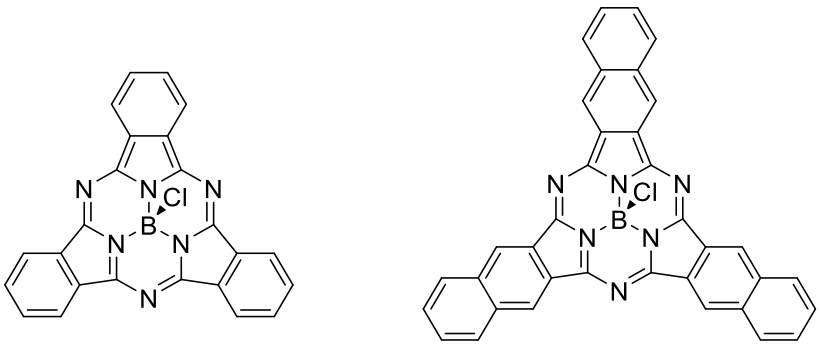

3 **4**

Figure 1.6 - Boron Subphthalocyanine Derivatives

1.1.6. Polymers as Donor Materials in Heterojunctions

Early donor materials in heterojunctions were mainly based on phenylenevinylene derivative polymers, such as poly[2-methoxy-5-(2^0-ethyl-hexyloxy)-1,4-phenylenevinylene] (**7**, Figure 1.7) and poly[2-methoxy-5-(3^0,7^0-dimethyloctyloxy)-1,4-phenylenevinylene] (**8**, Figure 1.7). These polymers

were chosen because of their conductance, but efficiencies with $PC_{71}BM$ did not exceed 3%, mainly due to the large bandgap (around 1.9 eV), which limited the number of photons that could be absorbed[31].

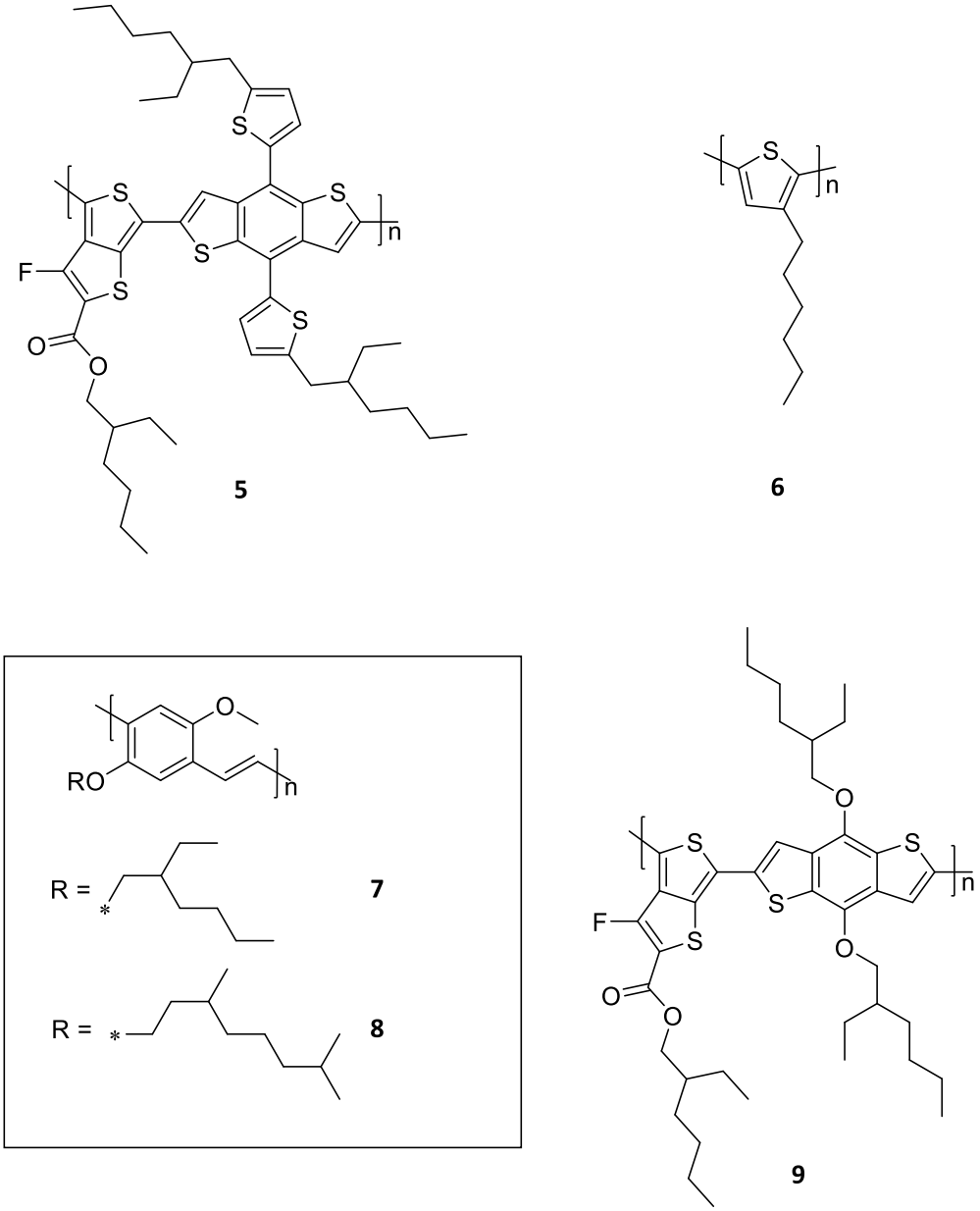

Figure 1.7 - Polymers Used as Donor Materials in Heterojunctions

Polythiophenes were the next group of donor materials to be investigated, most notably poly[3-hexylthiophene-2,5-diyl] (**6**, Figure 1.7), which in a heterojunction cell with PCBM utilising a layer of TiO_x as an optical spacer, managed to attain a PCE value of 5%[37]. The success of polythiophenes was due to better HOMO-LUMO alignment with PCBM and increased carrier mobility, leading to greater I_{SC} densities. However, optimisation of V_{OC} values of **6** became problematic, which led to the development of other low-bandgap polymers.

Following on from **6**, efforts were focused on fine tuning polymer properties for better matching HOMO-LUMO levels with acceptor materials which allowed for better charge transfer, and lowering bandgaps to allow for more efficient photon harvesting. Hundreds of polymers have been synthesised and investigated, including polymers based on thiophene, benzothiadiazole[38], isothianaphthene[39], thiazolothiazine[39], benzothiophene[40], benzodithiophene[41], thienoisoindoledione[42,43], thienoquinodimethane[44] and many other molecules.

Of the polymers investigated the most successful proved to be thieno[3,4-*b*]thiophene-based structures[45]. The most successful derivative being polythieno[3,4-*b*]thiophene-*co*-benzodithiophene (**9**, Figure 1.7), presenting low bandgaps, leading to efficiencies of 7-9%[46-49]. Following on from which derivatives of **9** were used in the first single junction heterojunction cells to break the 10% PCE barrier[50,51].

Another recent success story in polymer based heterojunctions came from designing a donor-acceptor co-polymer with a porphyrin-pyrene adduct (**10**, Figure 1.8) which showed panchromatic absorption and gave a promising PCE of 8.5% with $PC_{71}BM$[52].

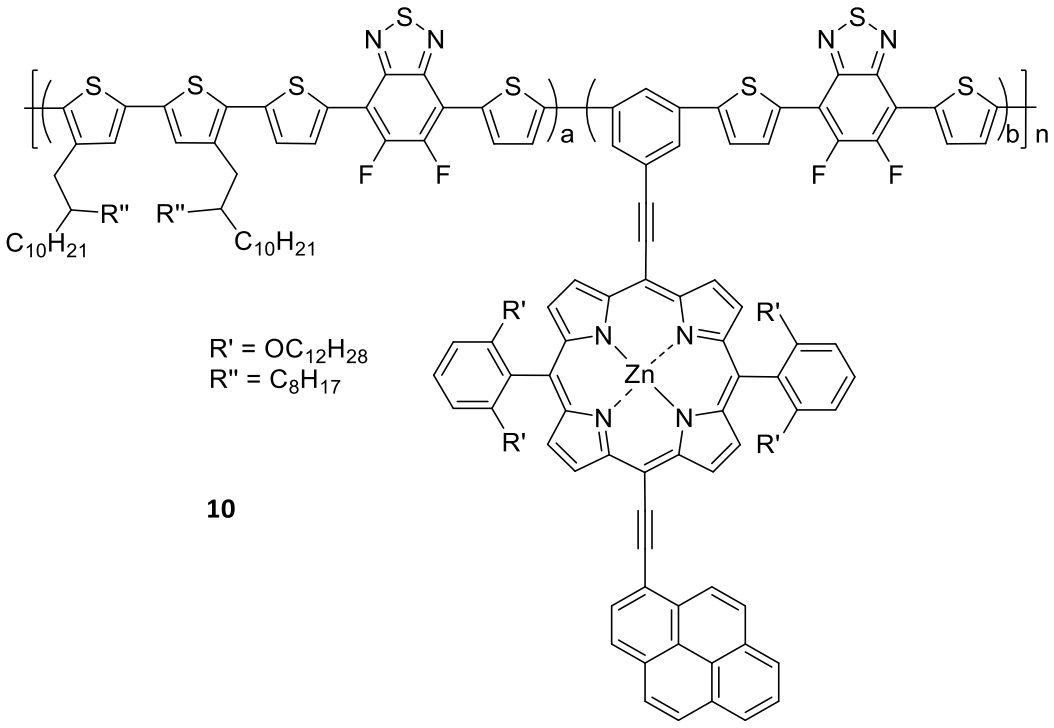

Figure 1.8 - Donor-Acceptor Co-Polymer with Porphyrin-Pyrene Adduct

1.1.7. Small Molecules as Donor Materials in Heterojunctions

Despite the advantages that can be found in the use of polymers as donor materials in heterojunctions, there are some disadvantages. Reproducibility of synthesis and difficulties with

purification, along with problems associated with the inherent electronic properties of polymers has meant that alternatives to polymer based donor and light harvesting materials have been investigated.

The first small molecules to be investigated were oligothiophenes and 3,4-ethylenedioxythiophene (EDOT) molecules, with a molecule consisting of oligothiophene chains around a trithienobenzene centre (**12**, Figure 1.9) giving the best PCE value of only 1.27%[53]. Oligothiophenes were studied early on in this process because of their interesting charge transfer characteristics and the potential to fine tune their optoelectronic properties[54]. Unfortunately, due to the poor absorption of these materials, early efficiencies were poor[55-57]. The best efficiencies reported with oligothiophene based donor materials comes from a series of methyl-substituted dicyanovinyl quinquethiophenes (**13-15**, Figure 1.9), with **15** achieving a PCE of 6.9% with $PC_{71}BM$[58].

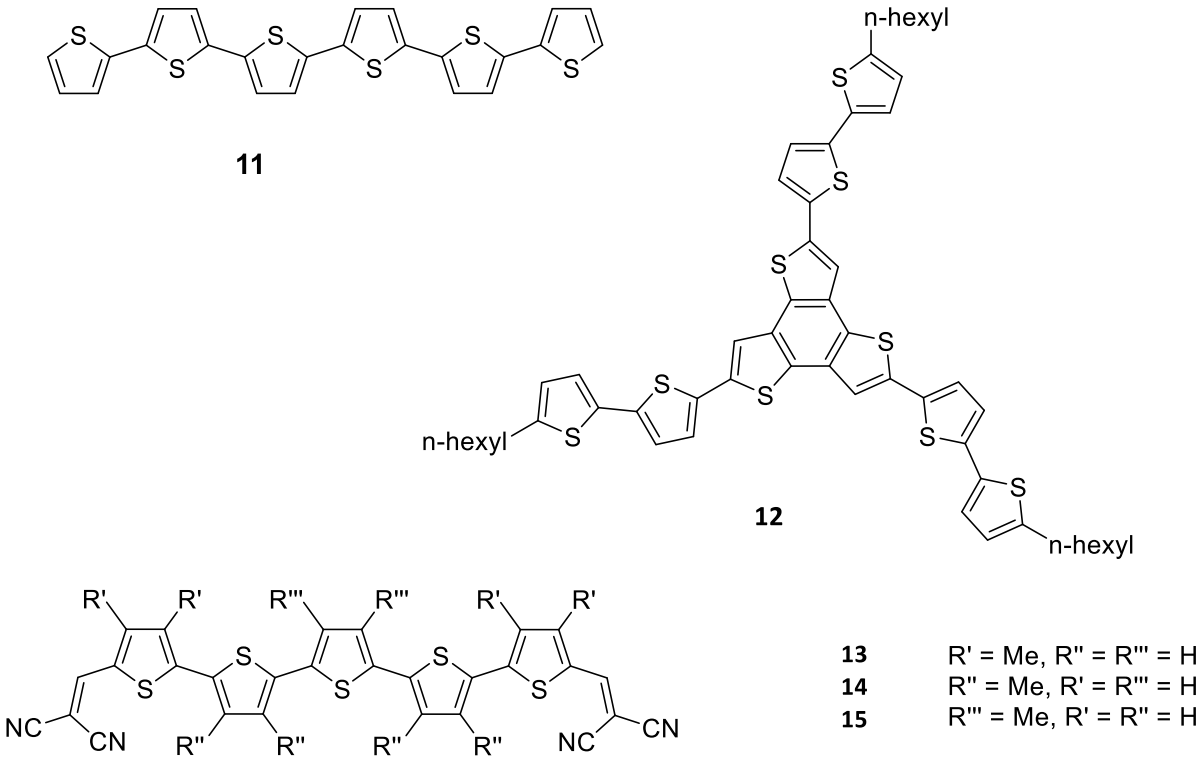

Figure 1.9 - Oligothiophene Derivatives Used as Donor Materials in Heterojunctions

Further molecular design led to the synthesis of molecules with improved absorption and thus improved I_{SC} values, and more branched alkyl chains to aid solubility. These improvements led to greatly improved performance, two such examples being the highly conjugated molecules **16** and **17** (Figure 1.10), which when combined with $PC_{71}BM$ gave PCE of 8.12%[59] and 8.02%[60] respectively, with a tandem device utilising **17** becoming the first small molecule to break the 10% PCE barrier.

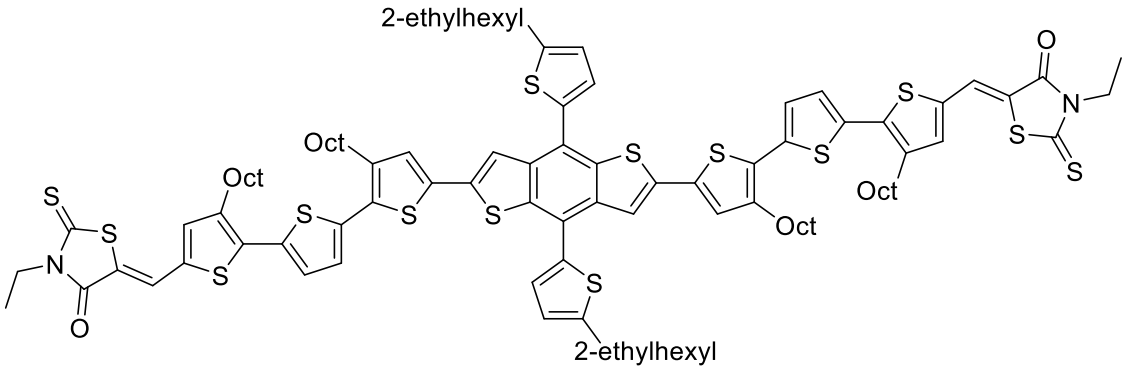

16

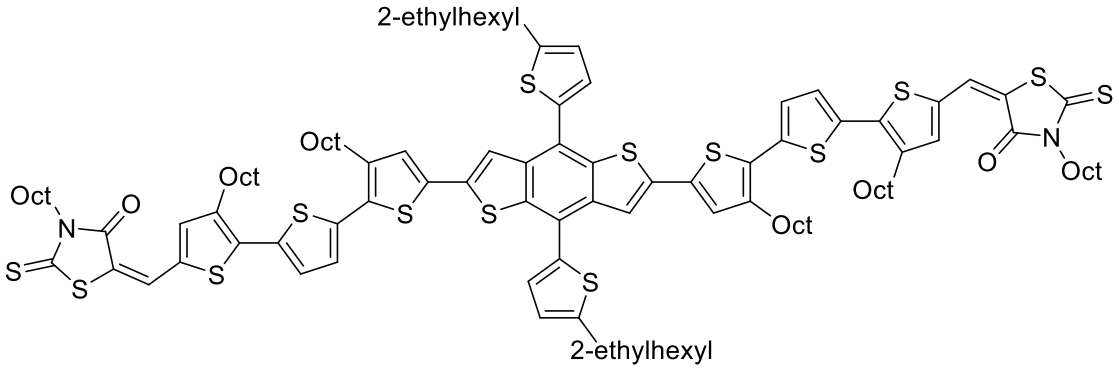

17

Figure 1.10 - Highly Efficient Organic Small Molecules as Donor Materials in Heterojunctions

Other interesting small organic molecules have been reported in literature, including oligacenes such as pentacene[61] and rubrene[62] which gave PCE values of around 3%. Squaraine dyes have been of interest in the design of small molecule donor materials because of their high extinction coefficients that can be made panchromatic with modification of the molecule, photochemical stability and ability to be modified to other small molecular structures[63]. After some optimisation the squaraine dye **18** (Figure 1.11) achieved a PCE of 5.5% with $PC_{71}BM$[64].

Triphenylamine moieties are very commonly found in organic photovoltaic materials, this is due to their high absorption and their excellent electron donating capabilities. The D-A-A molecule **19** (Figure 1.11) was an excellent middle ground between extending the spectral coverage to increase I_{SC} and matching HOMO-LUMO levels to increase V_{OC}, giving a PCE of 6.8% with $PC_{71}BM$[65].

Merocyanines are molecules that are known for their strong dipole character and high polarizability, which allows for high extinction coefficients[66]. Merocyanine molecule **20** (Figure 1.11) gave a PCE of 6.1% with PCBM[67].

Also worth mentioning are the results achieved by the D-A-A molecule **21** (Figure 1.11), based on a central pyrimidine group, attached to an electron rich ditolylaminothienyl structure, and an electron poor dicyanovinylene moiety. **21** achieved an impressive PCE of 6.4% with $PC_{71}BM$[68].

The previously discussed subphthalocyanines can also be used as small molecule donor materials in heterojunctions, with a **3**:PCBM heterojunction giving a PCE of 2.97%[69]. However a fullerene free **3**:**4** heterojunction recently gave an outstanding PCE of 6.4% [70]. The unexpected result of the fullerene-free heterojunction outperforming the fullerene-containing heterojunction was understood to be because of complementary absorption and reduced recombination at the interface due to excellent HOMO-LUMO alignment.

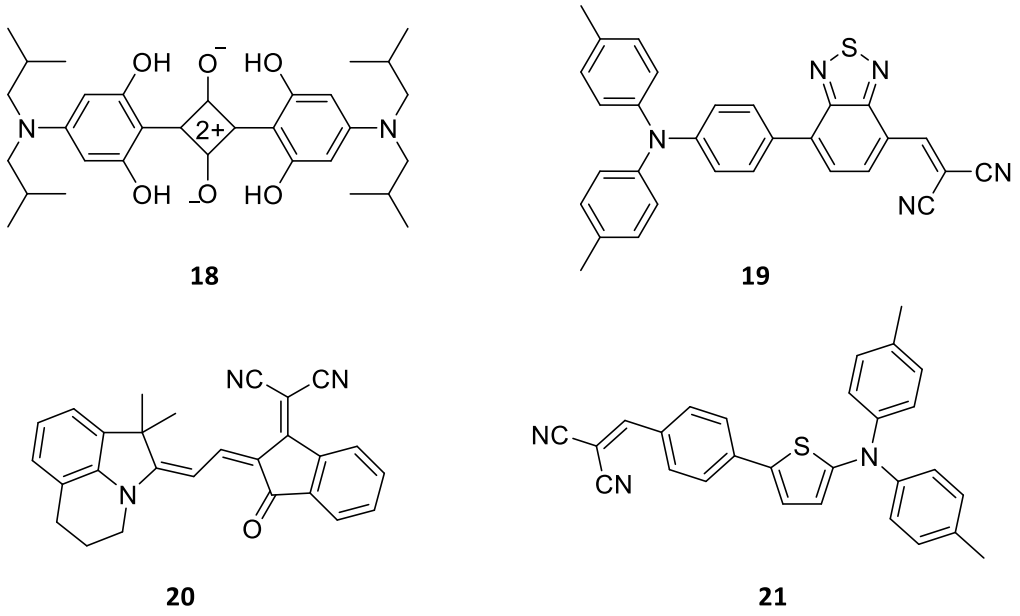

Figure 1.11 - Other Donor Materials Used in Heterojunctions

Lastly, porphyrins (although not strictly organic molecules) are mainly known for their application in dye sensitised solar cells, however they have shown some promise in small molecule heterojunction cells.

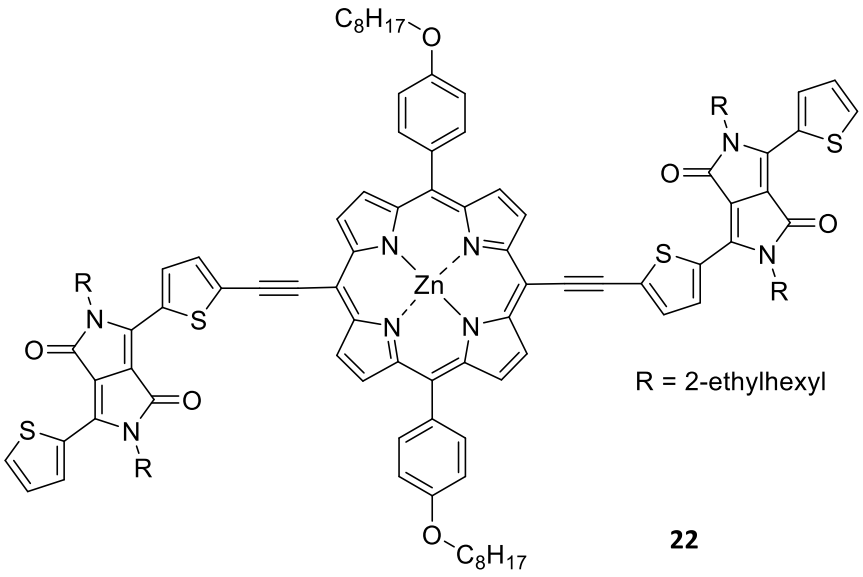

Figure 1.12 - Porphyrin Small Molecule Used as Donor Material in Heterojunctions

Porphyrins, with their 18π electron aromaticity have strong absorption in the visible region, and can act as electron donors. Porphyrin properties can also be fine-tuned by easily adding substituents, making them attractive for use in photovoltaics[71]. One such example of a porphyrin being used in heterojunctions is the molecule **22** (Figure 1.12), which is an electron rich porphyrin moiety, flanked by two electron poor diketopyrrolopyrrole molecules (diketopyrrolopyrroles will be discussed at length later in this report). **22** gave an efficiency of 7.23% with PCBM[72].

1.1.8. Tandem Configurations

One of the main limitations of standard heterojunctions is the limitation placed upon active layer thickness due to the lower charge carrier motilities of organic materials[73]. Thinner active layers result in poorer photon harvesting, therefore by employing tandem configurations greater photon harvesting and thus greater efficiencies can be achieved.

Another advantage of a tandem configuration being that two different photoactive materials can be used, allowing for greater absorption for a larger portion of the visible spectrum. Typically tandem heterojunctions are constructed of one low bandgap material and one high bandgap material, which allows for complementary not competitive absorption.

However, despite the V_{OC} of a double heterojunction cell being twice that of a single junction, the first efforts at making this kind of device returned poor efficiencies. It is believed the poor efficiencies were caused by the increased series resistance of the multilayer structure and the formation of a competing inverse heterojunction[74]. Overcoming the inverse heterojunction was first achieved by creating a multilayer cell consisting of two heterojunctions separated by a recombination layer, it was also necessary to fine tune the absorption properties to ensure that the photocurrent generated by both

heterojunctions was equal. The equality of the photocurrents in the individual heterojunctions eliminating the formation of the counterproductive inverse heterojunction in the tandem device[74]. The first tandem device constructed this way led to an efficiency value of 2.5%, as opposed to the equivalent single junction cell which yielded an efficiency value of 1.1%[74].

It has been hypothesised that employing a tandem configuration heterojunction allows for a theoretical maximum efficiency of 49%, as opposed to 30% in single junction cells[75]. This increase in theoretical maximum efficiency underlines the potential importance of the development of tandem configurations in heterojunctions. Developments in multi-junction configurations have resulted in excellent efficiencies of 10.6%[76] and 11.5%[77] for double and triple heterojunction configurations, respectively.

1.2. Dye-Sensitised Solar Cells

1.2.1. Development and Basic Principles

Dye-sensitised solar cells (DSSC) were first developed in 1991, with first efficiencies of 7.1-7.9% using a ruthenium based dye[78]. This initial success provided much excitement in the field of photovoltaics. DSSC have the attraction of having low production costs, ease of processing and high stability over a wide range of temperatures[79]. Also the standards of purity required for processing in DSSC are much lower than that of heterojunction cells, meaning that there is no need for processing under vacuum or at high temperatures[80].

DSSC are generally constructed of a fluoride doped tin dioxide anode, coated in TiO_2, onto which the dye sensitiser and electrolyte are coated. The electrolyte is most commonly an organic solvent containing a redox system such as iodide/triiodide couple. Although other redox couples have been investigated such as Br^-/Br_2, SCN^-/SCN_2 and $SeCN^-/SeCN_2$, none have shown the light-to-electricity conversion efficiency of I^-/I_3^- [81]. The circuit is then completed with a counter electrode. The counter electrode is almost always platinum, as platinum is stable and has high catalytic activity[82]. However platinum is a rare and expensive metal, therefore development of alternative counter electrode materials such as graphene/polymer composites[83], carbon nanotubes[84] and transition metal carbides[85] has been undertaken.

Dye-sensitised solar cells operate differently to heterojunction cells, and is comparable to photosynthesis. The basic principles are shown in Figure 1.13

1. Photoexcitation of the dye,
2. Electron injection into the conduction band of the TiO_2,
3. Electron transport to the working electrode,

4. Regeneration of the dye by electron donation from redox system in the electrolyte,
5. Oxidised redox couple is regenerated by the counter electrode.

The processes shown in green are the desirable processes, however there are some undesirable processes that occur in a DSSC (shown in red) that lead to inefficiency.

6. Relaxation of dye to ground state from excited state,
7. Recombination of injected electrons with the oxidised dye,
8. Recombination of injected electrons with redox couple (known as generation of dark currents).

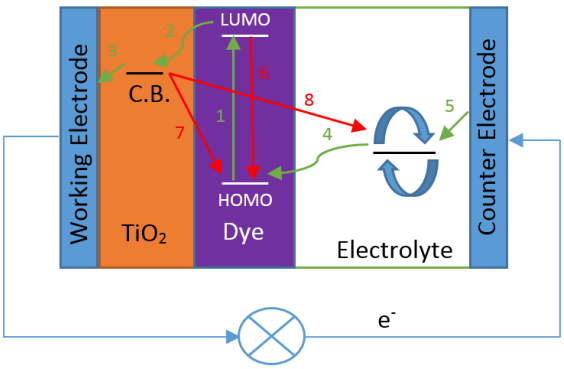

Figure 1.13 - Basic Principles of DSSC

For a DSSC to be successful, fine-tuning of the properties of the dye, the semi-conductor material and the redox couple in the electrolyte must take place to ensure all parts of the cell are working cohesively[86].

1.2.2. Dye Sensitiser

The most important part of a DSSC is probably the sensitiser. The sensitiser is responsible for harvesting photons and generating and transporting charges. Therefore design of molecules with the right properties is of the utmost importance[87]. For a sensitiser to be successful it must have:

- A LUMO level which allows for efficient electron injection into the conduction band of the semi-conducting material,
- A HOMO level which allows for efficient regeneration by the redox couple of the electrolyte,
- Broad absorption in the visible and NIR region.

As mentioned, the first dye sensitisers were ruthenium based. Ruthenium dyes were chosen because of their wide absorption in the visible and NIR region, their excellent charge transfer capabilities, and their thermal and photostabiltiy[78,88]. The most well-known ruthenium dye is Black Dye (**23**, Figure 1.14), which had a first PCE of 10.4% and was a breakthrough in the field[89]. Following on from black

dye, further molecular design was focused on the addition of p-conjugated systems to the bipyridyl ligand to help increase photon harvesting, the most successful of these attempts being **24** (Figure 1.14), which gave a PCE of 11.5%[90].

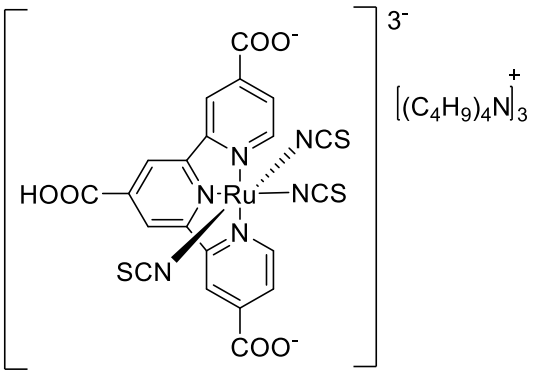

23

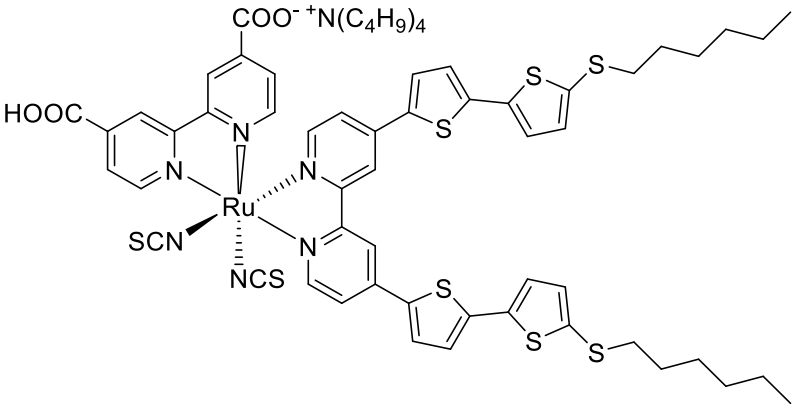

24

Figure 1.14 - Ruthenium Based Dyes Used in DSSC

Research then focused on finding metal free alternatives for use as dye sensitisers. Organic alternatives have the advantages that they do not use expensive and rare metals, are relatively easy to synthesise and allow for easier molecular tailoring[91]. Many different molecules have been tested over the years with varying results. Examples include polyene dyes, such as **25** (Figure 1.15), which gave a PCE of 6.8%[92]. Coumarin derivatives show some promise in DSSC because of their strong absorption in the visible region, good long term stability and appropriate LUMO levels for injection of electrons into the conduction of TiO_2. One such coumarin derivative that gave an impressive PCE of 8.2%[91] is **26** (Figure 1.15).

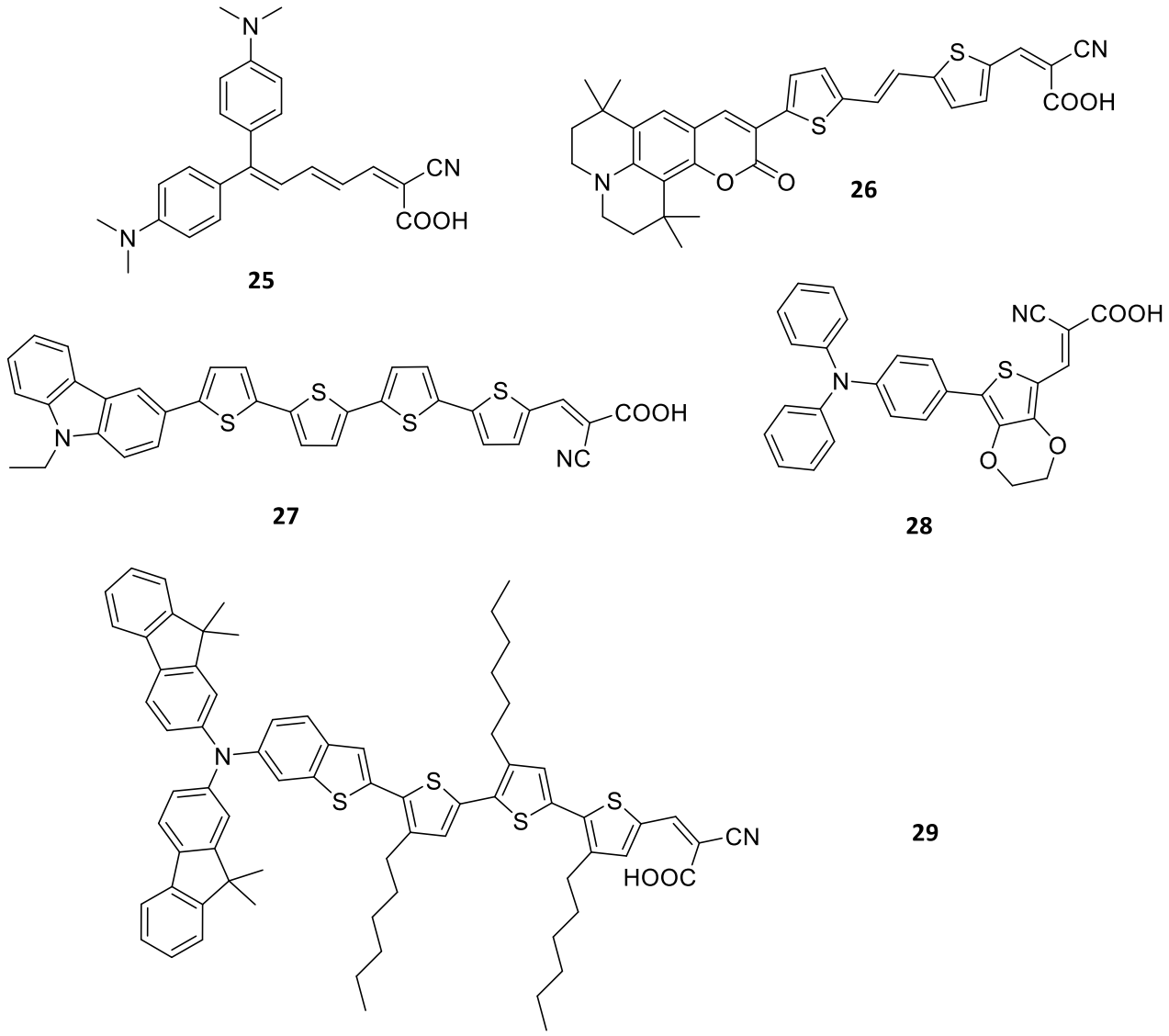

Figure 1.15 - Organic Dyes Used in DSSC

Following the donor-π bridge-acceptor (D-π-A) configuration, using carbazole as a donor **27** (Figure 1.15) was developed. The rationale for the hexyl chains on the thiophene moieties was to increase electron lifetimes by hindering the approach of acceptors in the electrolyte while the dye was bound to the TiO_2[93], a **27** DSSC gave a PCE of 7.7%. Another D-π-A molecule utilising alkyl chains to help to increase lifetimes is **28** (Figure 1.15), which gave a PCE of 8.6%[94]. As previously mentioned triphenylamine moieties are commonly found in organic photovoltaics due to their high absorption characteristics and electron donating abilities, the same can be said for DSSC, **29** (Figure 1.15) is one such example of a triphenylamine based dye that gave a PCE of 7.3%[95].

A more successful organic dye based on a triphenylamine moiety attached to a phenylenevinylene π-bridge with a cyanoacetic acid group **30** (Figure 1.16) was developed in 2007, bringing organic dye

sensitisers close to the efficiencies of their metal containing equivalents. **30** achieved a PCE value of 9.1%[96].

Another recent development is the use of rhodanine as opposed to cyanoacetic acid as an anchoring group in DSSC. Rhodanine encourages a strong push-pull system due to its electron withdrawing character. Rhodanine also allows for greater control of solubility as it can undergo N-alkylation[97]. One such example of rhodanine being used successfully as an anchoring group and to control solubility is **31** (Figure 1.16) which gave a PCE of 9.4%[98].

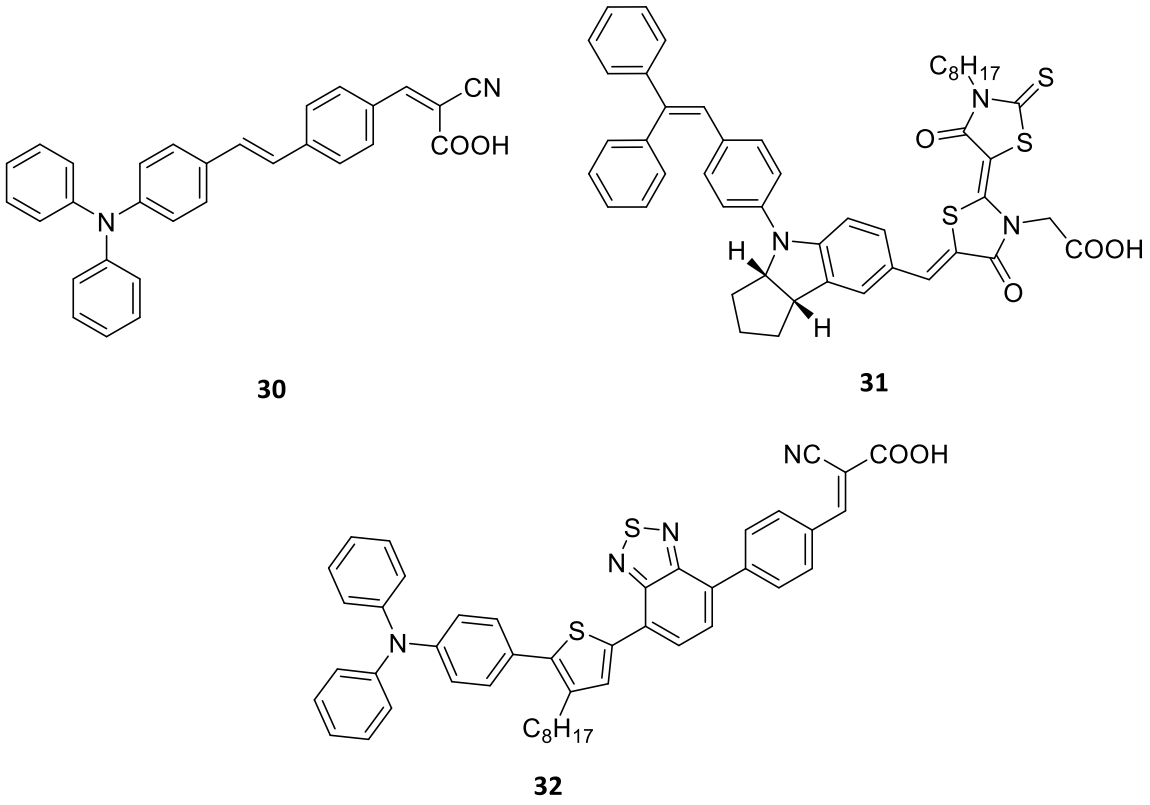

Figure 1.16 - Higher Efficiency Organic Dyes Used in DSSC

To date the best performing organic dye sensitiser is based on a triphenylamine donor group, an asymmetric π-bridge consisting of thiophene, benzothiadiazole and phenyl subunits and a cyanoacetic anchoring group. An octyl group is included in the π-bridge for the reasons previously discussed and the π-bridge is asymmetric in an attempt to avoid recombination. The dye **32** (Figure 1.16) gives an impressive PCE of 10.2%[99].

Porphyrins have attracted much interest due to their large absorption coefficients in the visible region and their potential to be molecularly engineered[100]. Porphyrins have almost panchromatic absorption and thus only a single benzothiadiazole subunit was required to sufficiently increase the absorbance.

Thus, the PCE record for DSSC belongs to the push-pull porphyrin **33** (Figure 1.17), which gave an excellent PCE of 13.0%[101].

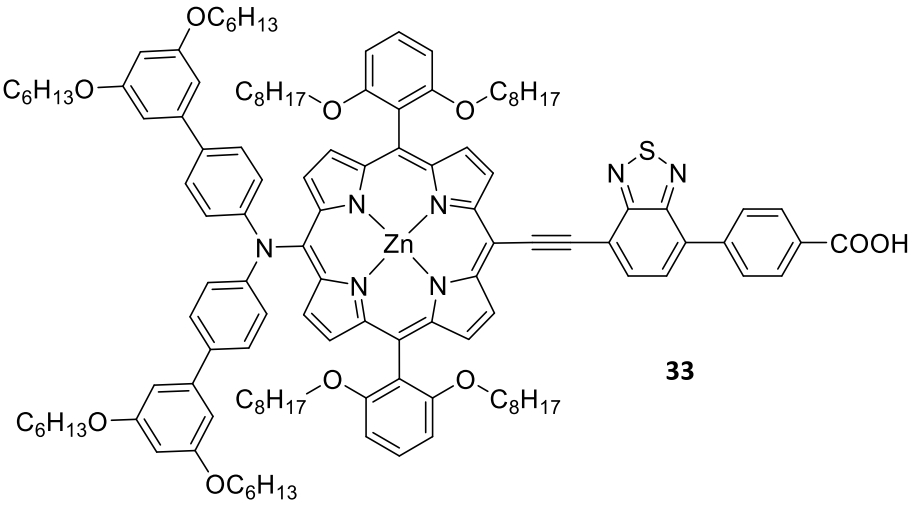

Figure 1.17 - Porphyrin Used in Highly Efficient DSSC

1.2.3. Electrolytes

As well as improving the sensitiser dye, DSSC efficiency can be improved by lowering the redox potential of the electrolyte and thus increasing the V_{OC} of the cell. The I^-/I_3^- redox couple is the most popular because of the slow recombination rate[102]. There have been many attempts to find an alternative redox couple in DSSC, examples such as Br^-/Br_3^- [103] which allowed for a greater V_{OC} and in some cases more efficient cells but the faster recombination reaction meant that increases in efficiency are only found in dyes with more positive potential than $E(Br^-/Br_3^-)$. Hydroquinone based redox couples were also investigated[104] but gave poor results.

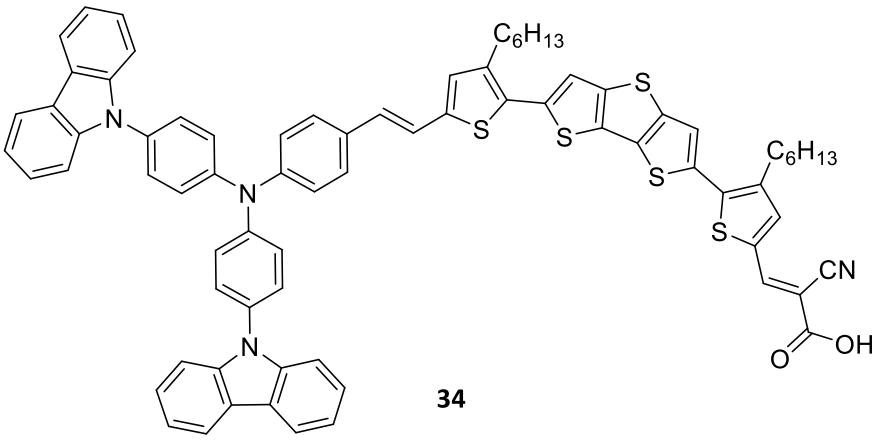

Figure 1.18 - Organic Dye Used with Ferrocene Redox Couple

Using the ferrocene redox couple Fc/Fc^{+} has shown some positive results, raising the efficiency of organic dye **34** (Figure 1.18) in the presence of a co-absorber from 6.1% to 7.5%[105]. Ferrocene also has the advantage of being readily commercially available.

The most promising results in recent times have come from using Co^{2+}/Co^{3+} electrolytes, the first example being $[Co(bpy)_3]^{2+/3+}$ which improved efficiencies of triphenylamine dyes over the cells constructed using I^-/I_3^- [106]. Cobalt complexes are attractive electrolytes due to the fact that their electronic and redox properties can be tuned by varying the ligand environment. Cobalt complexes with tridentate ligands have also been investigated, tridentate ligands have the advantages of making the complex more stable and by reducing or eliminating the chance of isomerisation. The cobalt complex $[Co(bpy\text{-}pz)_2]^{2+/3+}$ (bpy-pz being a tridentate ligand) was shown to increase the efficiency in DSSC[107]. The previously mentioned porphyrin dye **33** cell was constructed using the $[Co(bpy)_3]^{2+/3+}$ redox couple[101].

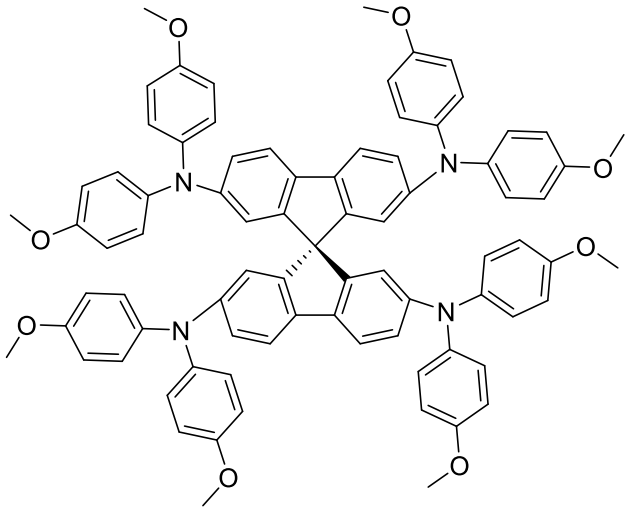

35

Figure 1.19 - Solid Hole Transporting Material

Conversely, there have been great efforts to eliminate the need for liquid electrolytes in DSSC. Liquid electrolytes have the disadvantages of being corrosive, volatile and thus have problems related with leakage. These problems present major challenges with mass production and thus much development has been undertaken to develop solid hole-transporting materials[108]. In solid state DSSC hole transfer takes place directly from the oxidised dye to the HOMO of the solid hole-transporting material, which transports the charge to the counterelectrode[109]. The best performing hole-transporting material to date is spiro-MeOTAD (**35**, Figure 1.19) which achieved PCEs of 7.2% with an organic dye[110] and 10.2% with an inorganic dye[111].

1.3. Background Information on Diketopyrrolopyrroles

As most of the work described in this thesis is based around diketopyrrolopyrroles (DPP) a brief introduction to its chemistry and applications in organic photovoltaics will now be produced.

1.3.1. Brief History

Diketopyrrolopyrroles were first synthesised in 1974 during the attempted synthesis of 2-azetinone **38**, however this reaction failed and the authors reported a red solid was formed and identified its structure as **39** (Scheme 1.1)[112].

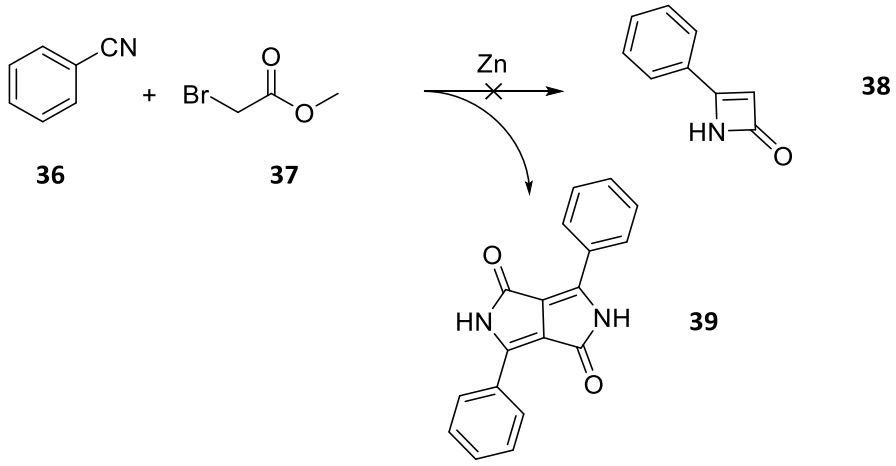

Scheme 1.1 - Failed Reaction Leading to the Discovery of DPP

Although no uses were originally found for DPPs, after some development by Ciba-Geigy before the first DPP pigment, C.I. Pigment Red 254 (**40**, Figure 1.20), was introduced to the market in 1986. Since then, functionalised DPPs have been applied in many fields, including paints, plastics, fibers and inks; before later finding uses in chemosensing and photovoltaics[113].

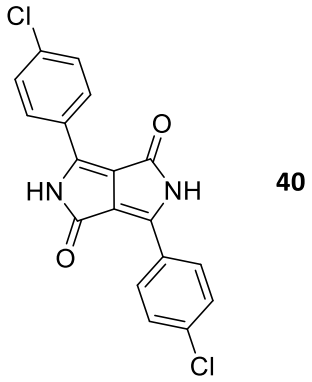

Figure 1.20 - First DPP Pigment on Market (C.I. Pigment 254)

1.3.2. Synthetic Routes

1.3.2.1. Reformatsky Route

Following on from the accidental synthesis of **39** it was proposed that DPP formation proceeded via an oxidative dimerisation, however this was proved not to be the case and that the DDP core was built first by condensation of the Reformatsky reagent with the cyanide group to yield the salt **41A**. Then an alkylation and ring closure gives the intermediate **41C**, a pyrrolinone ester, followed by another condensation to **41D** and a final cyclisation to yield the product **39** (Scheme 1.2)[114].

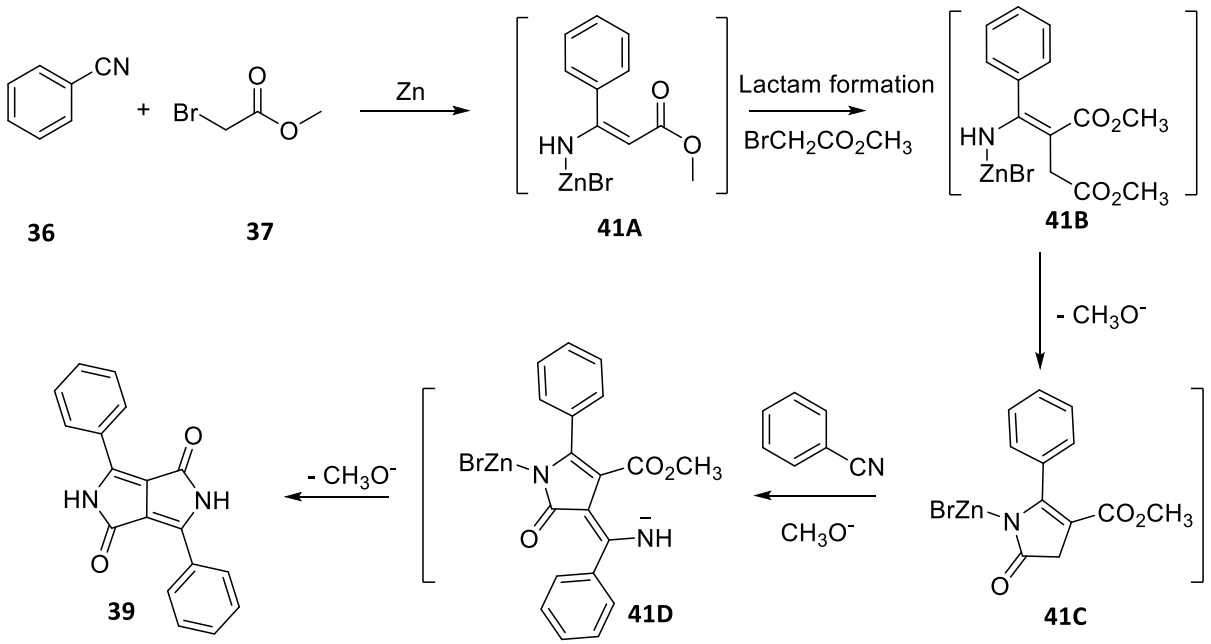

Scheme 1.2 - Reformatsky Synthesis of DPP

1.3.2.2. Succinic Ester Route

The succinic ester route of DPP synthesis was developed in 1983[114]. In this reaction, a succinic ester undergoes a condensation reaction with an aromatic nitrile, first by forming the enantiomer **43A** which is cyclised to the pyrrolinone ester **43B**, which reacts with another aromatic nitrile before a subsequent ring closure to form **39** (Scheme 1.3).

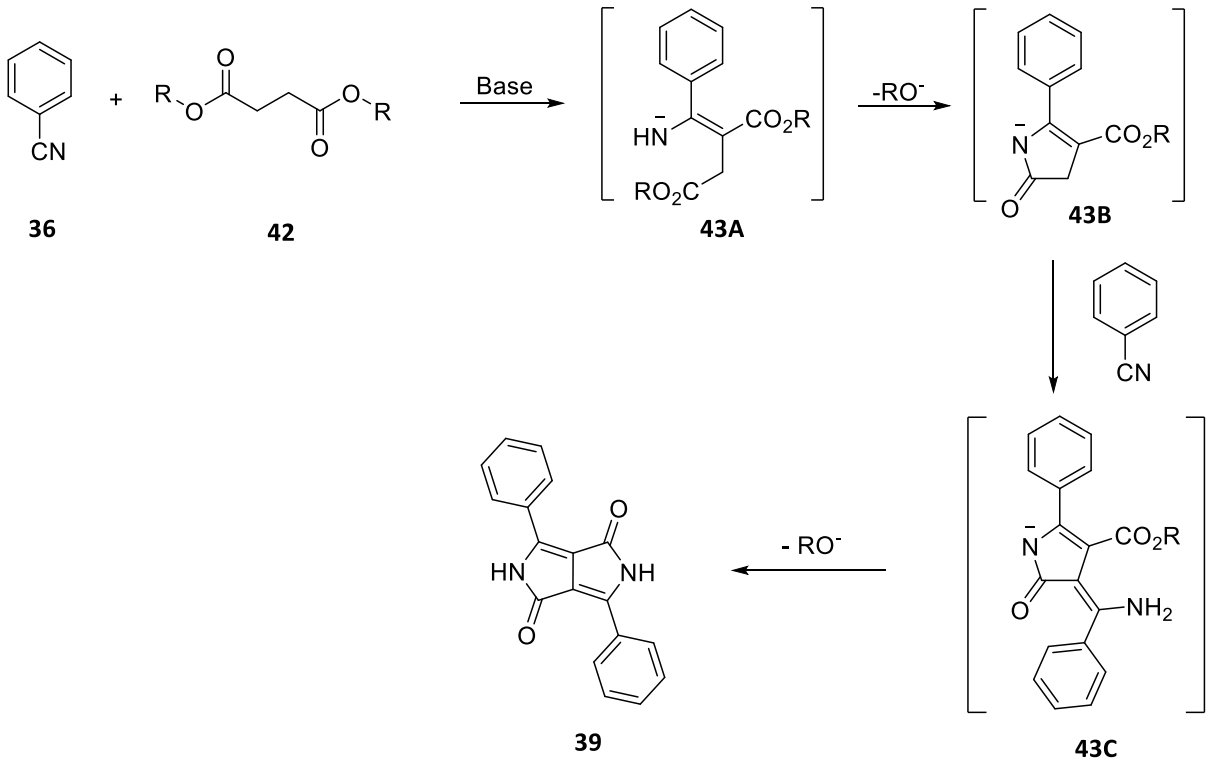

Scheme 1.3 -Succinic Ester Synthesis of DPP

1.3.2.3. Succinic Amide Route

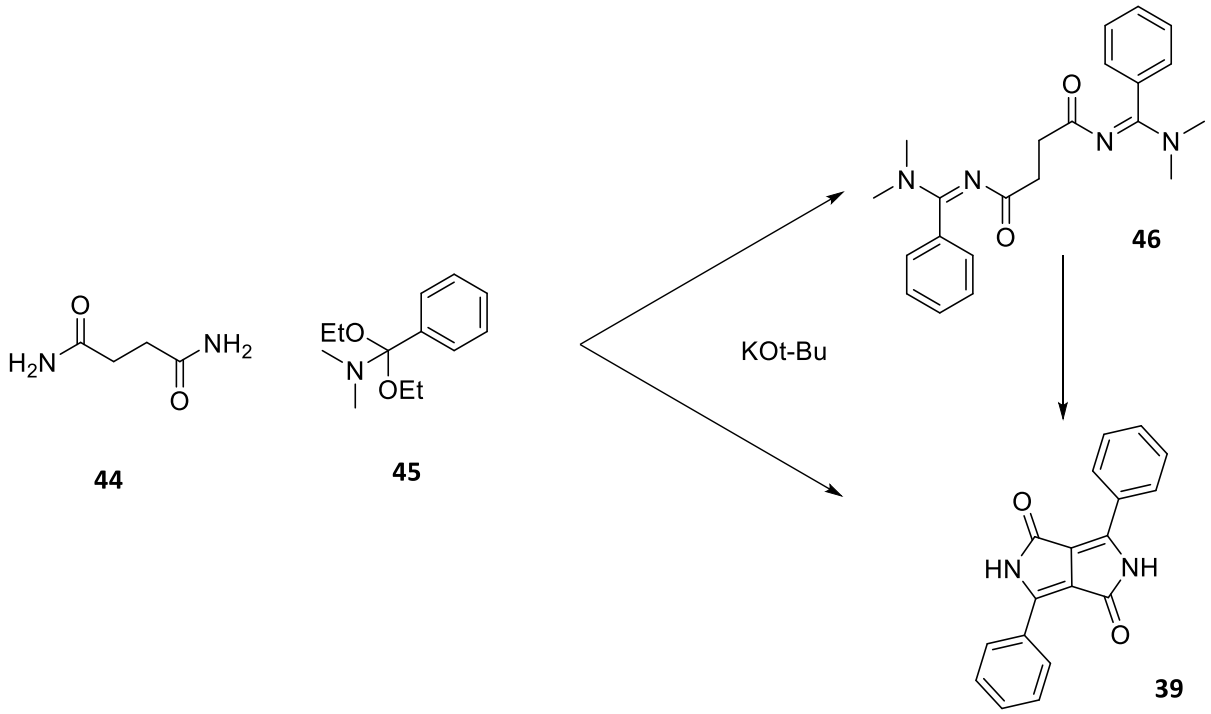

Scheme 1.4 - Succinic Amide Synthesis of DPP

Another useful synthetic route to DPPs is the succinic amide route[115], which uses a succinamide **44** and *N*,*N*-dimethylbenzamide diethylacetal **45** (Scheme 1.4).

1.3.3. Chemical Properties and Reactions

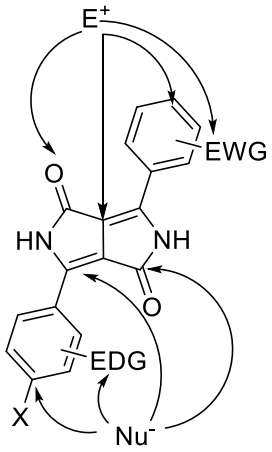

Figure 1.21 - Reactive Centres of DPP

Substitution of the phenyl rings in DPP makes the molecule susceptible to a number of electrophilic and nucleophilic substitution reactions. In addition to this, the pyrrolopyrrole core can undergo transformations depending on the conditions. A summary of the electrophilic and nucleophilic reactive sites can be seen in Figure 1.21[113].

1.3.3.1. Aromatic Substitutions

DPP **39** can be sulphonated to the disulphonic acid using fuming sulphuric acid, shown in scheme 1.5[113]. Group II and ammonium salts of **48** proved to be thermally stable compounds. The bromination of **39** also affords the stable compound **47**, however chlorination of **39** does not produce the chlorine analogue of **47** due to bromine being a better leaving group and a better nucleophile compared to chlorine[114].

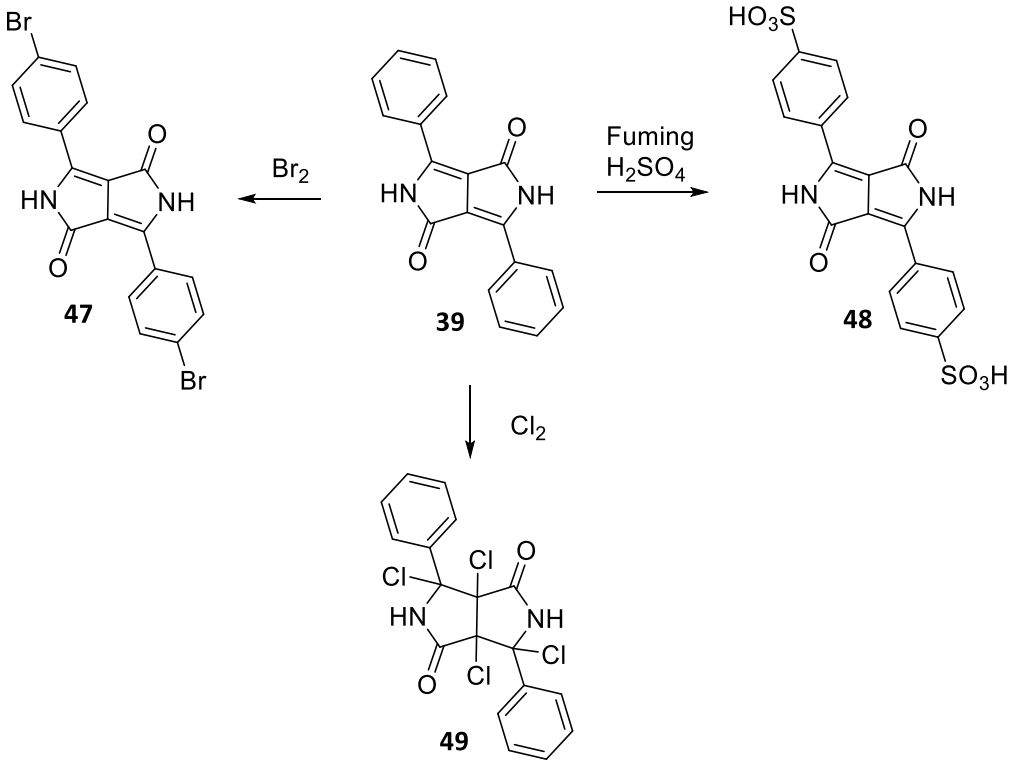

Scheme 1.5 - Substitution Reactions Associated with DPP

DPP **39** can also undergo nucleophilic aromatic substitution with amines to the diaminosubstituted DPP **50** (Scheme 1.6).

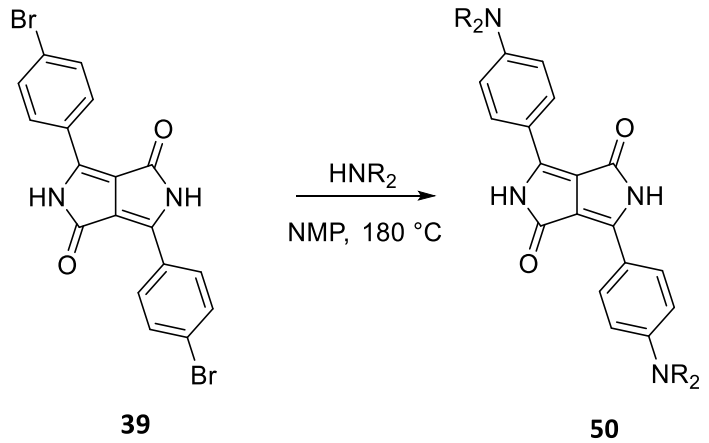

Scheme 1.6 - Nucleophilic Aromatic Substitution of DPP

1.3.3.2. N-Alkylation

DPP **39** can be alkylated at the nitrogen atoms of the DPP core, this alkylation can be carried out using alkyl halides or alkyl sulphonates, with potassium carbonate generally being used as a base. Upon alkylation of **39** the compound becomes drastically more soluble, due to the removal of the hydrogen bond donor that leads to aggregation in 39[113]. The two methods of alkylation can be seen in Scheme 1.7.

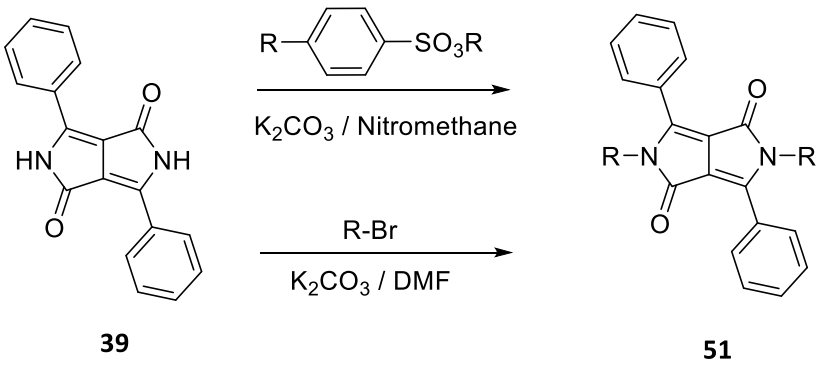

Scheme 1.7 - N-Alkylation of DPP

Despite being the favoured product, there are some undesirable side products (Figure 1.22) associated with the alkylation of DPP, due to alkylation occurring at the oxygen[116].

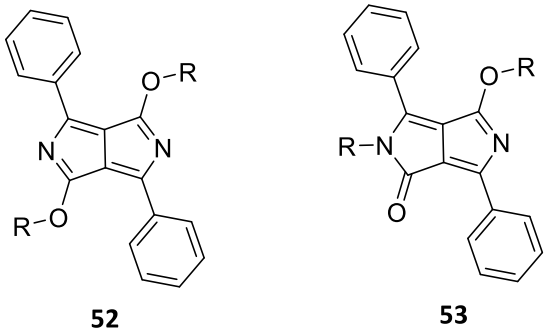

Figure 1.22 - Side Products of N-Alkylation of DPP

1.3.4. Diketopyrrolopyrroles in Photvoltaics

The DPP core has a well conjugated structure, allowing for π-π interaction as well as being electron withdrawing, which results in efficient charge transport. DPPs also have relatively low lying HOMO and LUMO levels and high absorption coefficients making them potentially useful in organic photovoltaics[117].

1.3.4.1. Diketopyrrolopyrrole Polymers in Heterojunctions

Examples of the most efficient DPP polymers used as donor materials in heterojunctions are shown in Figure 1.23. **54**, **55** and **56** had PCE values with $PC_{71}BM$ of 4.7%[118], 5.5%[119] and 8.0%[120], respectively.

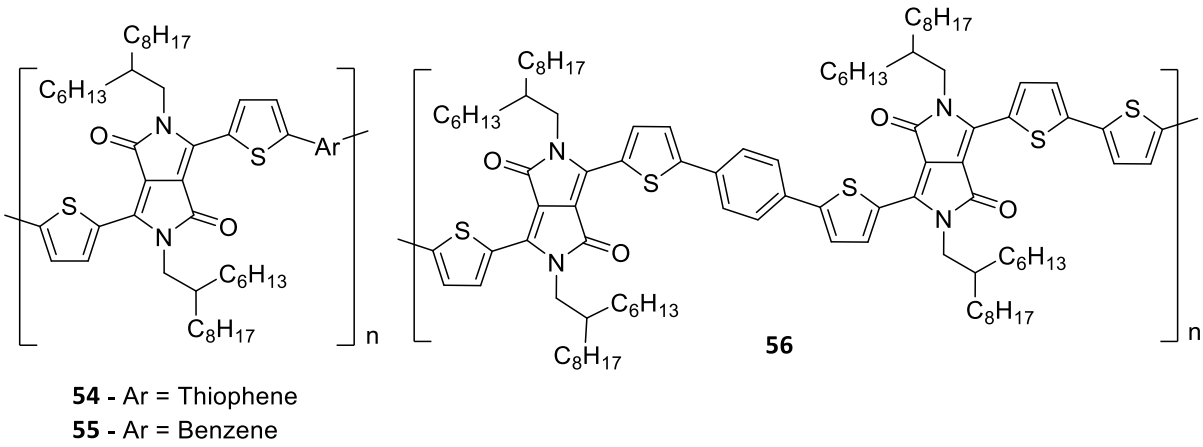

Figure 1.23 - DPP Polymers Used in Heterojunctions

1.3.4.2. Diketopyrrolopyrrole Small Molecules in Heterojunctions

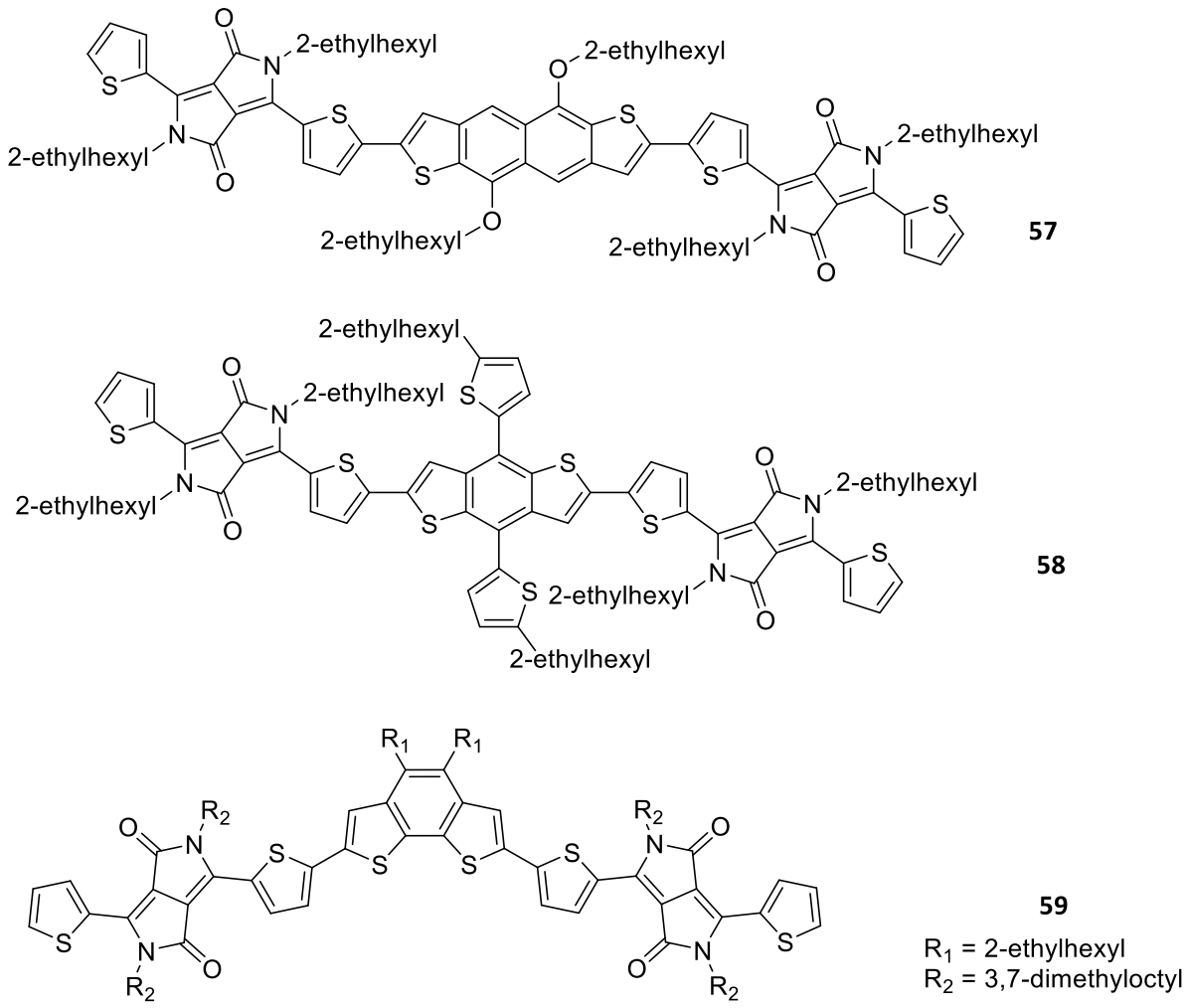

Figure 1.24 - DPP Small Molecules Used in Heterojunctions

DPPs have not performed as well as small molecule donors as their polymer equivalents, however reasonable efficiencies have been achieved with some DPP derivatives. Highlights include **57**, **58** and

59 (Figure 1.24), which gave efficiencies of 4.96% with PCBM[121], 5.29%[122] and 5.53%[123] with $PC_{71}BM$, respectively. However the most efficient small molecule donor material containing DPP is the previously mentioned **22**.

1.3.4.3. Diketopyrrolopyrroles in Dye-Sensitised Solar Cells

The high photochemical, mechanical and thermal stability of DPPs makes them ideal for use in DSSC[124]. The central planar chromophore of the DPP core is very well suited as a π-bridge in sensitisers, and the easy functionalization of the aromatic groups allows for great control of molecular design, also the straightforward N-alkylation of DPP allows the added solubility and hindrance of electrolyte molecules causing recombination as previously discussed. Thus DPPs have been extensively studied as dyes for DSSCs.

Some of the best examples of DPPs in DSSC include **60** (Figure 1.25) which gave a PCE of 7.7% and a PCE of 8.6% when combined with a co-sensitiser[125]. Another efficient DPP sensitiser is **61** (Figure 1.25) which gave a PCE of 9.1%[126]. However the best performing DPP dye was achieved using an asymmetric DPP core, with a large conjugated donor molecule and cyanoacetic acid acceptor group, DPP **62** (Figure 1.25) gave a PCE of 10.1%[127].

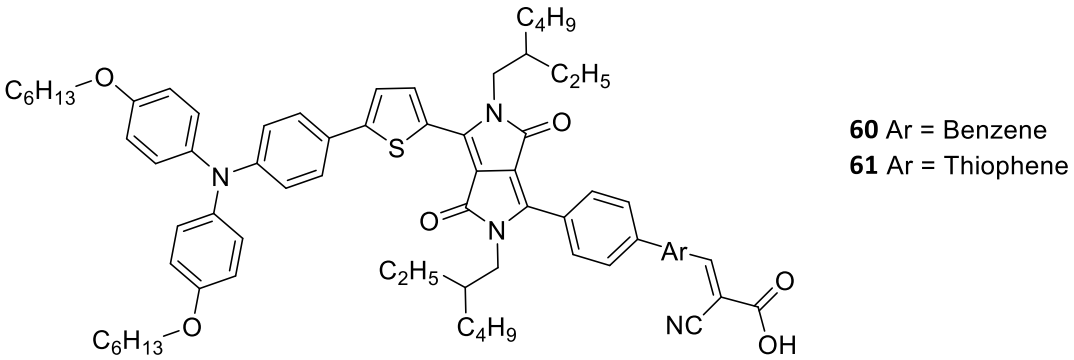

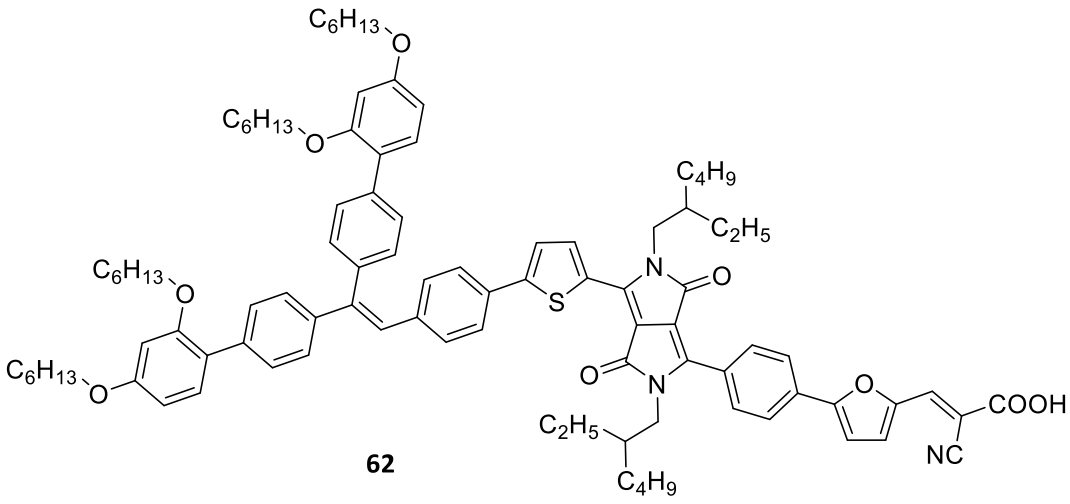

Figure 1.25 - DPPs Used in DSSC

2. Results and Discussion

2.1. Aims of Project

2.1.1. Small Molecules for Heterojunctions

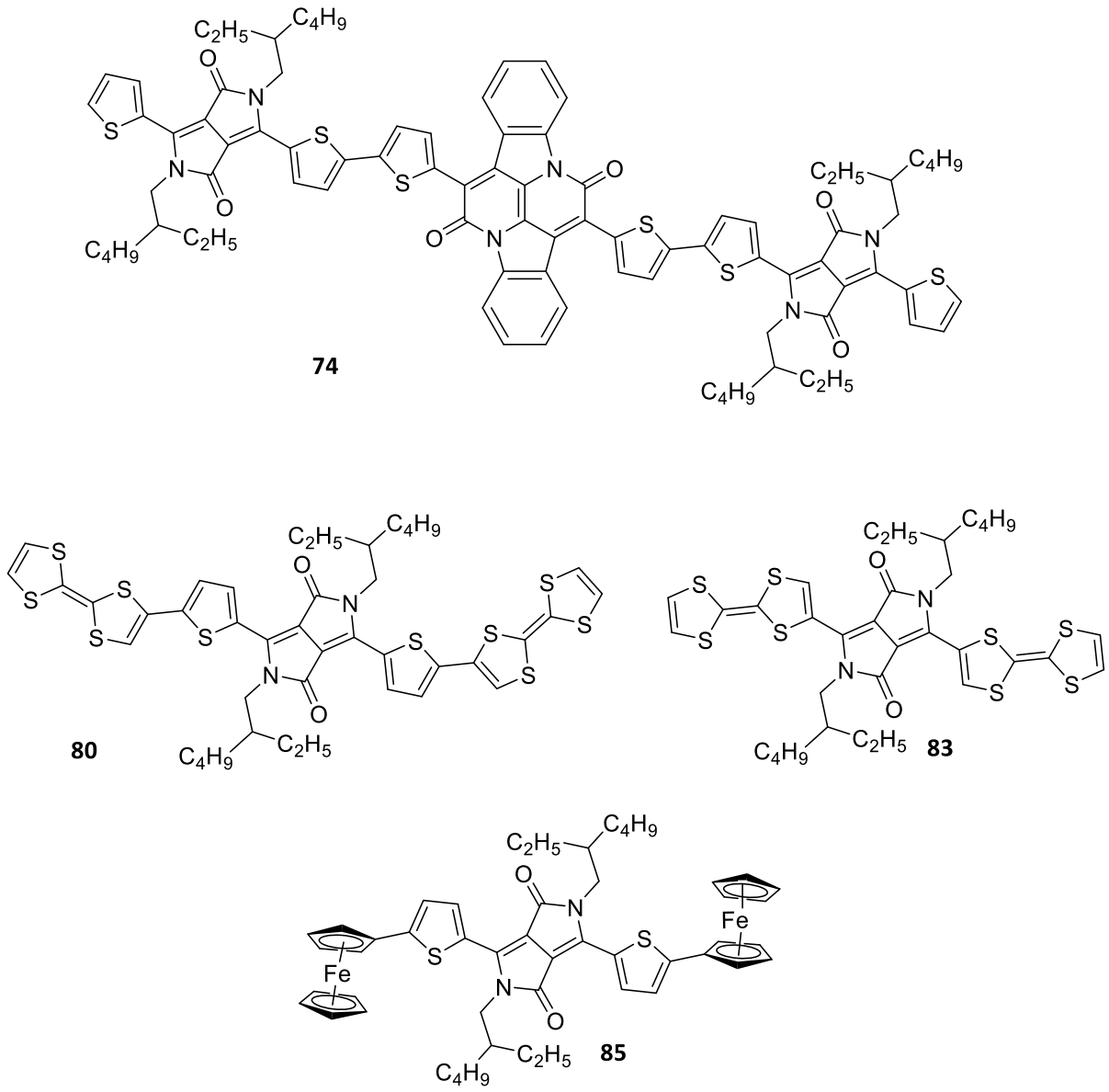

Figure 2.1 - Target Small Molecules for Use in Heterojunctions

The first target molecule **74** (Figure 2.1) was based on the recently developed bay-annulated indigo (BAI), flanked by two DPP subunits. BAI was found to be a good electron accepting unit with a low bandgap and potential for high electron mobility[128]. The second set of target molecules **80** and **83** (Figure 2.1), was again based on DPP however this time as the central moiety of the molecule flanked by two electron donating tetrathiafulvalene (TTF) moieties to create a donor-acceptor-donor molecule. TTF is an outstanding donor molecule that is readily oxidised to the di-cation, which makes

the molecule aromatic and thus more stable[129]. Thus TTF derivatives have been widely used in charge transfer complexes[130].

The final target small molecule for heterojunctions **85** (Figure 2.1) again utilises a central DPP moiety, which is flanked by two ferrocene moieties. Although not strictly organic, ferrocene undergoes many of the reactions associated with organic aromatic compounds. Ferrocene is also electron rich, is easily oxidised and thus acts as an electron donor[131].

2.1.2. Organic Dye for Dye-Sensitised Solar Cells

The target molecule **90** (Figure 2.2) for DSSC was based on the donor-π bridge-acceptor model for dye sensitisers. Using DPP as a π-bridge chromophore, a cyanoacetic acid group as the acceptor group and a strongly donating dimethyl aniline substituent. The triple bond, was chosen to bring an asymmetry to the π-bridge chromophore helping to slow down the recombination of charge carriers as previously discussed.

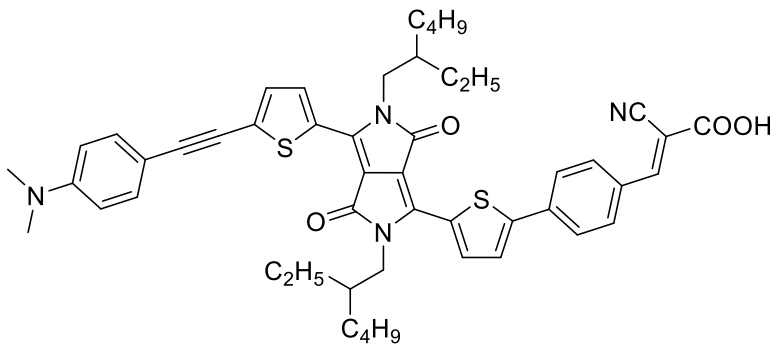

90

Figure 2.2 - Target Molecule for Use in DSSC

2.2. Results

The DPP chromophores in all molecules were prepared using the succinic ester route with a yield of 63%. The DPP **65** subsequently underwent *N*-alkylation using 2-ethylhexyl bromide to provide **66** in a yield of 30%. The poor yield of the alkylation step was due to the formation of the aforementioned isomers **52** and **53**. Branched alkyl chains were used to increase solubility and performance for the reasons previously mentioned. The alkylated DPP was then either mono or di brominated depending on the desired product using *N*-bromosuccinimide (NBS) to provide **67** and **68** in quantitative yields (Scheme 2.1).

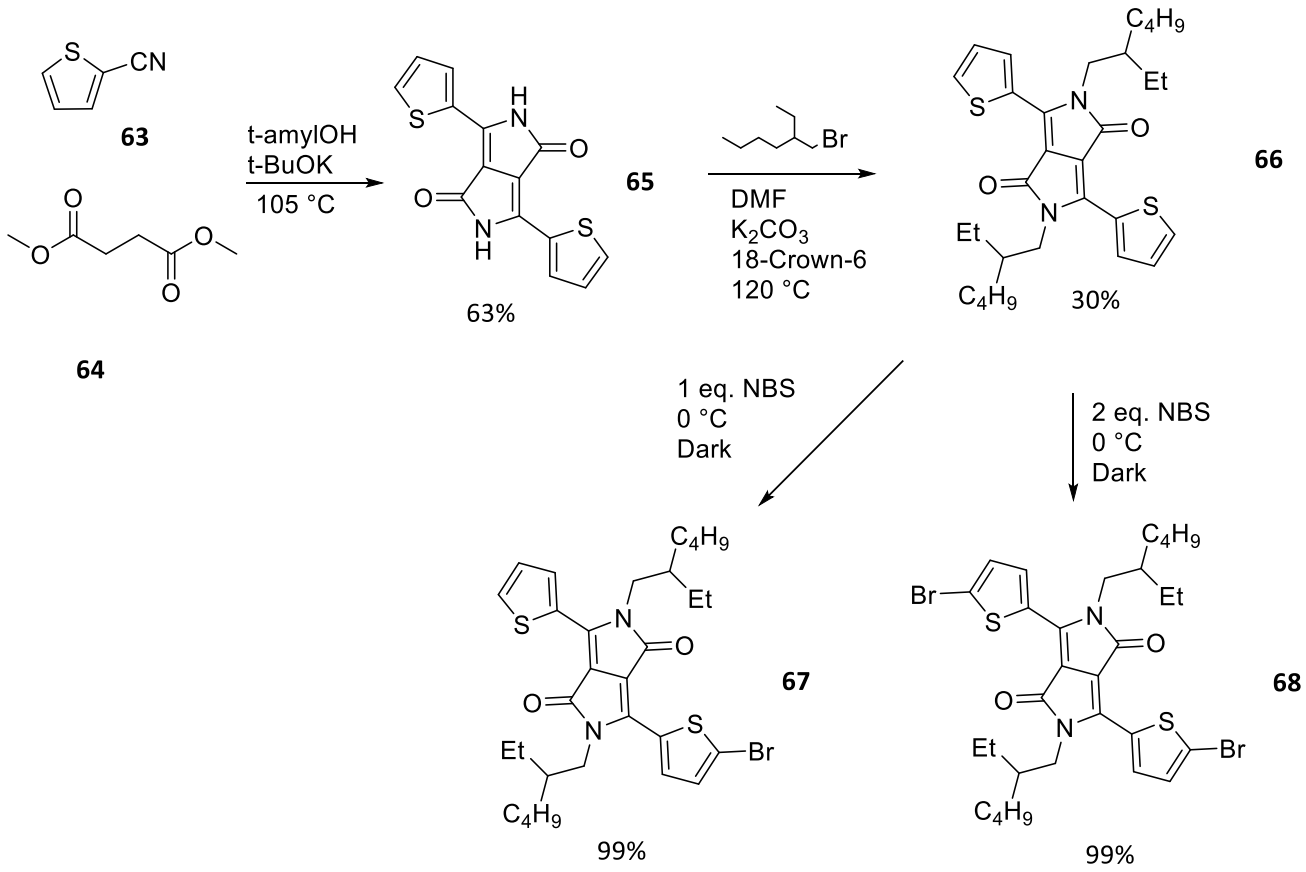

Scheme 2.1 - Synthesis of DPP moieties

2.2.1. Attempted Synthesis of **74**

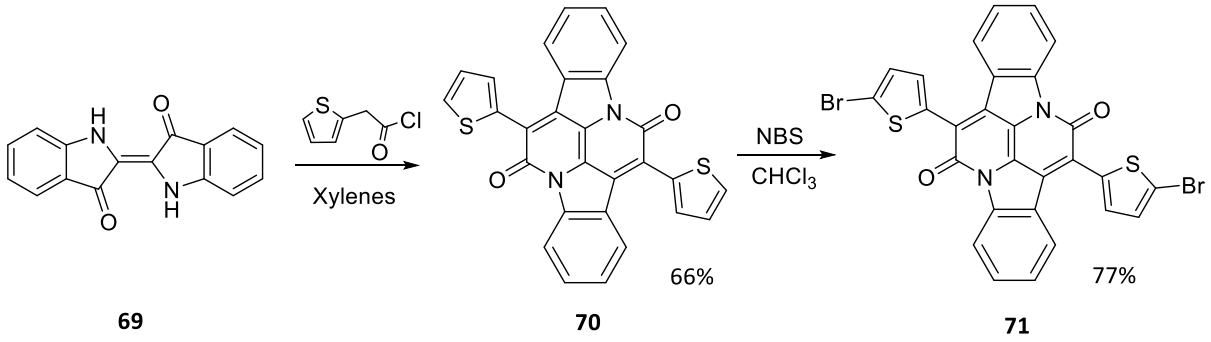

Scheme 2.2 - Synthesis of BAI and Bromination

Compound **70** was prepared using the literature procedure[128] in a yield of 60%, and subsequently brominated using NBS in accordance with the literature to provide **71** in a yield of 77% (Scheme 2.2).

Compound **67** was synthesised in accordance with Scheme 2.1. Compound **73** was prepared using a Miyaura borylation of **67** (Scheme 2.3) and used without further purification due to the pinacol

boronic ester being unstable on silica. A Suzuki-Miyaura cross coupling of **71** and **73** was attempted but was unsuccessful (Scheme 2.3). Miyaura borylations of **71** and of **70** directly were also attempted but were unsuccessful (Scheme 2.3). Lack of solubility is believed to be responsible for the poor reactivity of **70**.

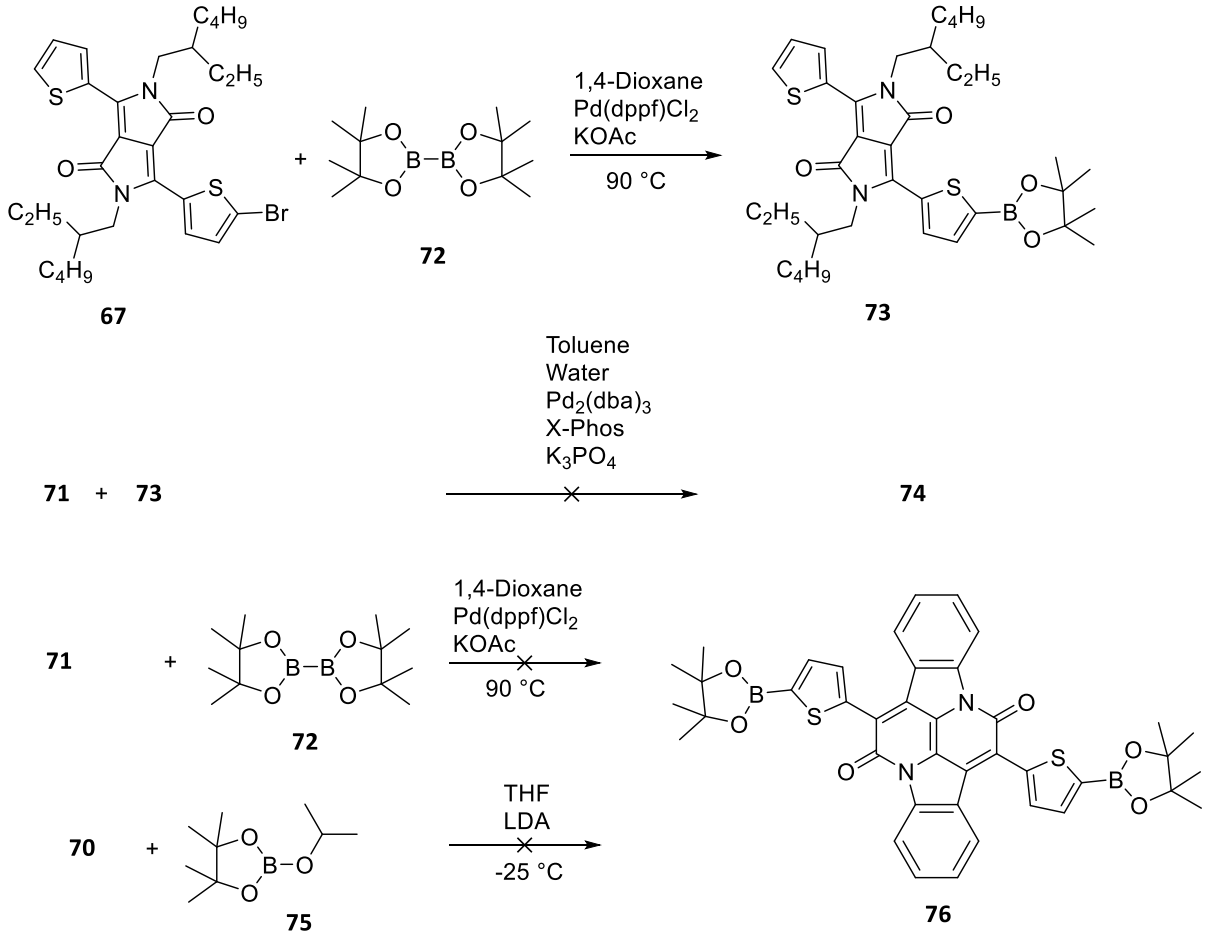

*Scheme 2.3 - Attempted Synthesis of **74***

2.2.2. Synthesis and Analysis of 80

Compound **68** was synthesised in accordance with Scheme 2.1. TTF was stannylated using tributyltin chloride to give **79** (Scheme 2.4), which was used without further purification due to the instability of the compound on silica. A successful Stille coupling of **68** and **79** was undertaken to give the product **80** with a yield of 73% (Scheme 2.4).

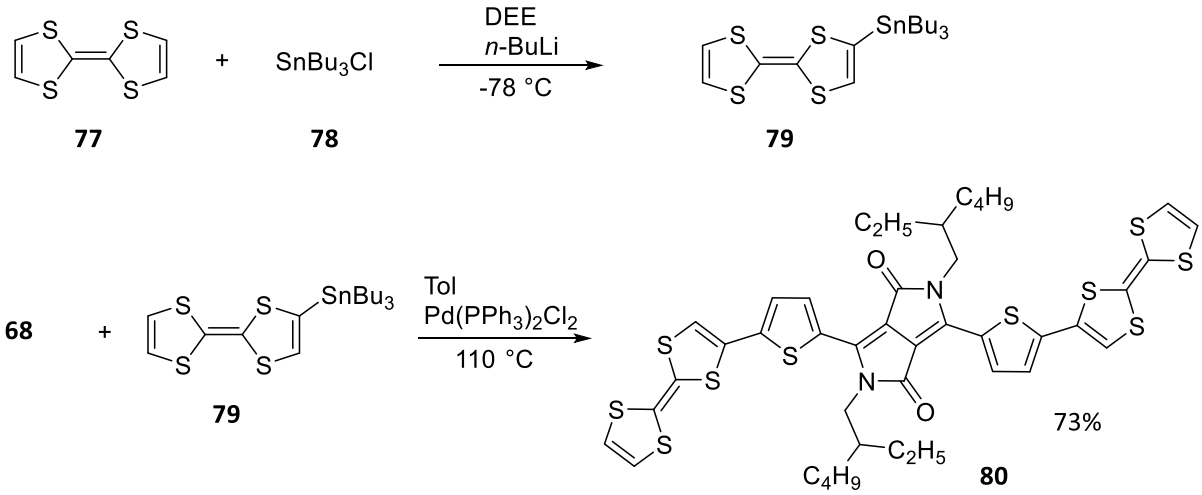

*Scheme 2.4 -Synthesis of **80***

The spectroscopic and electrochemical analysis of **80** was carried out by Mr Michele Cariello. The UV-vis spectrum of **80** can be seen in Figure 2.2, the molar absorptivity coefficient of **80**, despite being of a relatively high value, is slightly lower than expected from a donor-acceptor-donor DPP molecule with a value 49200 L mol^{-1} cm^{-1}. This lowering of absorptivity coefficient may be due to large intramolecular charge transfer (ICT) present in the molecule.

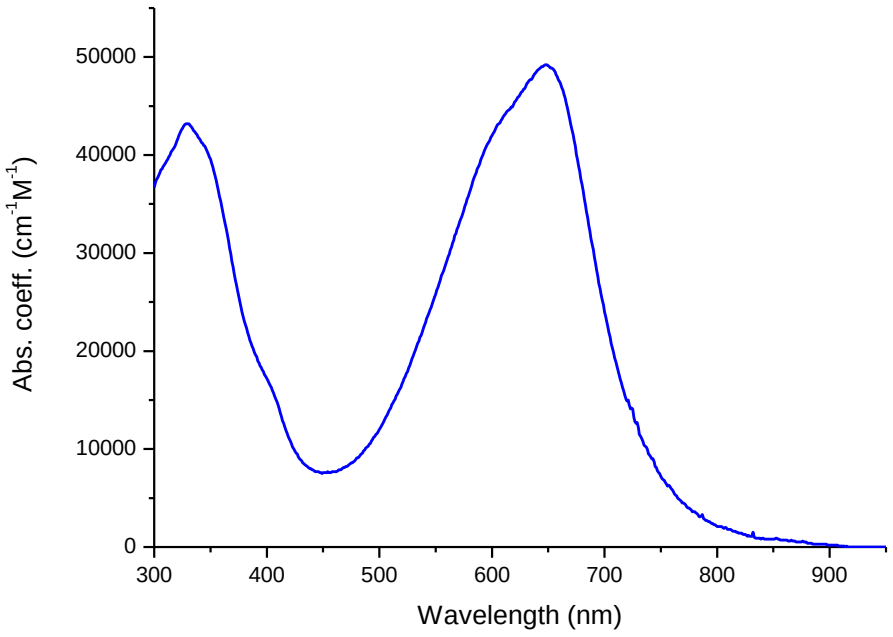

*Figure 2.2: UV-vis spectrum of **80** in $CHCl_3$ 1 × 10^{-3} M*

Absorptions associated with ICT states can be seen around 330-370 nm, the appearance of ICT bands can be indicative of effective charge separation in the molecule. The λ_{max} of **80** in $CHCl_3$ is 649 nm which shows a large bathochromic shift to that of an unsubstituted DPP, which has a λ_{max} of 504 nm[113]. Such bathochromic shifts are present in DPP molecules substituted with differing moieties, such as benzothiadiazole[132].

The high molar absorptivity coefficient indicates that there is potential for effective photon harvesting in **80**. The large bathochromatic shift indicates the lowering of the bandgap of DPP, allowing for absorption of lower energy radiation however the possibility of using **80** alongside other donor materials with complementary absorption properties in tandem configuration heterojunction cells may be hindered by the ICT absorptions of **80** at lower wavelengths.

The cyclic voltammogram and square wave voltammogram of **80** can be seen in Figure 2.3 and Figure 2.4, respectively. The electrochemical measurements were carried out with and without ferrocene as a standard. The results were then corrected against the redox potential of Fc/Fc^+, however the results presented in Figure 2.3 and Figure 2.4 do not include the Fc/Fc^+ oxidation for clarity.

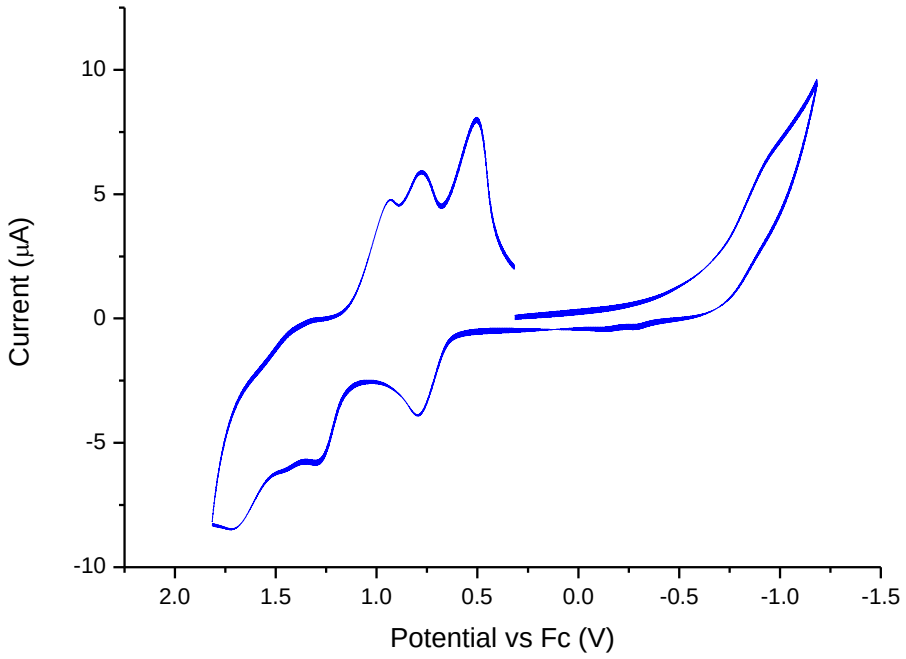

*Figure 2.3: CV trace of **80**: corrected against Fc/Fc^+ in $CHCl_3$ 1 × 10^{-3} M*

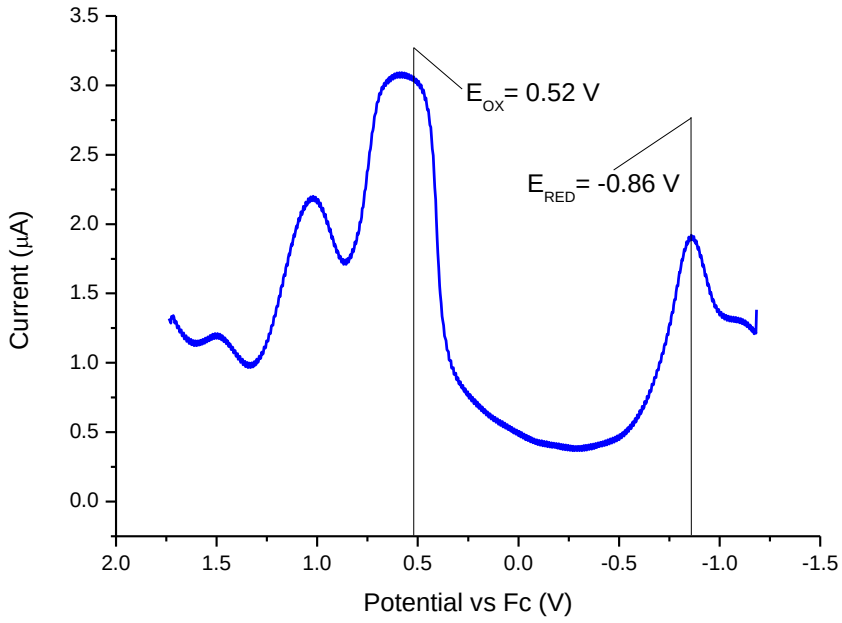

*Figure 2.4: SWV trace of **80**: corrected against Fc/Fc^{+} in $CHCl_3$ 1×10^{-3} M*

It can be seen that **80** has a low oxidation potential, due to the two TTF moieties being easily oxidisable. **80** also undergoes a second oxidation at 1.01 V. It is difficult to tell from the CV data collected whether the oxidations are reversible. The reduction of **80** occurs at -0.86 V.

Since the oxidation potential of ferrocene is well known, it can be used as a standard to calculate the HOMO and LUMO levels and thus the bandgap of the compound can be found. An example calculation can be seen below:

$$HOMO = Oxidation\ potential\ of\ Ferrocene - E_{ox}$$

$$HOMO = -4.80\ eV - 0.52\ eV$$

$$HOMO = -5.32\ eV$$

From the HOMO and LUMO the bandgap can then be calculated by simply subtracting the values obtained for the HOMO and LUMO levels. A summary of the optical and electrochemical data can be seen in Table 2.1 below. The approximations gathered for the bandgap of **80** from both the spectral and electrochemical measurements are in good agreement. 1.38 eV represents a relatively low bandgap. From both the spectral and electrochemical data collected it can be summarised that **80** has a good absorption profile in the visible region for harvesting incident light and can be easily be oxidised at low potential to generate cationic species. Thus, it is reasonable to expect that **80** could be effective as a donor molecule in heterojunctions.

*Table 2.1: Electronic and Optical Properties of **80***

	Electronic Properties					Optical Properties	
	Square Wave Voltammetry (V)					UV-Visible Spectrum	
	E_{diff} (ox)(V)	E_{diff} (red)(V)	E_{HOMO} (eV)	E_{LUMO} (eV)	E_{gap} (eV)	λ_{max} (nm)	E_{gap} (eV)
80	0.52	-0.86	-5.32	-3.94	1.38	649	1.36

2.2.3. Attempted Synthesis of 83

The proposed synthetic route for **83** can be seen in Scheme 2.5. By making compound **82**, the TTF molecule would have the required nitrile for the succinic ester synthesis of DPP, thus attaching TTF moieties directly on to the DPP core without the thiophene units found in **80**. However attempts to make and purify **83** were unsuccessful, due to the instability of **82** under the reaction conditions used.

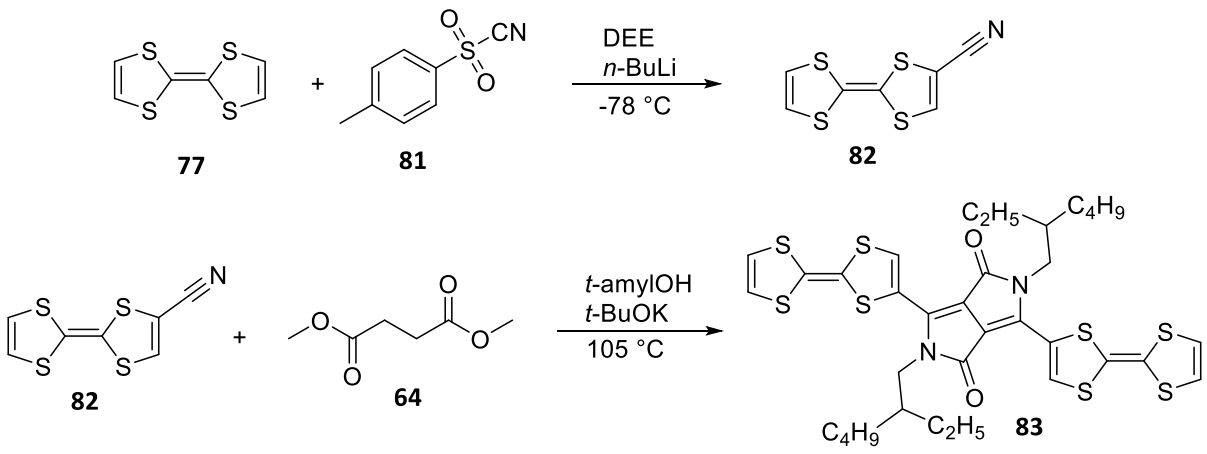

*Scheme 2.5 - Proposed Synthetic Route for **83***

2.2.4. Synthesis and Analysis of 85

Compound **68** was synthesised in accordance with Scheme 2.1. A successful Suzuki-Miyaura cross coupling reaction of **68** and ferrocene boronic acid **84** was undertaken to give the product **85** with a yield of 40% (Scheme 2.6).

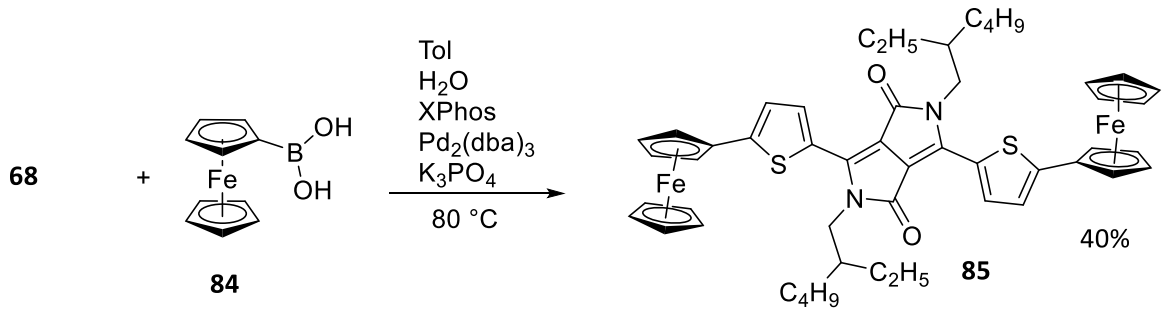

*Scheme 2.6 - Synthesis of **85***

A sample of **85** was sent to collaborators at St. Andrews University for testing as a donor material in heterojunction cells. The UV-vis spectrum of **85** can be seen in Figure 2.5, the molar absorptivity coefficient of **85** falls into the anticipated range of a donor-acceptor-donor DPP molecule with a value 72900 L mol^{-1} cm^{-1}. The λ_{max} of **85** in DCM is 632 nm which shows a large bathochromic shift to that of an unsubstituted DPP, which has a λ_{max} of 504 nm[113].

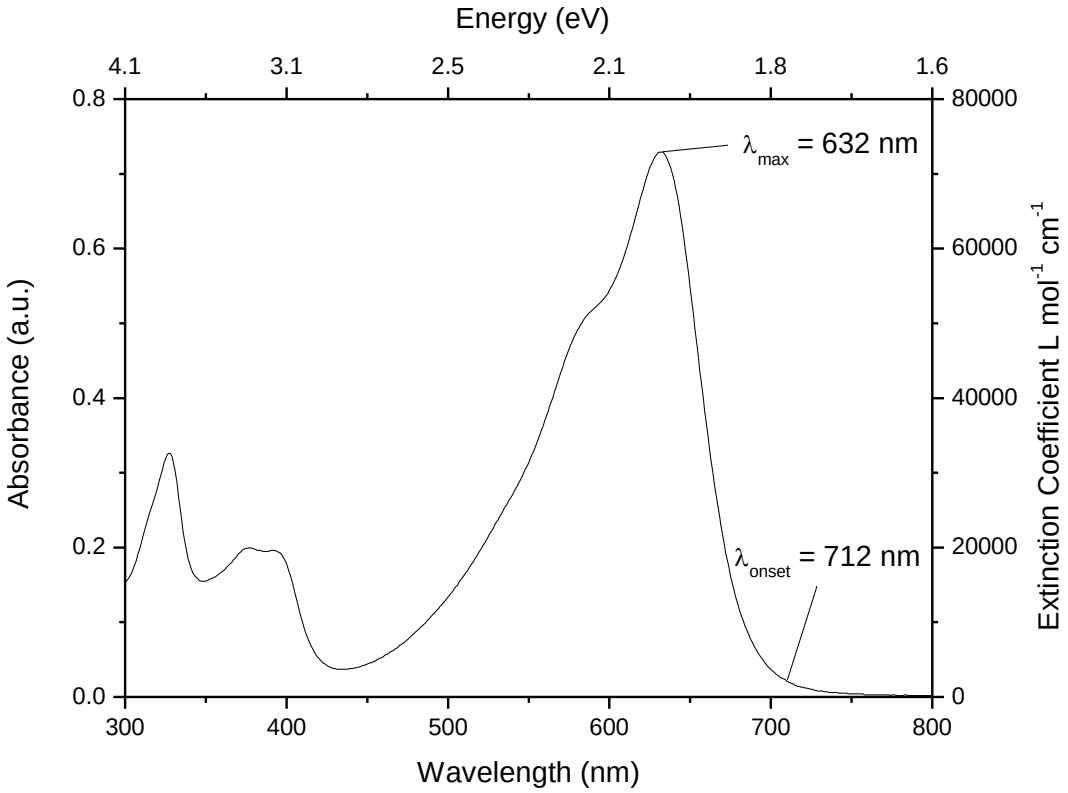

Figure 2.5 - UV-vis spectrum of **85** in DCM 1 × 10^{-5} M

The high molar absorptivity coefficient indicates that there is potential for effective photon harvesting in **85**. The large bathochromatic shift indicates the lowering of the bandgap of DPP, allowing for absorption of lower energy radiation and the possibility of using **85** alongside other donor materials

with complementary absorption properties in tandem configuration heterojunction cells. The UV-vis spectrum of **85** also shows a small shoulder that can be attributed to vibronic coupling. Absorptions associated with ICT states can be seen around 330-400 nm.

The cyclic voltammogram and square wave voltammogram of **85** can be seen in Figure 2.6 and Figure 2.7, respectively. The electrochemical measurements were again carried out with and without ferrocene as a standard. The results were then corrected against the redox potential of Fc/Fc^+, however the results presented in Figure 2.6 and Figure 2.7 do not include the Fc/Fc^+ oxidation for clarity.

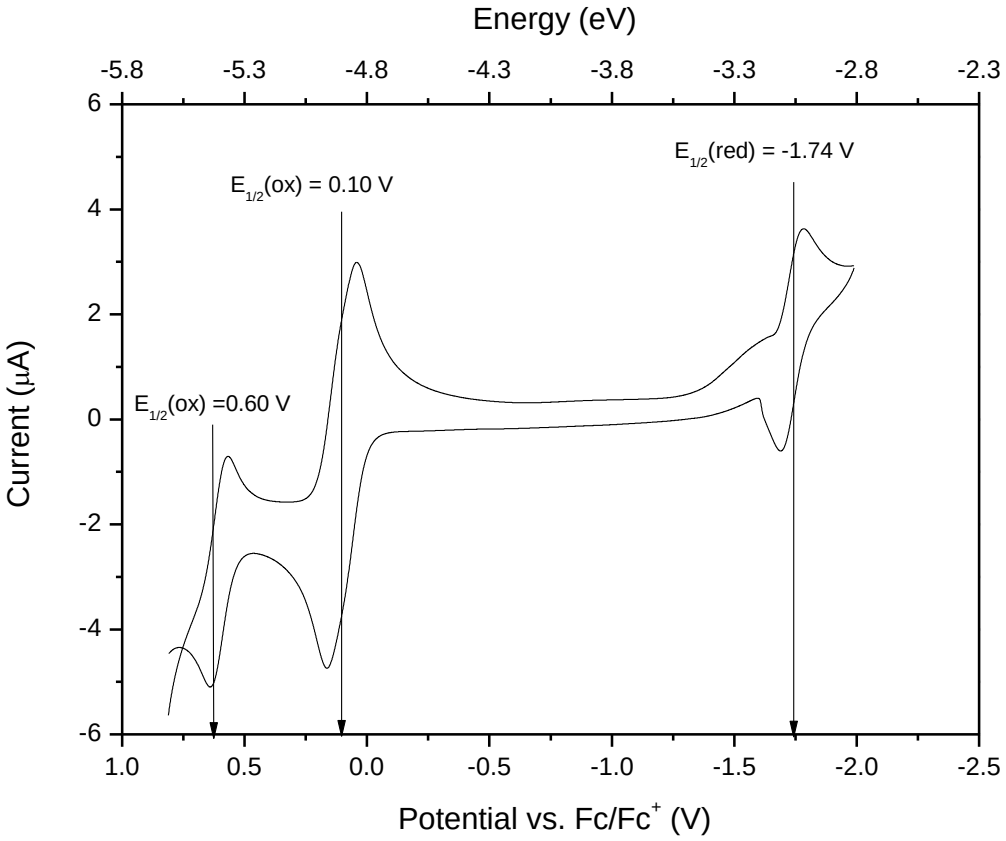

*Figure 2.6 - CV trace of **85**: corrected against Fc/Fc^+ in DCM 5×10^{-4} M*

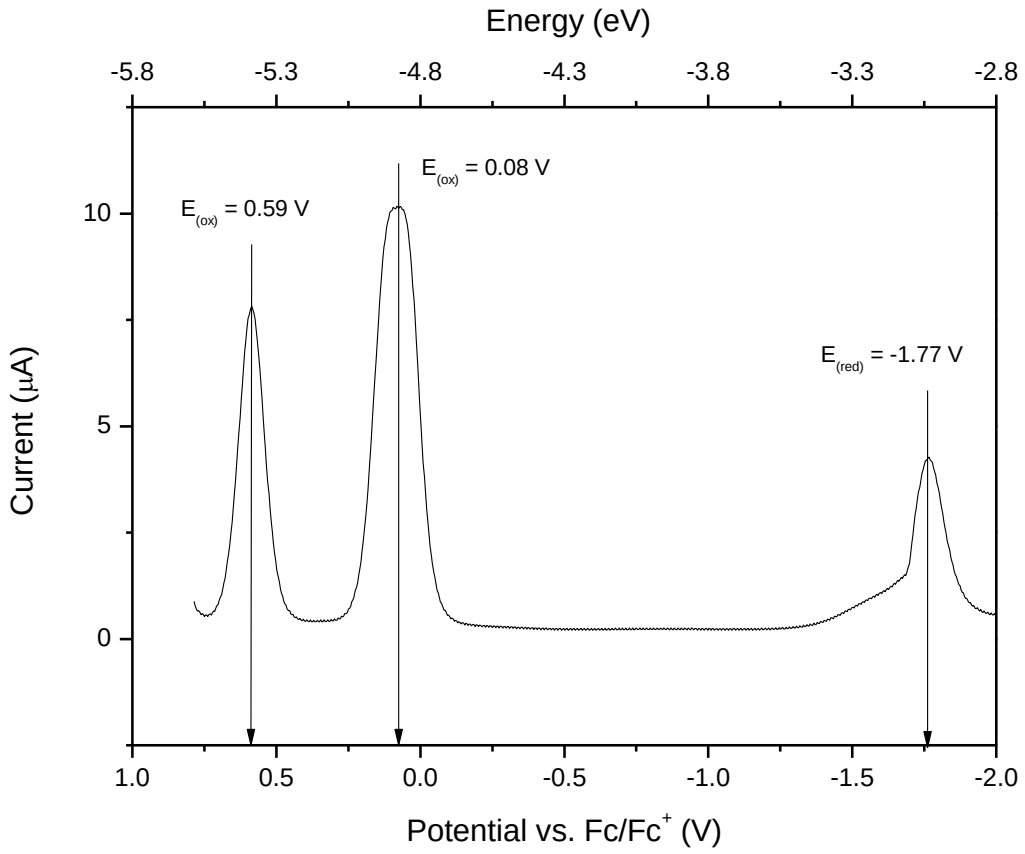

*Figure 2.7 - SWV trace of **85**: corrected against Fc/Fc^{+} in DCM 5×10^{-4} M*

It can be seen that **85** has a very similar oxidation potential to that of ferrocene (only 0.1 V of a difference), due to the two ferrocene moieties being easily oxidisable. **85** also undergoes a second oxidation at 0.60 V. Both oxidations are reversible. The reversible reduction of **85** occurs at -1.74 V.

From the electrochemical data the bandgap of the HOMO and LUMO levels can be calculated as 1.85 eV (calculations the same as those carried out in section 2.2.2.). This approximation is in keeping with the UV-vis data collected and represents a relatively low bandgap. The results obtained from the spectral and electrochemical measurements can be found in Table 2.2.

*Table 2.2: Electronic and Optical Properties of **85***

	Electronic Properties								Optical Properties	
	Cyclic Voltammetry (V)			Square Wave Voltammetry (V)					UV-Visible Spectrum	
	$E_{1/2}$ (ox)	$E_{1/2}$ (red)	E_{gap} (eV)	E_{diff} (V) (ox)	E_{diff} (V) (red)	E_{HOMO} (eV)	E_{LUMO} (eV)	E_{gap} (eV)	λ_{max} (nm)	λ_{onset} (nm)
85	0.10	-1.74	1.84	0.08	-1.77	-4.88	-3.03	1.85	632	712

From both the spectral and electrochemical data collected it can be summarised that **85** has a good absorption profile in the visible region for harvesting incident light and can be easily be oxidised at

low potential to generate cationic species. Thus, it is reasonable to expect that **85** could be effective as a donor molecule in heterojunctions.

2.2.5. Synthesis and Analysis of 90

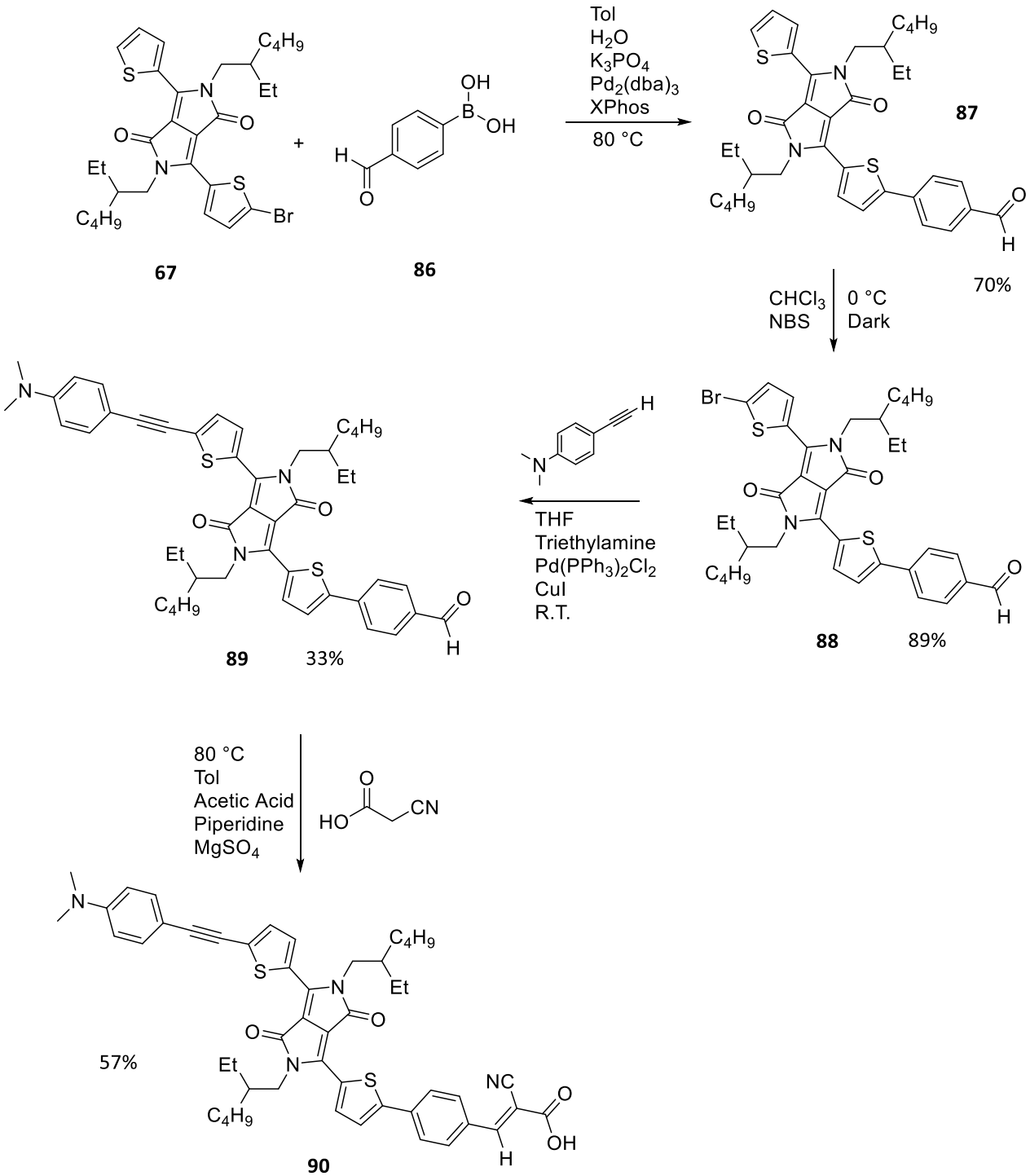

*Scheme 2.7 - Synthesis of **90***

The synthesis of **90** is outlined in Scheme 2.7. **67** was synthesised in accordance with Scheme 2.1. A Suzuki-Miyaura cross coupling of **67** and 4-formylphenylboronic acid **86** was successfully undertaken to give **87** in a yield of 70%, a subsequent mono bromination of **87** using NBS gave the compound **88** in a yield of 89%. A Sonogashira coupling of **88** and 4-Bromo-*N*,*N*-dimethylaniline was successfully undertaken to give **89** with 33% yield, and the final step of a Knovenagel condensation reaction of **89** with cyanoacetic acid gave the product **90** with a yield of 57%.

The UV-vis spectrum of **90** can be seen in Figure 2.8. **90** has a high molar absorption coefficient of 88700 L mol^{-1} cm^{-1}, indicating that **67** has the potential to effectively harvest photons in DSSC. The λ_{max} of **90** occurs at 626 nm, which represents a large bathochromatic shift when compared to the λ_{max} of 504 nm of an unsubstituted DPP[113]. In the previously reported DPP molecules **60**[125] and **61**[126] bathochromatic shifts were observed, but not to the same extent as present in **90**. The most efficient DPP in DSSC, **62**, had a λ_{max} of 602 nm[127], which was a promising sign that the low optical bandgap of **90** would translate to good efficiency in DSSC.

The UV-vis spectrum of **90** also showed a shoulder to the maximum absorption band due to vibronic coupling and similar ICT bands to that of **85**. The ICT bands found in **90** are more intense than that of **85**, implying that the charge transfer states of **90** could be better stabilised. The increased stability of the charge transfer states can be attributed to the aforementioned asymmetry of the π-bridge, helping to slow down the recombination of separated charges.

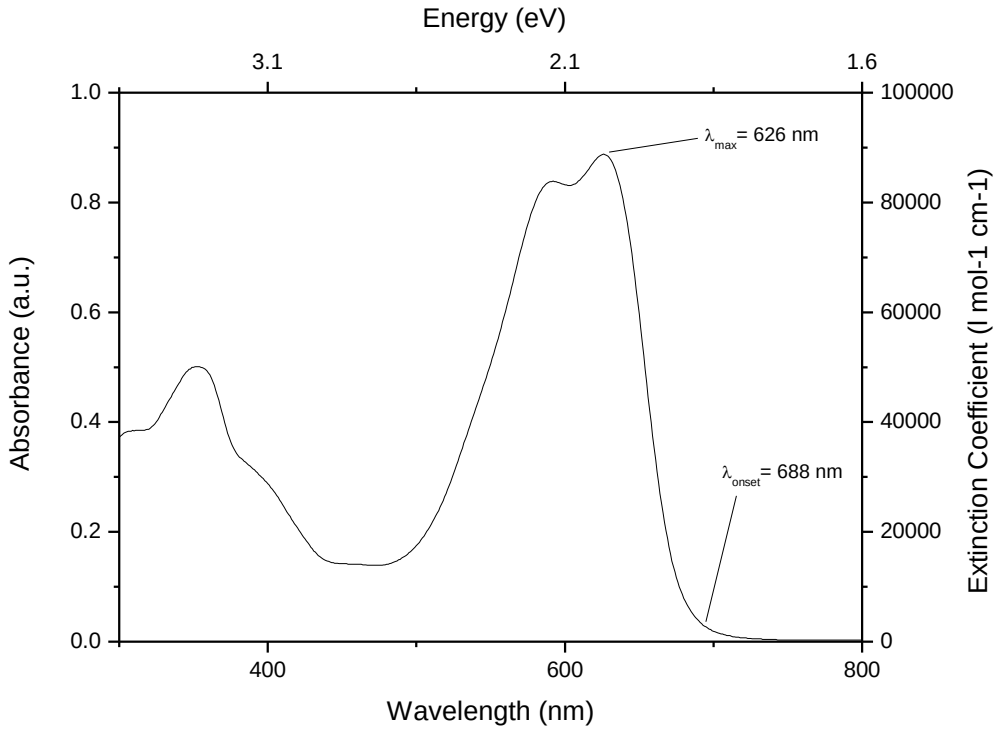

*Figure 2.8 - UV-vis Spectrum of **90** in DMF 1 × 10^{-5} M*

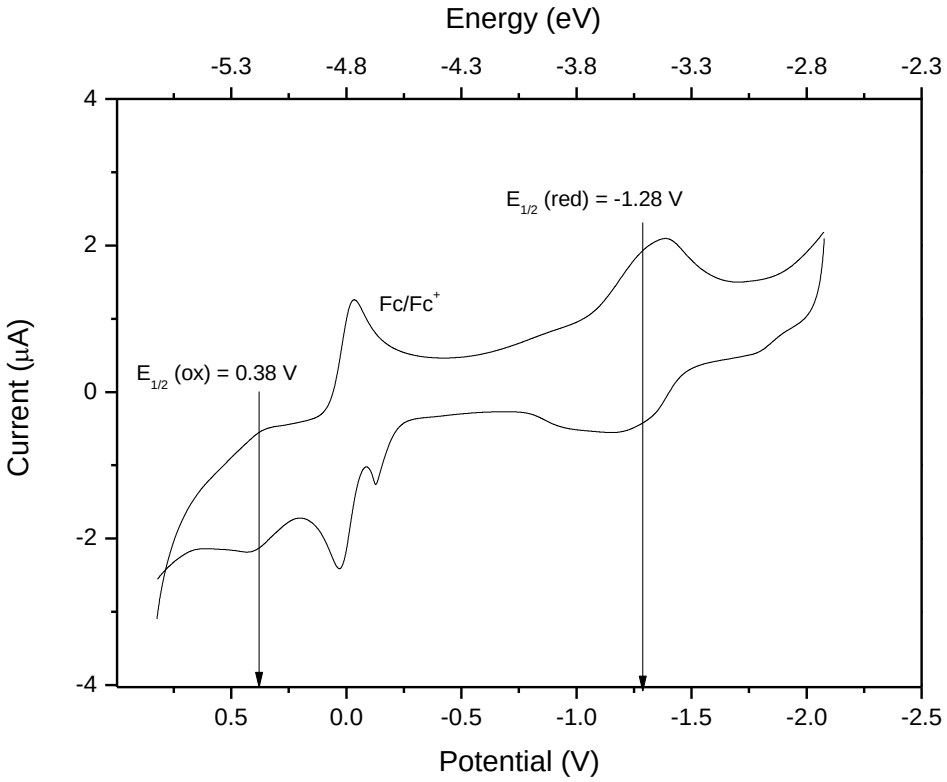

*Figure 2.9 - CV trace of **90**: corrected against Fc/Fc^{+} in DMF 5×10^{-4} M*

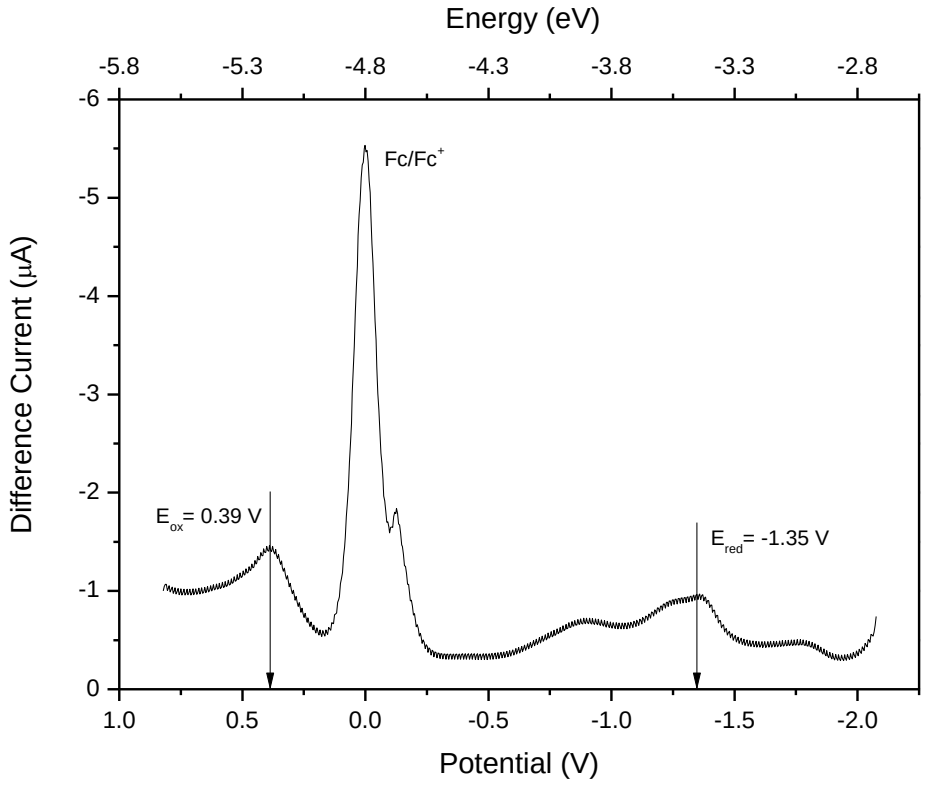

*Figure 2.10 - SWV trace of **90**: corrected against Fc/Fc^{+} in DMF 5×10^{-4} M*

The cyclic voltammogram and square wave voltammogram of **90** can be seen in Figure 2.9 and Figure 2.10, respectively. The electrochemical measurements were carried out with and without ferrocene as a standard. The results were then corrected against the redox potential of Fc/Fc^+, the results presented in Figure 2.6 and Figure 2.7 do include the Fc/Fc^+ oxidation as a reference.

It can be seen that **90** has a low oxidation potential of 0.39 V. The reversible reduction of **90** occurs at -1.28 V in the CV and -1.35 V in the square wave. From the electrochemical data obtained from the square wave voltammogram, the bandgap of the HOMO and LUMO levels can be calculated as 1.74 eV (calculations the same as section 2.2.2.). This approximation is in keeping with the UV-vis data collected and represents a low bandgap. The results obtained from the spectral and electrochemical measurements can be found in Table 2.3.

*Table 2.3: Electronic and Optical Properties of **90***

	Electronic Properties								Optical Properties	
	Cyclic Voltammetry (V)			Square Wave Voltammetry (V)					UV-Visible Spectrum	
	$E_{1/2}$ (ox)	$E_{1/2}$ (red)	E_{gap} (eV)	E_{diff} (V) (ox)	E_{diff} (V) (red)	E_{HOMO} (eV)	E_{LUMO} (eV)	E_{gap} (eV)	λ_{max} (nm)	λ_{onset} (nm)
90	0.38	-1.28	1.66	0.39	-1.35	-5.19	-3.45	1.74	626	688

From both the spectral and electrochemical data collected it can be summarised that **90** has a good absorption profile in the visible region for harvesting incident light and can be easily be oxidised at low potential to generate cationic species. Thus, it is reasonable to expect that **90** could be effective as a dye-sensitiser in DSSC. A sample of **90** was taken to École Polytechnique Fédérale de Lausanne by Mr Michele Cariello for device fabrication and testing. The best result obtained a power conversion efficiency of 3.98%. Further optimisation is to be carried out.

2.3. Conclusions and Future Work

Compounds **80** and **85** was successfully synthesised and results regarding their performance as donor molecules in bulk heterojunction solar cells is expected in due course. Compound **90** was successfully synthesised and successful device fabrication was undertaken by collaborators to give a promising first power conversion efficiency of 3.98%. Further optimisation of devices containing **90** is to be undertaken to improve PCE further.

Further efforts will be made to synthesise **74**, including investigating different coupling methods and different reaction conditions for the final coupling. Further efforts to synthesise **83** will be made, including producing more of compound **82** and improving purity to increase the likelihood of the final reaction being successful.

3. Synthesis and Characterisation

Experimental Terms and Methods

Flash Column Chromatography: Using silica gel (Merk) 40-63 µm 60 Å and solvent system is specified in each experiment.

TLC: Were performed using 5×4 cm SiO_2 coated aluminium

Dry Solvents: Innovative Technology *inc* Pure Solv 400-5-MD solvent purification system (activated alumina columns)

Reaction Temperatures: Room temperature refers to 20-25 °C other temperatures were obtained using ice-water bath for 0 °C and acetone-dry ice bath for -78°C.

Analytical Methods

MS: Mass spectrometry was performed by Jim Tweedie mass spectrometry technician at the University of Glasgow.

M.P.: Recorded on a SMP-10 Stuart Scientific melting point machine. Melting points are uncorrected.

NMR: Performed on either Bruker Avance 500, Bruker Avance 400. All spectra were characterised from ^{1}H, ^{13}C, HMQC methods, and were analysed using the Mestrelab research iNMR© package and Spinworks© 4.0.

CV: Performed using a CH Instrument Electrochemical Workstation (CHI 440a). Samples were analysed at 10^{-4} M concentrations using 0.1 M $TBA.PF_6$ as electrolyte and using Pt, Pt wire and Ag wire electrodes.

UV: Performed using a PerkinElmer Lambda 25 spectrometer.

3.1. Synthesis and Characterisation

2,5-Dihydro-1,4-dioxo-3,6-dithienylpyrrolo[3,4-c]-pyrrole: **65**[133]

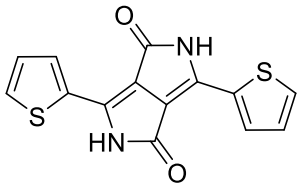

Potassium 2-methyl-2-propanolate (6.20 g, 55 mmol) was dissolved in 2-methyl-2-butanol (44 ml) under an Ar atmosphere and stirred at 105 °C for 1 hr. 2-Thiophenecarbonitrile (4.3 ml, 46 mmol) was added to the mixture, stirring was continued at 105 °C for 30 min. A solution of dimethyl succinate (2.4 ml, 18 mmol) in 2-methyl-2-butanol (8 ml) was added dropwise over 2 hrs. The mixture was allowed to stir at 105 °C for a further 2 hrs, then cooled to 50 °C and a mixture of methanol (28 ml) and water (7 ml) was added to quench the reaction. The mixture was then heated under reflux for 45 min before being allowed to cool to room temperature. The mixture was poured over ice (46 g) then HCl (35% aq., 14 ml) and methanol (51 ml) were added and the mixture was stirred for 45 min. The mixture was filtered and the precipitate washed with methanol (18 ml), before being suspended in water (92 ml) and stirred for 30 min. The mixture was filtered again and washed with methanol (18 ml), before being allowed to dry under vacuum to give the product as a purple solid (2.95 g, 63%); δ_H (500 MHz, DMSO-*d6*) 7.29 (2H, dd, *J*(Hz) 4.96, 3.80, C(4',4'')H), 7.95 (2H, dd, *J*(Hz) 4.97, 1.13, C(3',3'')H), 8.21 (2H, dd, *J*(Hz) 3.79, 1.14, C(5',5'')H), 11.25 (2H, s, NH); δ_C (125 MHz, DMSO-*d6*) 108.69 (C(3a,6a)), 128.84 (C(4',4'')H), 130.88 (C(5',5'')H), 131.37 (C(2',2'')), 132.83 (C(3',3'')H), 136.28 (C(3,6)), 161.70 (C(1,4)); *m/z* (ESI) 322.9902 $[M+Na]^+$ ($C_{14}H_8N_2NaO_2S_2$ requires 322.9925).

2,5-Bis(2-ethylhexyl)-3,6-di(thiophen-2-yl)pyrrolo[3,4-c]pyrrole-1,4(2H,5H)-dione: **66**[134]

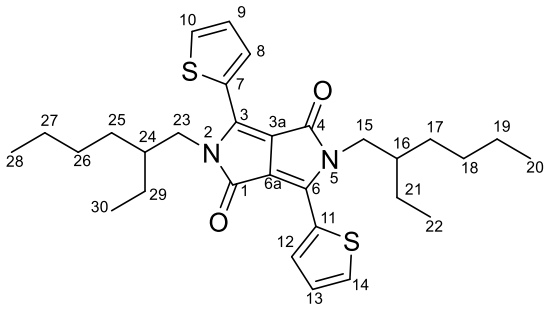

2,5-Dihydro-1,4-dioxo-3,6-dithienylpyrrolo[3,4-c]-pyrrole (3.0 g, 10.0 mmol) and potassium carbonate (4.14 g, 30.0 mmol) were dissolved in anhydrous DMF (100 ml) under an argon atmosphere. The solution was heated with stirring at 120 °C for 1 hour. 2-Ethylhexyl bromide (4.4 ml, 25.0 mmol) was added dropwise over 30 minutes. The mixture was heated with stirring overnight at 130 °C. The reaction mixture was cooled to room temperature before being poured into distilled water (400 ml) to quench. The product was extracted using CH_2Cl_2, and the organic layer collected. The solvent was evaporated and yield the impure product. The compound was then purified by column chromatography, first with petroleum ether and CH_2Cl_2 (1:4) and then with chloroform. The solvent was evaporated to yield the compound as a red solid (0.818 g, 30%); (500 MHz, $CDCl_3$) 0.86 (12H, m), 1.31 (16H, m), 1.86 (2H, m, C(16,24)H), 4.01-4.05 (4H, m, C(15,23)H_2), 7.27 (2H, m, C(8,12)H), 7.62 (2H, d, *J*(Hz) 1.19, C(9,13)H), 8.90 (2H, d, *J*(Hz) 1.18, C(10,14)H); δ_C (125 MHz, $CDCl_3$) 10.57 (C(20,28)H_3), 14.04 (C(22,30)H_3), 23.14 (C(19,27)H_2), 23.68 (C(21,29)H_2), 28.45 (C(18,26)H_2), 30.29 (C(17,25)H_2), 39.29 (C(16,24)H), 46.01 (C(15,23)H_2), 108.07 (C(3a,6a)), 128.50 (C(8,12)H), 129.80 (C(7,11)), 130.67 (C(9,13)H), 135.44 (C(10,14)H), 140.43 (C(3,6)), 161.93 (C(1,4)); *m/z* (EI^+) 524.3 $[M]^+$ ($C_{30}H_{40}N_2O_2S_2$ requires 524.3).

3-(5-Bromo-2-thienyl)-2,5-bis(2-ethylhexyl)-2,5-dihydro-6-(2-thienyl)-Pyrrolo[3,4-*c*]pyrrole-1,4-dione: **67**[135]

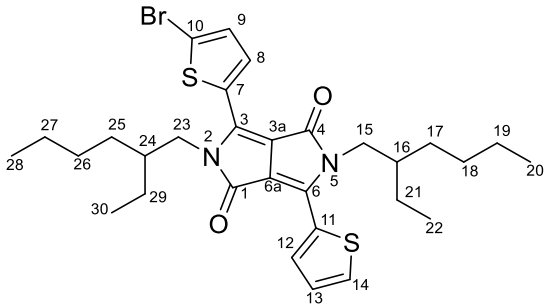

2,5-Bis(2-ethylhexyl)-3,6-di(thiophen-2-yl)pyrrolo[3,4-c]pyrrole-1,4(2H,5H)-dione (680 mg, 1.30 mmol) was dissolved in $CHCl_3$ (30ml). The reaction was cooled to 0 °C kept in the dark. *N*-Bromosuccinimide (0.254 g, 1.43 mmol) was dissolved in $CHCl_3$ and added dropwise to the reaction over 6 hours. The reaction was allowed to warm to room temperature overnight. The solvent was evaporated and the residue purified by column chromatography (PE:DCM, 1:1) to yield the title compound as a purple solid (0.449 g, 57%); δ_H (500 MHz, $CDCl_3$) 0.87 (12H, m), 1.19-1.39 (16H, m), 1.84 (2H, m, C(16,24)H), 3.94 (2H, m, C(15 or 23)H_2), 4.02 (2H, m, C(15 or 23)H_2), 7.23 (1H, d, *J*(Hz) 4.20, C(9)H), 7.28 (1H, m, C(13)H), 7.64 (1H, dd, *J*(Hz) 5.03, 1.16, C(12)H), 8.63 (1H, d, *J*(Hz) 4.19, C(8)H), 8.91 (1H, dd, *J*(Hz) 3.92, 1.17, C(14)H); δ_C (125 MHz, $CDCl_3$) 10.63 (C(22,30)H_3), 14.17 (C(20,28)H_3), 23.16 (C(19 or 27)H_2), 23.18 (C(19 or 27)H_2), 23.64 (C(21 or 29)H_2), 23.68 (C(21 or 29)H_2), 28.46 (C(18 or 26)H_2), 30.26 (C(18 or 26)H_2), 30.29 (C(17 or 25)H_2), 30.32 (C(17 or 25)H_2), 39.18 (C(16 or 24)H), 39.23 (C(16 or 24)H), 46.03 (C(15 or 23)H_2), 46.06 (C(15 or 23)H_2), 107.89 (C(3a or 6a)), 108.24 (C(3a or 6a)), 118.79 (C(10)Br), 128.55 (C(13)H), 129.86 (C(11)), 130.97 (C(12)H), 131.40 (C(9)H), 131.53 (C(7)), 135.21 (C(8)H), 135.64 (C(14)H), 138.97 (C(6)), 141.02 (C(3)), 161.61 (C(1 or 4)), 161.78 (C(1 or 4); *m/z* (ESI) 627.1504 $[M+Na]^+$ ($C_{30}H_{39}BrN_2NaO_2S_2$ requires 627.1514).

2,5-Bis(2-ethylhexyl)-2,5-dihydro-3,6-bis(5-bromo-2-thienyl)-Pyrrolo[3,4-*c*]pyrrole-1,4-dione: **68**[136]

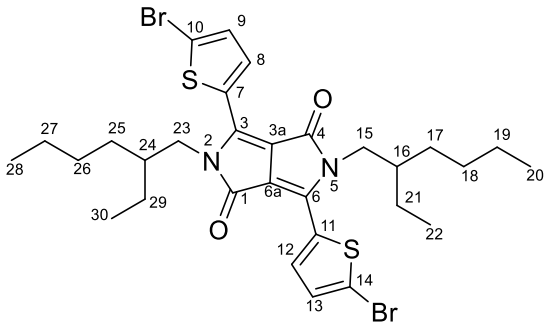

2,5-Bis(2-ethylhexyl)-3,6-di(thiophen-2-yl)pyrrolo[3,4-c]pyrrole-1,4(2H,5H)-dione (0.50 g, 0.95 mmol) was dissolved in $CHCl_3$ (30 ml). *N*-Bromosuccinimide (0.35 g, 1.95 mmol) was dissolved in $CHCl_3$ (15 ml) and added dropwise over 45 minutes to the mixture at 0 °C in the dark. The reaction was allowed to stir to completion as judged by TLC. The reaction was quenched with water and the organic layer was extracted using CH_2Cl_2 (30 ml). The organic layer was dried with $MgSO_4$ and filtered before removing the solvent under reduced pressure to afford the title compound in quantitative yield; δ_H (500 MHz, $CDCl_3$) 0.87 (12H, m), 1.17-1.39 (16H, m), 1.83 (2H, m, C(16,24)H)), 3.93 (4H, m, (C(15,23)H_2), 7.23 (2H, d, *J*(Hz) 3.93, C(8,12)H), 8.65 (2H, d, *J*(Hz) 4.01, C(9,13)H); δ_C (125 MHz, $CDCl_3$) 10.73 (C(22,30)H_3), 14.30 (C(20,28)H_3), 23.31 (C(19,27)H_2), 28.60 (C(21,29)H_2), 29.94 (C(18,26)H_2), 30.45 (C(17,25)H_2), 39.39 (C(16,24)H), 46.31 (C(15,23)H_2), 108.31 (C(3a,6a)), 119.30 (C(10,14)), 131.45 (C(8,12)H), 131.70 (C(7,11)), 135.62 (C(9,13)), 139.66 (C(3,6)), 161.65 (C(1,4)); *m/z* (EI^+) 680.10 $[M]^+$ ($C_{30}H_{38}Br_2N_2O_2S_2$ requires 680.07).

7,14-Di-2-thienyl-6*H*-Diindolo[3,2,1-*de*:3',2',1'-*ij*][1,5]naphthyridine-6,13-dione: **70**[128]

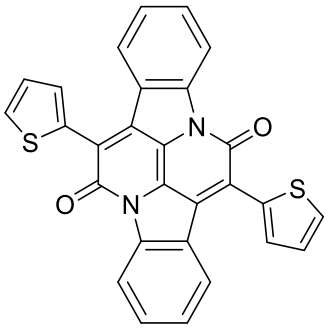

Indigo (2.00 g, 7.62 mmol) was added to mixed xylenes (100 ml) under an argon atmosphere and brought to reflux. 2-Thiopheneacetyl chloride (3.77 ml, 30.5 mmol) in xylenes (10 ml) was added to the mixture over 1 hour. The reaction was monitored by TLC until no semi-annulated product remained. The reaction was then allowed to cool to room temperature before being filtered and rinsed with THF to yield the product as a red solid (2.71 g, 75%); δ_H (400 MHz, $CHCl_3$) 7.14 (2H, t, *J*(Hz) 7.42), 7.58 (2H, t, *J*(Hz) 7.84), 7.72 (4H, dd, *J*(Hz) 16.71, 4.12), 8.17 (2H, d, *J*(Hz) 8.03), 8.56 (2H, d, *J*(Hz) 7.86; δ_C unavailable due to lack of solubility; *m/z* (ESI) 475.1525 $[M+H]^+$ ($C_{28}H_{15}N_2O_2S_2$ requires 475.0575).

7,14-bis(5-bromothiophen-2-yl)diindolo[3,2,1-de:3',2',1'-ij][1,5]naphthyridine-6,13-dione: **71**[128]

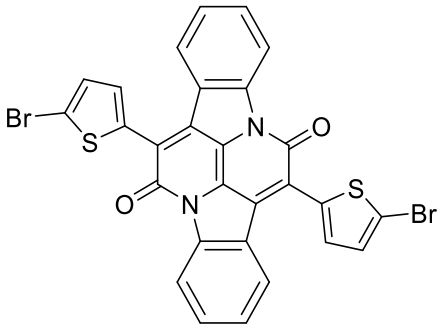

Compound **70** (2 g 4.22 mmol) was suspended in $CHCl_3$ (200 ml). *N*-Bromosuccinimide (1.57 g, 8.86 mmol, 2.1 eq.) was added in portions. The reaction was left to stir overnight before adding water (50 ml) to quench the reaction. The suspension was filtered and washed with water, acetone and $CHCl_3$ to give the product as a purple solid (2.05 g, 77%); δ_H (400 MHz, $CDCl_3$) 7.21 (2H, d, *J*(Hz) 4.0), 7.33 (2H, t, *J*(Hz) 7.3), 7.54 (2H, d, *J*(Hz) 4.0), 7.62 (2H, t, *J*(Hz) 7.8), 8.24 (2H, d, *J*(Hz) 7.7), 8.56 (2H, d, *J*(Hz) 8.0); δ_C unavailable due to lack of solubility; *m/z* (ESI) 632.92 $[M+H]^+$ ($C_{28}H_{13}Br_2N_2O_2S_2$ requires 632.88).

3-(5-(4,4,5,5-Tetramethyl-1,3,2-dioxaborolan-2-yl)-2-thienyl)-2,5-bis(2-ethylhexyl)-2,5-dihydro-6-(2-thienyl)-Pyrrolo[3,4-*c*]pyrrole-1,4-dione: **73**

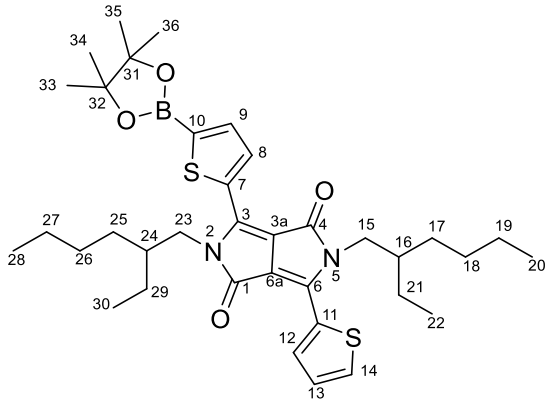

Compound **67** (0.50 g, 0.83 mmol), bis(pinacolato)diboron (0.320 g, 1.24 mmol) and potassium acetate (0.243 g, 2.48 mmol) were dissolved in anhydrous 1,4-dioxane (15 ml). The solution was degassed for 45 minutes before addition of [1,1'-bis(diphenylphosphino)ferrocene]dichloropalladium(II) (30 mg), and the reaction was heated at 90 °C overnight. The solvent was evaporated and the residue washed with petroleum ether, affording the product as a purple solid (0.450 g, 83%); δ_H (500 MHz, $CDCl_3$) 0.84-0.97 (12H, m), 1.27 (12H, s, C(33,34,35,36)$\underline{H}_3$), 1.28-1.32 (16H, m), 1.91 (2H, broad s, C(16,24)$\underline{H}$), 4.01-4.13 (4H, m, C(15,23)$\underline{H}_2$), 7.31 (1H, dd, *J*(Hz) 5.01, 3.92), 7.46 (1H, d, *J*(Hz) 4.19), 7.67 (1H, dd, *J*(Hz) 5.02, 1.14), 8.96 (1H, dd, *J*(Hz) 3.90, 1.13), 8.99 (1H, d, *J*(Hz) 4.22); compound **73** was used without further purification.

Tributylstannyl tetrathiafulvalene: **79**[137]

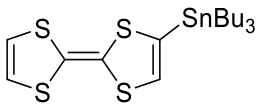

Tetrathiafulvalene (1.00 g, 4.89 mmol) was dissolved in diethyl ether (200 ml) and cooled to -78 °C. *n*-Butyllithium (4.20 ml, 1.26 M, 4.89 mmol) was added and the reaction was allowed to stir at -78 °C for 1 hour to allow the formation of the yellow tetrathiafulvalene anion. Tributyltin chloride (1.4 ml, 4.89 mmol) was added and the reaction was allowed to stir for a further 1 hour at -78 °C before being allowed to warm to room temperature. Water was added to quench the reaction (50 ml) and the organic layer was extracted using ethyl acetate. The organic layer was dried using $MgSO_4$, filtered and the solvent evaporated under vacuum to give the crude product as a brown oil which was used in the next step without further purification.

3,6-Bis(5-([2,2'-bi(1,3-dithiolylidene)]-4-yl)thiophen-2-yl)-2,5-bis(2-ethylhexyl)pyrrolo[3,4-c]pyrrole-1,4(2H,5H)-dione: **80**

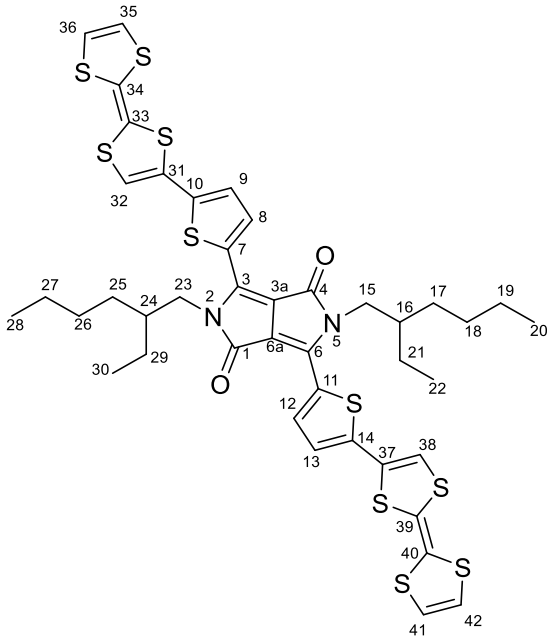

Compound **68** (0.10 g, 0.15 mmol) and compound **79** (0.29 g, 0.59 mmol) were dissolved in anhydrous toluene (15 ml) and the solution was degassed for 30 minutes before adding bis(triphenylphosphine)palladium(II) dichloride (20 mg). The reaction was heated at reflux for 24 hours. Water (20 ml) was added to quench the reaction and the organic layer was extracted using CH_2Cl_2 (30 ml). The organic layer was dried using $MgSO_4$, filtered and the solvent removed under reduced pressure. The residue was then absorbed onto silica, flushed with petroleum ether to remove residual TTF and recollected by dissolution in DCM, the solvent was removed to afford the product as a blue solid (0.10 g, 73%); δ_H (500 MHz,$CDCl_3$) 0.87 (12H, m) 1.24-1.38 (16H, m), 1.86 (2H, m, C(16, 24)H), 3.95-4.04 (4H, m, C(15,23)H_2), 6.34 (4H, s, C(35, 36, 41, 42)H), 6.64 (2H, s, C(32, 37)H), 7.11 (2H, d, *J*(Hz) 4.16, C(9,13)H), 8.85 (2H, d, *J*(Hz) 4.17, C(8,12)H); *m/z* (NSI) $[M+H]^+$ 929.0680 ($C_{42}H_{45}N_2O_2S_{10}$ requires 929.0683).

2,5-Bis(2-ethylhexyl)-2,5-dihydro-3,6-bis(5-ferrocene-2-thienyl)-Pyrrolo[3,4-*c*]pyrrole-1,4-dione: **85**

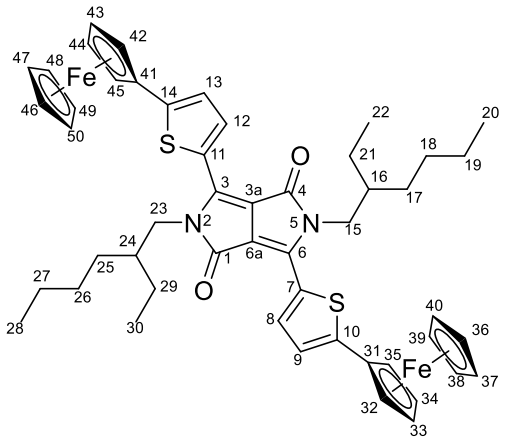

2,5-Bis(2-ethylhexyl)-2,5-dihydro-3,6-bis(5-bromo-2-thienyl)-Pyrrolo[3,4-*c*]pyrrole-1,4-dione (0.20 g, 0.29 mmol), ferroceneboronic acid (0.20 g, 0.88 mmol) and tribasic potassium phosphate (0.30 g, 1.5 mmol) were dissolved in anhydrous toluene (6 ml) and water (1 ml). The solution was degassed for 30 minutes before adding tris(dibenzylideneacetone)dipalladium(0) (8 mg) and Xphos (8 mg). The reaction was heated to 80 °C and stirred until completion. Water was added to the reaction then the organic layer was extracted using ethyl acetate and dried using $MgSO_4$. After filtering off the drying agent the solvents were removed under reduced pressure. The crude product was then purified by column chromatography (CH_2Cl_2:Petroleum Ether, 1:1) to yield the product as a dark blue solid (0.105 g, 40%); δ_H (500 MHz,$CDCl_3$) 0.86-0.97 (12H, m), 134-1.46 (16H, m), 1.91-1.99 (2H, m, C(16,24)H), 4.07 (4H, m, C(15,23)H_2), 4.12 (10H, s, C(36,37,38,39,40,46,47,48,49,50)H), 4.42 (2H, s, C(32,35,42,45)H), 4.69 (2H, s, C(33,34,43,44)H), 7.14 (2H, d, *J*(Hz) 4.05, C(8,12)H), 8.90 (2H, d, *J*(Hz) 4.05, C(9,13)H); δ_C (125 MHz, $CDCl_3$) 10.77 (C(20,28)H_3), 14.30 (C(22,30)H_3), 23.33 (C(19,27)H_2), 23.79 (C(21,29)H_2), 28.69 (C(18,26)H_2), 30.49 (C(17,25)H_2), 39.45 (C(16,24)H), 46.04 (C(15,23)H_2), 67.52 (C(33,34,43,44)H), 70.04 (C(32,35,42,45)H), 70.62 (C(36,37,38,39,40,46,47,48,49,50)H), 78.34 (C(31,41)) 107.73 (C(3a,6a)), 123.70 (C(8,12)H), 127.22 (C(7,11)), 136.73 (C(9,13)H), 139.59 (C(3,6)), 150.62 (C(10,14)), 161.96 (C(1,4)); *m/z* (NSI) 893.2551 $[M+H]^+$ ($C_{50}H_{57}Fe_2N_2O_2S_2$ requires 893.2557).

4-(5-(2,5-Bis(2-ethylhexyl)-3,6-dioxo-4-(thiophen-2-yl)-2,3,5,6-tetrahydropyrrolo[3,4-c]pyrrol-1-yl)thiophen-2-yl)benzaldehyde: **87**[138]

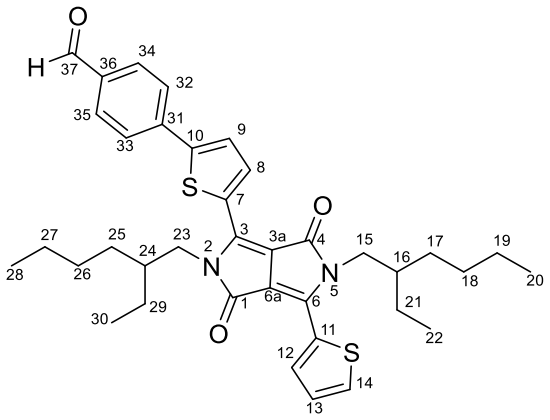

3-(5-Bromo-2-thienyl)-2,5-bis(2-ethylhexyl)-2,5-dihydro-6-(2-thienyl)-Pyrrolo[3,4-*c*]pyrrole-1,4-dione (0.50 g, 0.83 mmol), K_3PO_4 (0.530 g, 2.48 mmol) and 4-formylphenylboronic acid (0.190 g, 1.24 mmol) were dissolved in anhydrous toluene (15 ml) and water (1ml). The solution was degassed for 45 minutes before adding X-Phos (5%mol) and tris(dibenzylideneacetone)dipalladium(0) (5%mol). The reaction was heated to 80 °C and stirred to completion. The reaction was quenched with water (20 ml) and the organic layer was extracted using ethyl acetate (30 ml). The organic layer was dried using $MgSO_4$ and filtered before the solvent was evaporated under reduced pressure. The residue was purified by column chromatography (PE:DCM, 1:5) to give the product as a purple solid (0.367 g, 70%); δ_H (500 MHz, $CDCl_3$) 0.82-0.94 (12H, m), 1.19-1.42 (16H, m), 1.89 (2H, m, C(16,24)H), 4.06 (4H, m, C(15,23)H_2), 7.28 (1H, dd, *J*(Hz) 5.03, 3.93, C(13)H), 7.60 (1H, d, *J*(Hz) 4.17 C(8)H), 7.65 (1H, dd, *J*(Hz) 5.02, 1.17, C(12)H), 7.83 (2H, d, *J*(Hz) 8.26, C(34,35)H), 7.94 (2H, d, *J*(Hz) 8.58, C(32,33)H), 8.90 (2H, m C(9,14)H), 10.04 (1H, s, C(37)HO); δ_C (125 MHz, $CDCl_3$) 10.73 (C(22 or 30)H_3), 10.81 (C(22 or 30)H_3), 14.27 (C(20 or 28)H_3), 14.33 (C(20 or 28)H_3), 23.31 (C(19 or 27)H_2), 23.34 (C(19 or 27)H_2), 23.77 (C(21 or 29)H_2), 23.93 (C(21 or 29)H_2), 28.58 (C(18 or 26)H_2), 28.83 (C(18 or 26)H_2), 30.43 (C(17 or 25)H_2), 30.58 (C(17 or 25)H_2), 39.32 (C(16 or 24)H), 39.54 (C(16 or 24)H), 46.18 (C(15 or 23)H_2), 53.67 (C(15 or 23)H_2), 108.28 (C(3a or 6a)), 109.01 (C(3a or 6a)), 126.4 (C(8)), 126.58 (C(34,35)), 128.77 (C(13)), 130.00 (C(7, 11, or 36)), 130.81 (C(32,33)H), 130.90 (C(12)H), 131.15 (C(7, 11, 31 or 36)), 135.90 (C(9 or 14)H), 136.15 (C(7, 11, 31 or 36)), 136.68 (C(9 or 14)), 138.95 (C(7, 11, or 31)), 139.63 (C(10)), 141.10 (C(3 or 6)), 147.43 (C(3 or 6)), 161.88 (C(1 or 4), 161.97 (C(1 or 4), 191.46 (C(37)HO); *m/z* (ESI) 651.2914 $[M+Na]^+$ ($C_{37}H_{44}N_2NaO_3S_2$ requires 651.2691).

4-(5-(4-(5-Bromothiophen-2-yl)-2,5-bis(2-ethylhexyl)-3,6-dioxo-2,3,5,6-tetrahydropyrrolo[3,4-c]pyrrol-1-yl)thiophen-2-yl)benzaldehyde: **88**[138]

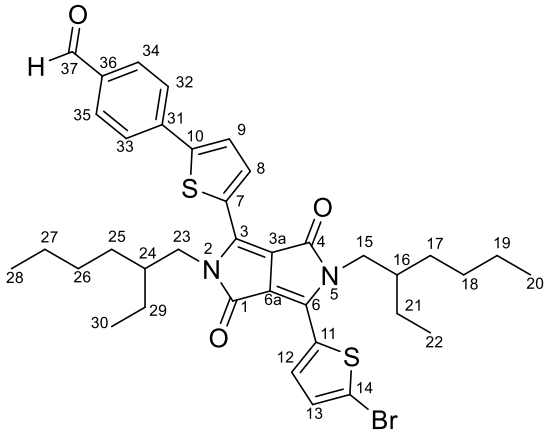

Compound **87** (0.20 g, 0.32 mmol) was dissolved in $CHCl_3$ (15 ml), the mixture was cooled to 0 °C in the dark before adding *N*-bromosuccinimide (0.068 g, 0.38 mmol). The reaction was stirred until completion as judged by TLC. The reaction was quenched with water and the organic layer extracted using $CHCl_2$ (20 ml), the organic layer was washed with water (30 ml) three times before being dried with $MgSO_4$. The organic layer was then filtered and the solvent removed under vacuum to afford the product as a purple solid (0.220g, 98%); δ_H (500 MHz, $CDCl_3$) 0.83-0.94 (12H, m), 1.20-1.43 (16H, m), 1.83-1.93 (2H, broad d, C(16,24)H), 3.95 (2H, m, C(15 or 23)H_2), 4.05 (2H, m, C(15 or 23)H_2), 7.23 (1H, d, *J*(Hz) 4.18, C(8 or 12)H), 7.59 (1H, d, *J*(Hz) 4.17, C(8 or 12)H), 7.83 (2H, d, *J*(Hz) 8.27, C(32,33)H), 7.93 (2H, d, *J*(Hz) 8.51, C(34,35)H), 8.68 (1H, d, *J*(Hz) 4.19, C(9 or 13)H), 8.94 (1H, d, *J*(Hz) 4.16, C(9 or 13)H), 10.04 (1H, s, C(37)HO); δ_C (125 MHz, $CDCl_3$) 10.73 (C(22 or 30)H_3), 10.80 (C(22 or 30)H_3), 14.28 (C(20 or 28)H_3), 14.33 (C(20 or 28)H_3), 23.29 (C(19 or 27)H_2), 23.34 (C(19 or 27)H_2), 23.82 (C(21 or 29)H_2), 23.92 (C(21 or 29)H_2), 28.57 (C(18 or 26)H_2), 28.82 (C(18 or 26)H_2), 30.41 (C(17 or 25)H_2), 30.59 (C(17 or 25)H_2), 39.37 (C(16 or 24)H), 39.54 (C(16 or 24)H), 46.26 (C(15 or 23)H_2), 53.67 (C(15 or 23)H_2), 108.50 (C(3a or 6a)), 108.88 (C(3a or 6a)), 119.35 (C(14)), 126.46 (C(8 or 12)H), 126.62 (C(32,33)H, 130.77 (C(3, 6, 7, 10, 11, 31 or 36)), 130.84 (C(34,35)H), 131.42 (C(8 or 12)), 131.74 (C(3, 6, 7, 10, 11, 31 or 36)), 135.72 (C(9 or 13)H), 136.22 (C(3, 6, 7, 10, 11, 31 or 36)), 136. 95 (C(9 or 13)H), 138.89 (C(3, 6, 7, 10, 11, 31 or 36)), 139.62 (C(3, 6, 7, 10, 11, 31 or 36)), 140.10 (C(3, 6, 7, 10, 11, 31 or 36)), 147.76 (C(3, 6, 7, 10, 11, 31 or 36)), 161.73 (C(3 or 6)), 161.81 (C(3 or 6)), 191.47 (C(37)HO); *m/z* (ESI) 729.1776 $[M+Na]^+$ ($C_{37}H_{43}BrN_2NaO_3S_2$ requires 729.1796).

4-(5-(4-(5-((4-(Dimethylamino)phenyl)ethynyl)thiophen-2-yl)-2,5-*bis*(2-ethylhexyl)-3,6-dioxo-2,3,5,6-tetrahydropyrrolo[3,4-c]pyrrol-1-yl)thiophen-2-yl)benzaldehyde **89**.

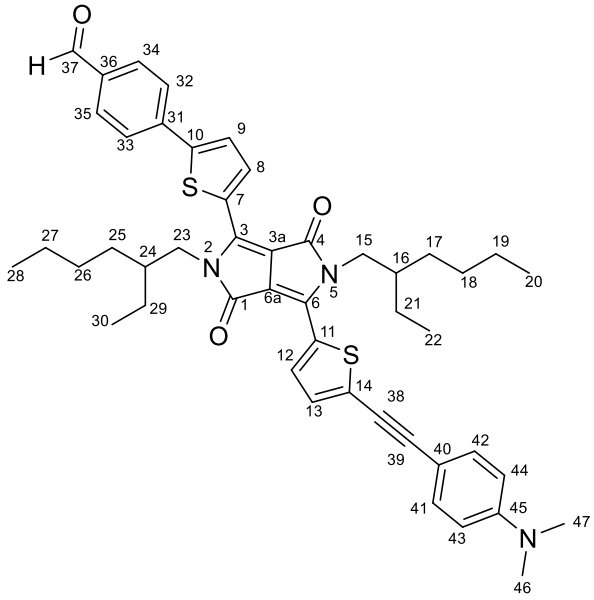

Compound **88** (200 mg, 0.28 mmol) and 4-ethynyl-*N*,*N'*-dimethylaniline (50 mg, 0.34 mmol) were dissolved in dry-THF (8 ml) and dry-TEA (8 ml) under an Ar atmosphere. The solution was degassed with Ar for 20 minutes. $Pd(PPh_3)_2Cl_2$ (6 mg, 3% mmol), and CuI (1.6 mg, 3% mmol) were then added to the mixture and the solution was stirred at room temperature overnight. The reaction was then diluted with CH_2Cl_2 (50 ml) and washed with brine (3 × 50 ml). The organic extract was dried over $MgSO_4$, filtered, and the solvent removed under reduced pressure. The crude product was purified by column chromatography (P.E.:DCM, 1:1) to yield the product as a blue solid (180 mg, 83%); M.p. 230-231 °C; ^{1}H NMR (500 MHz, $CDCl_3$) δ = 0.89 (12H, m, C(20, 22, 28, 30)H), 1.20-1.46 (16H, m, C(17, 18, 19, 21, 25, 26, 27, 29)H), 1.83-1.99 (2H, m, C(16, 24)H), 3.01 (6H, s, C(46, 47)H_3), 3.95-4.15 (4H, m, C(15, 23)H_2), 6.66 (2H, d, J(Hz) 8.9, C(43, 44)H), 7.31 (1H, d, *J*(Hz) 4.1, C(13)H), 7.41 (2H, d, *J*(Hz) 8.9, C(41, 42)H), 7.59 (1H, d, *J*(Hz) 4.1, C(9)H), 7.82 (2H, d, *J*(Hz) 8.0, C(32, 33)H), 7.93 (2H, d, *J*(Hz) 8.0, C(34, 35)H), 8.93 (1H, d, J(Hz) 4.2, C(8)H), 8.97 (1H, d, J(Hz) 4.2, C(12)H), 10.03 (1H, s, C(37)H); ^{13}C NMR (125 MHz, $CDCl_3$) δ = 10.6, 10.6 C(22, 30), 14.0 C(20, 28), 23.1, 23.6, 23.7 C(18, 19, 26, 27), 28.3, 28.6, 30.2, 30.4 C(17, 21, 25, 29), 39.1, 39.3 C(16, 24), 40.1 C(46, 47), 46.0, 46.2 C(15, 23), 80.9 C(38), 100.2 C(39), 108.3, 108.6 C(3a, 6a), 111.7 C(43, 44), 126.1 C(9), 126.3 C(32, 33), 130.5 C(34, 45), 131.8 C(13), 132.9 C(41, 42), 136.2 C(12), 136.4 C(8), 109.0, 129.3, 130.7, 135.9, 138.7, 138.8, 140.2, 147.0, 150.6 C(3, 6, 7, 10, 11, 14, 31, 36, 40, 45), 161.4, 161.7, C(17, 20), 191.2 C(42); *m/z* (ESI^+) 772.3606 [$M+H^+$] ($C_{47}H_{54}N_3O_3S_2$ requires 772.3601)

3-[4-[5-[4-[5-[2-[4-(Dimethylamino)phenyl]-ethynyl]-2-thienyl]-2,5-bis(2-ethylhexyl)-2,3,5,6-tetrahydro-3,6-dioxopyrrolo[3,4-c]pyrrol-1-yl]-2-thienyl]phenyl]-2-cyano-2-propenoic acid: **90**

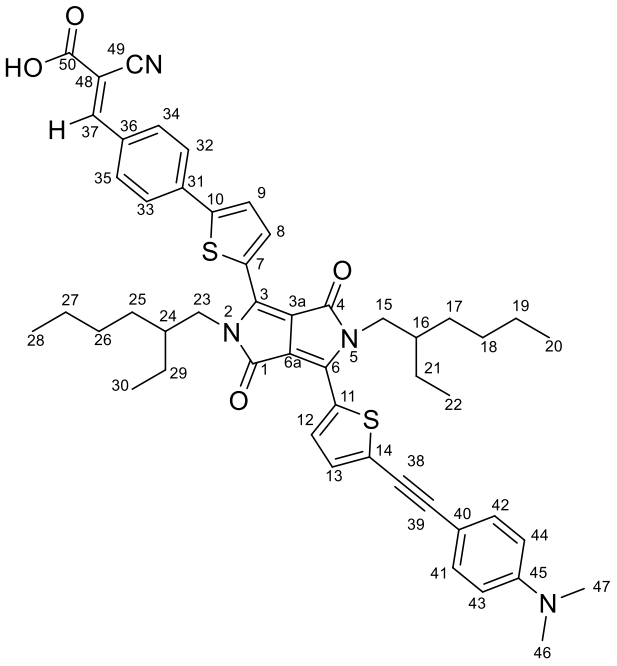

Compound **89** (80 mg, 0.10 mmol), $MgSO_4$ (10 mg, 0.042 mmol) and cyanoacetic acid (110 mg, 0.12 mmol) were dissolved in anhydrous toluene (20 ml). Acetic acid (0.05 ml) and piperidine (2 drops) were then added to the reaction. The reaction was heated to 80 °C overnight. The reaction was quenched with water (20 ml) and the organic layer was extracted using CH_2Cl_2, dried using $MgSO_4$ and filtered. The solvent was then evaporated under vacuum and the residue purified by column chromatography (1:2:97, acetic acid:methanol:CH_2Cl_2) to afford the product as a blue solid (50 mg, 57%); a good quality NMR of **90** was unobtainable due to lack of solubility of the molecule in deuterated solvents; *m/z* (ESI) 838.3585 $[M]^+$ ($C_{50}H_{54}N_4O_4S_2$ requires 838.3586).

References

1. IEA, *Energy Technology Perspectives (ETP)*, OECD/IEA, Paris, 2014
2. N. Lewis and D. Nocera, *Proc. Natl. Acad. Sci.*, 2006, **103**, 15729
3. EIA, *Annual Energy Outlook 2014*
4. http://www.nrel.gov/ncpv/ [Accessed 20/04/2015]
5. F. Dimroth, M. Grave, P. Beutel, U.Fiedeler, C. Karcher, T. Tibbits, E. Oliva, G. Siefer, M. Schachtner, A. Wekkeli, A. Bett, R. Krause, M. Piccin, N. Blanc, C. Drazek, E. Guiot, B. Ghyselen, T. Salvetat, A. Tauzin, T. Signamarcheix, A. Dobrich, T. Hannappel and K. Schwarzburg, *Prog. Photovolt: Res. Appl.*, 2014, **22**, 277
6. IEA, *Technology Roadmap Solar Photovoltaic Energy*, OECD/IEA, Paris, 2014
7. G. Carr, *The Economist*, 2012
8. D. Kearns and M. Calvin, *J. Chem. Phys.*, 1958, **29**, 950
9. C. Brabec, N. Sariciftci and J. Hummelen, *Adv. Funct. Mater.*, 2001, **11**, 15
10. C. Tang, *Appl. Phys. Lett.*, 1986, **48**, 183
11. F. Padinger, R.Rittberger and N. Sariciftci, *Adv. Funct. Mater.*, 2003, **13**, 85
12. T. Umeyama and H. Imahori, *J. Mater. Chem. A*, 2014, **2**, 11545
13. J. Choi, M. Jin, C. An, D. Kim and H. Jung, *Appl. Mater. Interfaces*, 2014, **6**, 11047
14. Y. Sun, C. Takacs, S. Cowan, J. Seo, X. Gong, A. Roy and A. Heeger, *Adv. Mater.*, 2011, **23**, 2226
15. C. Chu, V. Shrotriya, G. Li and Y. Yang, *Appl. Phys. Lett.*, 2006, **88**, 153504
16. M. Scharber, D. Mühlbacher, M. Koppe, P. Denk, C. Waldauf, A. Heeger and C.Brabec, *Adv. Mater.*, 2006, **18**, 789
17. G. Wang, T. Hirasa, D. Moses and A. Heeger, *Synth. Met.*, 2004, **146**, 127
18. H. Heil, T. Finnberg, N. von Malm, R. Schmechel and H. von Seggern, *J.Appl. Phys.*, 2003, **93**, 1636
19. Z. Bao, A. Dodabalapur and A. Lovinger, *Appl. Phys. Lett.*, 1996, **69**, 4108
20. M. Surin, P. Leclère, R. Lazzaroni, J. Yuen, G. Wang, D. Moses, A. Heeger, S.Cho and K. Lee, *J. Appl. Phys.*, 2006, **100**, 033712
21. H. Chen, W. Lin and F. Wu, *Appl. Phys. Lett.*, 2009, **94**, 223302
22. A. Moulé and K. Meerholz, *Adv. Mater.*, 2008, **20**, 240
23. J. Peet, J. Kim, N. Coates, W. Ma, D. Moses, A. Heegar and G. Bazan, *Nature Mater.*, 2007, **6**, 497
24. T. Erb, U. Zhokhavets, G. Gobsch, S. Raleva, B. Stühn, P. Schilinsky, C. Waldauf and C.Brabec, *Adv. Funct. Mater.*, 2005, **15**, 1193

25. A. Heeger, *Adv. Mater.*, 2014, **26**, 10
26. S. Cowan, A. Roy and A. Heeger, *Phys. Rev. B*, 2010, **82**, 245207
27. S. Cowan, R. Street, S. Cho and A. Heeger, *Phys. Rev. B*, 2011, **83**, 035205
28. C. Brabec, S. Gowrisanker, J. Halls, D. Laird, S. Jia and S. Williams, *Adv. Mater.*, 2010, **22**, 3839
29. Y. He and Y. Li, *Phys. Chem. Chem. Phys.*, 2011, **13**, 1970
30. J. Delgado, P. Bouit, S. Filippone, M. Herranz and N. Martin, *Chem. Commun.*, 2010, **46**, 4853
31. M. Wienk, J. Kroon, W. Verhees, J. Knol, J. Hummelen, P. van Hal and R. Janssen, *Angew. Chem. Int. Ed.*, 2003, **42**, 3371
32. S. Park, A. Roy, S. Beaupŕe, S. Cho, N. Coates, J. Moon, D. Moses, M. Leclerc, K. Lee and A. Heeger, *Nature Photon.*, 2009, **3**, 297
33. Y. Zhong, M. Trinh, R. Chen, W. Wang, P. Khlyabich, B. Kumar, Q. Xu, C. Nam, M. Sfeir, C. Black, M. Steigerwald, Y. Loo, S. Xiao, F. Ng, X. Zhu and C. Nuckolls, *J. Am. Chem. Soc.*, 2014, **136**, 15215
34. Y. Zang, C. Li, C. Chueh, S. Williams, W. Jiang, Z. Wang, J. Yu and A. Jen, *Adv. Mater.*, 2014, **26**, 5708
35. H. Xu, X. Jiang, E. Chan, W. Fong and D. Ng, *Org. Biomol. Chem.*, 2007, **5**, 3987
36. K. Cnops, B. Rand, D. Cheyns, B. Verreet, M. Empl and P. Heremans, *Nature Commun.*, 2014, **5**, 3406
37. J. Kim, S. Kim, S. Kim, H. Lee, K. Lee, W. Ma, X. Gong and A. Heeger, *Adv. Mater.*, 2006, **18**, 572
38. J. Kim, Y. Qin, D. Stevens, V. Kalihari, M. Hillmyer and C. Frisbie, *J. Phys. Chem. C*, 2009, **113**, 21928
39. T. Umeyama, K. Hirose, K.Noda, K. Matsushige, T. Shishido, H. Saarenpää, N. Tkachenko, H. Lemmetyinen, N. Ono and H. Imahori, *J. Phys. Chem. C*, 2012, **116**, 17414
40. M. Raj, S. Anandan, *RSC Advances*, 2013, **3**, 14595
41. J. Douglas, G. Griffini, T. Holcombe, E. Young, O. Lee, M. Chen and J. Fréchet, *Macromolecules*, 2012, **45**, 4069
42. W. Braunecker, Z. Owczarczyk, A. Garcia, N. Kopidakis, R. Larsen, S. Hammond, D. Ginley and D. Olsen, *Chem. Mater.*, 2012, **24**, 1346
43. Y. Wu, Y. Jing, X. Guo, S. Zhang, M. Zhang, L. Huo and J. Hou, *Polym. Chem.*, 2013, **4**, 536
44. T. Umeyama, Y. Watanabe, M. Oodoi, D. Evgenia, T. Shishido and H. Imahori, *J. Mater. Chem.*, 2012, **22**, 24394
45. Y. Liang, D. Feng, Y. Wu, S. Tsai, G. Li, C. Ray and L. Yu, *J. Am. Chem. Soc.*, 2009, **131**, 7792
46. S. Woo, W. Kim, H. Kim, Y. Yi, H. Lyu and Y. Kim, *Adv. Energy Mater.*, 2014, **4**, 1301692

47. Z. He, C. Zhong, S. Su, M. Xu, H. Wu and Y. Cao, *Nat. Photon.*, 2012, **6**, 591
48. S. Liu, K. Zhang, J. Lu, J. Zhang, H. Yip, F. Huang and Y. Cao, *J. Am. Chem. Soc*., 2013, **135**, 15326
49. B. Lee, E. Jung, Y. Nam, M. Jung, J. Park, S. Lee, H. Choi, S. Ko, N. Shin, Y. Kim, S. Kim, J. Kim, H. Shin, S. Cho and M. Song, *Adv. Mater.*, 2014, **26**, 494
50. J. Chen, C. Cui, Y. Li, L. Zhou, Q. Ou, C. Li, Y. Li and J. Tang, *Adv. Mater.*, 2015, **27**, 1035
51. S. Liao, H. Jhuo, P. Yeh, Y. Cheng, Y. Li, Y. Lee, S. Sharma and S. Chen, *Sci. Rep.*, 2014, **4**, 6813
52. Y. Chao, J. Jheng, J. Wu, K. Wu, H. Peng, M. Tsai, C. Wang, Y. Hsiao, C. Wang, C. Lin and C. Hsu, *Adv. Mater.*, 2014, **26**, 5205
53. R. Bettignies, Y. Nicolas, P. Blanchard, E. Levillain, J. Nunzi and J. Roncali, *Adv. Mater.*, 2003, **15**, 1939
54. T. Noda, H. Ogawa, N. Noma and Y. Shirota, *Adv. Mater.*, 1997, **9**, 720
55. J. Sakai, T. Taima and K. Saito, *Org. Elect.*, 2008, **9**, 582
56. N. Camaioni, G. Ridolfi, V. Fattori, L. Favaretto, and G. Barbarella, *Appl. Phys. Lett.*, 2004, **84**, 1901
57. L. Guan, J. Wang, J. Huang, C. Jiang, M. La, P. Liu and W. Deng, *Synth. Commun.*, 2011, **41**, 3662
58. R. Fitzner, E. Osteritz, A. Mishra, G. Schulz, E.Reinold, M. Weil, C.Körner, H. Ziehlke, C. Elschner, K. Leo, M. Riede, M.Pfeiffer, C. Uhrich and P. Bäuerle, *J. Am. Chem. Soc.*, 2012, **134**, 11064
59. J. Zhou, Y. Zuo, X. Wan, G. Long, Q. Zhang, W. Ni, Y. Liu, Z. Li, G. He, C. Li, B. Kan, M. Li and Y. Chen, *J. Am. Chem. Soc.*, 2013, **135**, 8484
60. Y. Liu, C. Chen, Z. Hong, J. Gao, Y. (Michael) Yang, H. Zhou, L. Dou, G. Li and Y. Yang, *Scientific Reports*, 2013, **3**, 3356
61. S. Yoo, B. Domercq and B. Kippelen, *Appl. Phys. Lett.*, 2004, **85**, 5427
62. A. Pandey and J. Nunzi, *Adv. Mater.*, 2007, **19**, 3613-3617
63. D.Keil, H. Hartmann and T. Moschny, *Dyes and Pigments*, 1991, **17**, 19
64. G. Wei, S. Wang, K. Sun, M. Thompson and S. Forrest, *Adv. Energy Mater.*, 2011, **1**, 184
65. Y. Chen, L. Lin, C. Lu, F. Lin, Z. Huang, H. Lin, P. Wang, Y. Liu, K. Wong, J. Wen, D. Miller and S. Darling, *J. Am. Chem. Soc.*, 2012, **134**, 13616
66. S. Marder and J. Perry, *Adv. Mater.*, 1993, **5**, 804
67. V. Steinmann, N. Kronenberg, M. Lenze, S. Graf, D. Hertel, K. Meerholz, H. Bürckstümmer, E. Tulyakova and F. Würthner, *Adv. Energy Mater.*, 2011, **1**, 888
68. S. Chiu, L. Lin, H. Lin, Y. Chen, Z. Huang, Y. Lin, F. Lin, Y. Liu and K. Wong, *Chem. Commun.*,

2012, **48**, 1857

69. P. Sullivan, A. Duraud, l. Hancox, N. Beaumont, G. Mirri, J. Tucker, R. Hatton, M. Shipman and T. Jones, *Adv. Energy Mater.*, 2011, **1**, 352
70. B. Verreet, K. Cnops, D. Cheyns, P. Heremans, A. Stesmans, G. Zango, C. Claessens, T. Torres and B. Rand, *Advanced Energy Materials*, 2014, **4**, 1301413
71. T. Tanaka and A. Osuka, *Chem. Soc. Rev.*, 2015, **46**, 943
72. H. Qin, L. Li, F. Guo, S. Su, J. Peng, Y. Cao and X. Peng, *Energy Environ. Sci.*, 2014, **7**, 1397.
73. O. Adebanjo, B. Vaagensmith and Q. Qiao, *J. Mater. Chem. A,* 2014, **2**, 10331
74. A. Yakimov and S. Forrest, *Appl. Phys. Lett.,* 2002, **80**, 1667
75. A. De Vos, *J. Phys. D: Appl. Phys,* 1980, **13**, 839
76. J. You, L.Dou, K. Yoshimura, T.Kato, K. Ohya, T. Moriarty, K.Emery, C. Chen, J. Gao, G. Li and Y. Yang, *Nature Commun.,* 2012, **41**, 1446
77. C. Chen, W. Chang, K. Yoshimura, K. Ohya, J. You, J. Gao, Z. Hong and Y. Yang, *Adv. Mater,* 2014, **26**, 5670
78. B. O'Regan and M. Grätzel, *Nature*, 1991, **353**, 737
79. M. Grätzel, *Prog. Photovolt. Res. Appl.*, 2000, **8**, 171
80. M. Grätzel, *Acc. Chem. Res.*, 2009, **42**, 1788
81. J. Wu, Z. Lan, S. Hao, P. Li, J. Lin, M. Huang, L. Fang and Y. Huang, *Pure Appl. Chem.*, 2008, **80**, 2241
82. S. Thomas, T. Deepak, G. Anjusree, T. Arun, S. Nair and A. Nair, *J. Mater. Chem. A*, 2014, **2**, 4474
83. G. Wang, S. Zhuo and W. Xing, *Materials Letters*, 2012, **69**, 27
84. J. Trancik, S. Barton and J. Hone, *Nano Letters*, 2008**, 8**, 982
85. M. Wu, X. Lin, Y. Wang, L. Wang, W. Guo, D. Qi, X. Peng, A. Hagfeldt, M. Grätzel and T. Ma, *J. Am. Chem. Soc.*, 2012, **134**, 3419
86. B. Hardin, H. Snaith and M. McGehee, *Nature Photon.*, 2012, **6**, 162
87. D. Hagberg, J. Yum, H. Lee, F. De Angelis, T. Marinado, K. Karlsson, R. Humphry-Baker, L. Sun, A. Hagfeldt, M. Grätzel and M. Nazeeruddin, *J. Am. Chem. Soc.*, 2008, **130**, 6259
88. J. Yin, M. Velayudham, D. Bhattacharya, H. Lin and K. Lu, *Coord. Chem. Rev.*, 2012, **256**, 3008
89. P. Péchy, T. Renouard, S. Zakeeruddin, R. Humphry-Baker, P. Comte, P. Liska, L. Cevey, E. Costa, V. Shklover, L. Spiccia, G. Deacon, C. Bignozzi and M. Grätzel, *J. Am. Chem. Soc.*, 2001, **123**, 1613
90. C. Chen, M. Wang, J. Li, N. Pootrakulchote, L. Alibabaei, C. Ngoc-le, J. Decoppet, J. Tsai, C. Grätzel, C. Wu, S. Zakeeruddin and M. Grätzel, *ACS Nano*, 2009, **3**, 3103

91. Z. Wang, Y. Cui, Y. Dan-oh, C. Kasada, A. Shinpo and K. Hara, *J. Phys. Chem. C*, 2007, **111**, 7224
92. K. Hara, M. Kurashige, S. Ito, A. Shinpo, S. Suga, K. Sayama and H. Arakawa, *Chem. Commun.*, 2002, 252
93. N. Koumura, Z. Wang, S. Mori, M. Miyashita, E. Suzuki and K. Hara, *J. Am. Chem. Soc.*, 2006, **128**, 14256
94. H. Choi, C. Baik, S. Kang, J. Ko, M. Kang, M. Nazeeruddin and M. Grätzel, *Angew. Chem.*, 2009, **121**, 1739
95. W. Liu, I. Wu, C. Lai, C. Lai, P. Chou, Y. Li, C. Chen, Y. Hsu and Y. Chi, *Chem. Commun.*, 2008, 5152
96. S. Hwang, J. Lee, C. Park, H. Lee, C. Kim, C. Park, M. Lee, W. Lee, J. Park, K. Kim, N. Park and C. Kim, *Chem. Commun.*, 2007, 4887.
97. S. Holliday, R. Ashraf, C. Nielsen, M. Kirkus, J. Röhr, C. Tan, E. Collado-Fregoso, A. Knall, J. Durrant, J. Nelson and I. McCulloch, *J. Am. Chem. Soc.*, 2015, **137**, 898
98. S. Ito, H. Miura, S. Uchida, M. Takata, K. Sumioka, P. Liska, P. Comte, P. Pãchy and M. Grätzel, *Chem. Commun.*, 2008, 5194
99. D. Joly, L. Pellejà , S. Narbey, F. Oswald, J. Chiron, J. Clifford, E. Palomares and R. Demadrille, *Sci. Rep.*, 2014, **4**, 4033
100. A. Yella, H. Lee, H. Tsao, C. Yi, A. Chandiran, M. Nazeeruddin, E. Diau, C. Yeh, S. Zakeeruddin and M. Gratzel, *Science*, 2011, **334**, 629
101. S. Mathew, A. Yella, P. Gao, R. Humphry-Baker, B. Curchod, N. Ashari-Astani, I. Tavernelli, U. Rothlisberger, M. Nazeeruddin and M. Grätzel, *Nature Chem.*, 2014, **6**, 242
102. S. Huang, G. Schlichthörl, A. Nozik, M. Grätzel and A. Frank, *J. Phys. Chem. B*, 1997, **101**, 2576
103. Z. Wang, K. Sayama and H. Sugihara, *J. Phys. Chem. B*, 2005, **109**, 22449
104. F. Pichot and B. Gregg, *J. Phys. Chem. B*, 2000, **104**, 6
105. T. Daeneke, T. Kwon, A. Holmes, N. Duffy, U. Bach and L. Spiccia, *Nature Chem.*, 2011**, 3**, 213
106. S. Feldt, E. Gibson, E. Gabrielsson, L. Sun, G. Boschloo and A. Hagfeldt, *J. Am. Chem. Soc.*, 2010, **132**, 16714
107. J. Yum, E. Baranoff, F. Kessler, T. Moehl, S. Ahmad, T. Bessho, A. Marchioro, E. Ghadiri, J. Moser, C. Yi, M. Nazeeruddin and M. Grätzel, *Nature Commun.*, 2012, **3**, 631
108. P. Docampo, S. Guldin, T. Leijtens, N. Noel, U. Steiner and H. Snaith, *Adv. Mater.*, 2014, **26**, 4013
109. H. Snaith and L. Schmidt-Mende, *Adv. Mater.*, 2007, **19**, 3187
110. J. Burschka, A. Dualeh, F. Kessler, E. Baranoff, N. Cevey-Ha, C. Yi, M. Nazeeruddin and M. Grätzel, *J. Am. Chem. Soc.*, 2011, **133**, 18042

111. I. Chung, B. Lee, J. He, R. Chang and M. Kanatzidis, *Nature*, 2012, **485**, 486

112. D. Farnum, G. Mehta, G. Moore and F. Siegal, *Tetrahedron Letters*, 1974, **15**, 2549

113. E. Faulkner and R. Schwartz, *High performance pigments*, Wiley-VCH, Weinheim, 2009

114. A. Iqbal, R. Kirchmayr, J. Pfenninger, A. Rochat and O. Wallquist, *Bull. Soc. Chim. Belg*, 1988, **97**, 615

115. F. Closs and R. Gompper, *Angew. Chem.*, 1987, **99**, 566

116. B. Zhao, K. Sun, F. Xue and J. Ouyang, *Org. Elect.*, 2012, **13**, 2516

117. S. Qu and H. Tian, *Chem. Commun.*, 2012, **48**, 3039

118. J. Bijleveld, A. Zoombelt, S. Mathijssen, M. Wienk, M. Turbiez, D. de Leeuw and R. Janssen, *J. Am. Chem. Soc.*, 2009, **131**, 16616

119. J. Bijleveld, V. Gevaerts, D. Di Nuzzo, M. Turbiez, S. Mathijssen, D. de Leeuw, M. Wienk and R. Janssen, *Adv. Mater.*, 2010, **22**, E242

120. K. Hendriks, G. Heintges, V. Gevaerts, M. Wienk and R. Janssen, *Angew. Chem.*, 2013, **125**, 8499

121. S. Loser, C. Bruns, H. Miyauchi, R. Ortiz, A. Facchetti, S. Stupp and T. Marks, *MRS Proc.*, 2012, 1390

122. J. Huang, C. Zhan, X. Zhang, Y. Zhao, Z. Lu, H. Jia, B. Jiang, J. Ye, S. Zhang, A. Tang, Y. Liu, Q. Pei and J. Yao, *ACS Appl. Mater. Interfaces*, 2013, **5**, 2033

123. T. Harschneck, N. Zhou, E. Manley, S. Lou, X. Yu, M. Butler, A. Timalsina, R. Turrisi, M. Ratner, L. Chen, R. Chang, A. Facchetti and T. Marks, *Chem. Commun.*, 2014, **50**, 4099

124. S. Qu and H. Tian, *Chem. Commun.*, 2012, **48**, 3039

125. J. Yum, T. Holcombe, Y. Kim, J. Yoon, K. Rakstys, M. Nazeeruddin and M. Grätzel, *Chem. Commun.*, 2012, **48**, 10727

126. S. Li, K. Jiang, F. Zhang, J. Huang, S. Li, M. Chen, L. Yang and Y. Song, *Org. Elect.*, 2014, **15**, 1579

127. J. Yum, T. Holcombe, Y. Kim, K. Rakstys, T. Moehl, J. Teuscher, J. Delcamp, M. Nazeeruddin and M. Grätzel, *Sci. Rep.*, 2013, **3**, 2446

128. B. He, A. Pun, D. Zherebetskyy, Y. Liu, F. Liu, L. Klivansky, A. McGough, B. Zhang, K. Lo, T. Russell, L. Wang and Y. Liu, *J. Am. Chem. Soc.*, 2014, **136**, 15093

129. F. Wudl, G. Smith and E. Hufnagel, *J. Chem. Soc. D*, 1970, 1453

130. D. Cortizo-Lacalle, S. Arumugam, S. Elmasly, A. Kanibolotsky, N. Findlay, A. Inigo and P. Skabara, *J. Mater. Chem.*, 2012, **22**, 11310

131. D. Bao, B. Millare, W. Xia, B. Steyer, A. Gerasimenko, A. Ferreira, A. Contreras and V. Vullev, *J. Phys. Chem. A*, 2009, **113**, 1259

132. P. Sonar, E. Williams, S. Singh, S. Manzhos and A. Dodabalapur, *Phys. Chem. Chem. Phys.,* 2013, **15**, 17064

133. A. Lafleur-Lambert, S. Rondeau-Gagné, A. Soldera and J. Morin, *Tetrahedron Letters*, 2011, **52**, 5008

134. C. Woo, P. Beaujuge, T. Holcombe, O. Lee and J. Fréchet, *J. Am. Chem. Soc.*, 2010, **132**, 15547

135. S. Loser, C. Bruns, H. Miyauchi, R. Ortiz, A. Facchetti, S. Stupp and T. Marks, *J. Am. Chem. Soc.*, 2011, **133**, 8142

136. E. Zhou, S. Yamakawa, K. Tajima, C. Yang and K. Hashimoto, *Chem. Mater.*, 2009, **21**, 4055

137. J. lovell, R. Beddoes and J. Joule, *Tetrahedron*, 1996, **52**, 4745

138. T. Holcombe, J. Yum, J. Yoon, P. Gao, M. Marszalek, D. Censo, K.Rakstys, M. Nazeeruddin and M. Grätzel, *Chem. Commun.*, 2012, **48**, 10724

Appendix A – ^{1}H and ^{13}C NMR

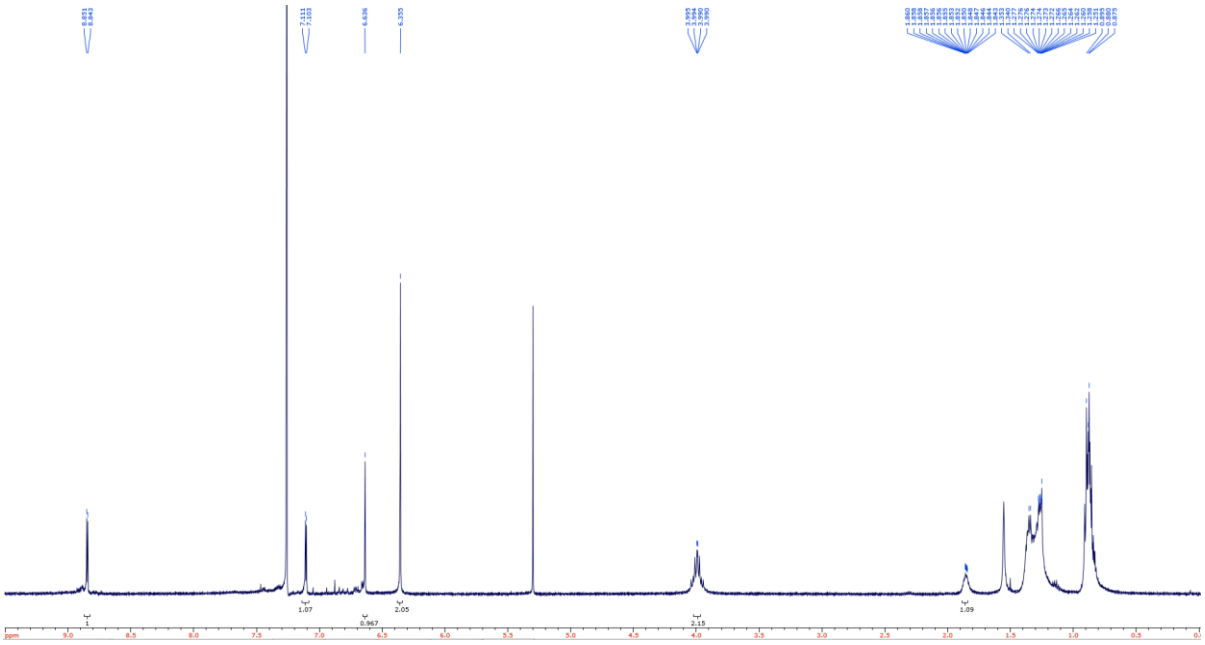

^{1}H NMR of **64** in $CDCl_3$ (calibrated against residual $CHCl_3$ in the $CDCl_3$ 7.26 ppm)

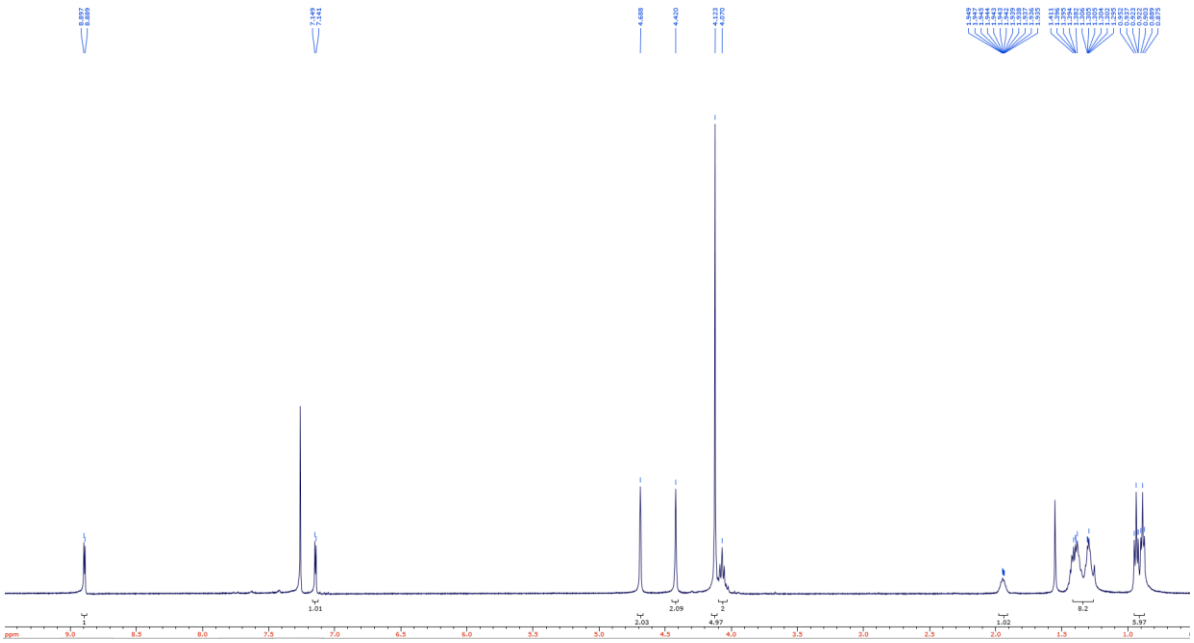

^{1}H NMR of **66** in $CDCl_3$ (calibrated against residual $CHCl_3$ in the $CDCl_3$ 7.26 ppm)

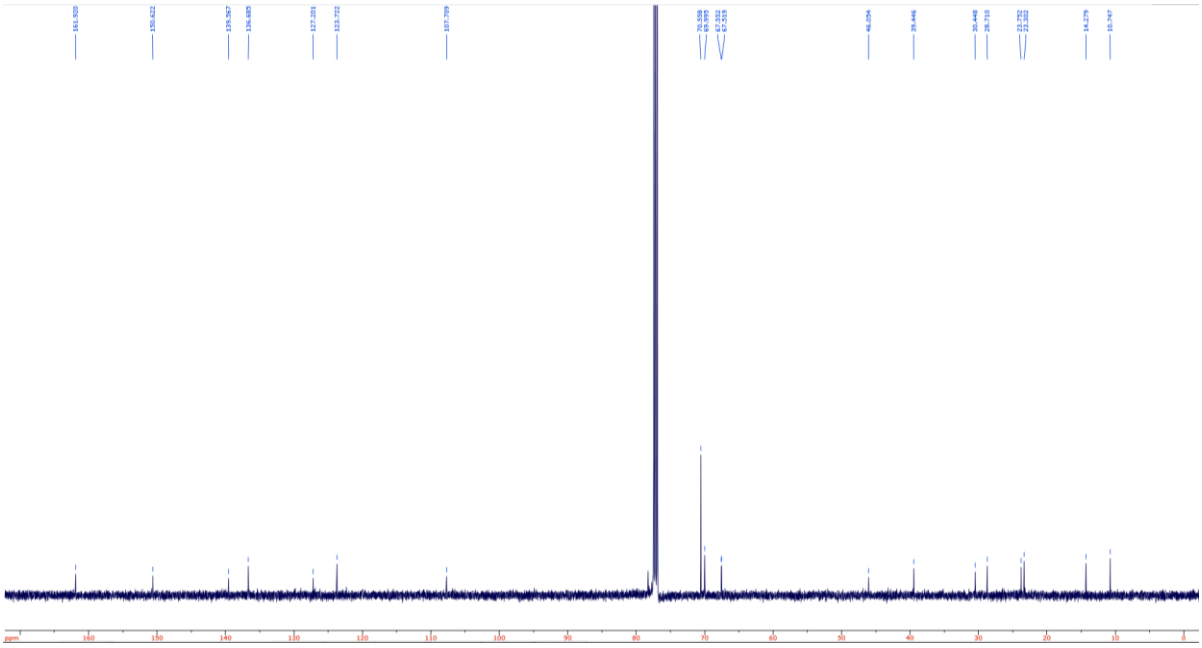

^{13}C NMR of **66** in $CDCl_3$ (calibrated against $CDCl_3$ 77.16 ppm)

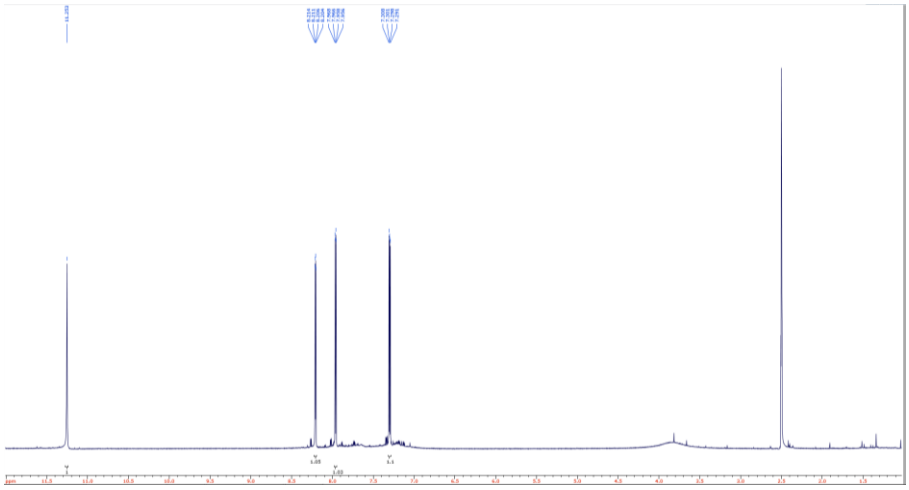

^{1}H NMR of **70** in DMSO-*d6* (calibrated against TMS 0 ppm)

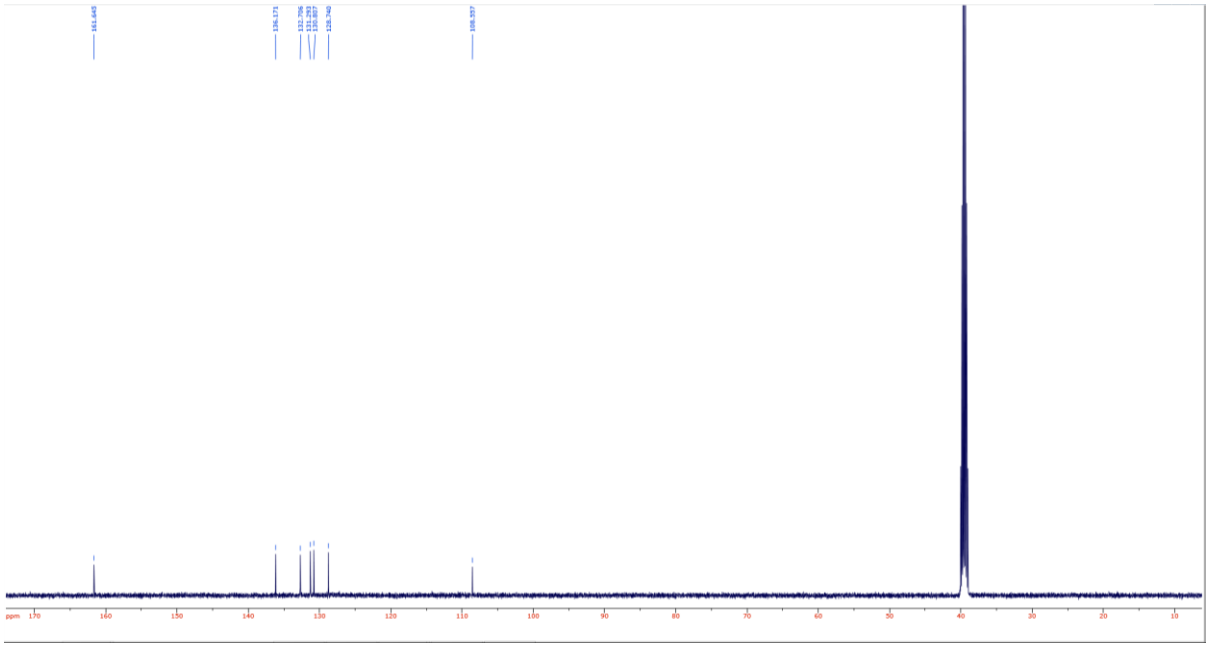

^{13}C NMR of **70** in DMSO-*d6* (calibrated against DMSO-*d6* 39.52 ppm)

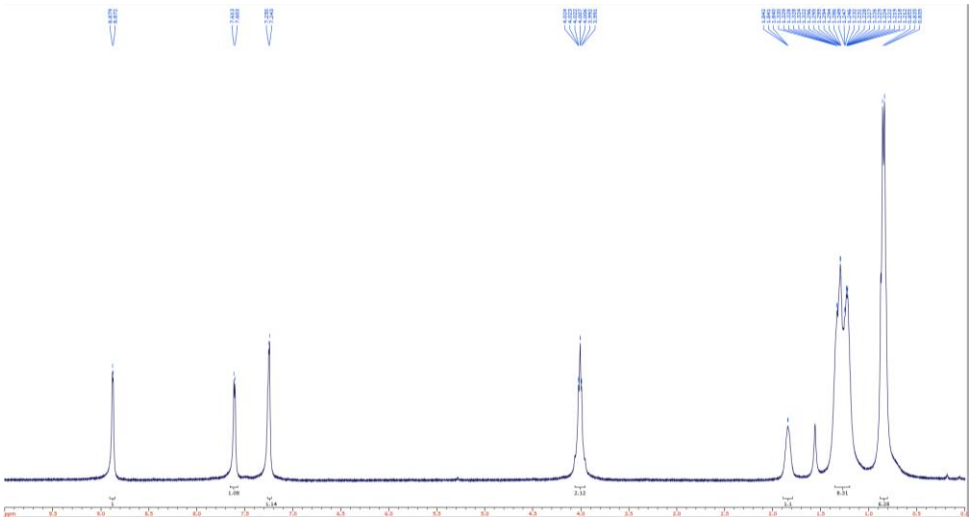

^{1}H NMR of **71** in $CDCl_3$ (calibrated against residual $CHCl_3$ in the $CDCl_3$ 7.26 ppm)

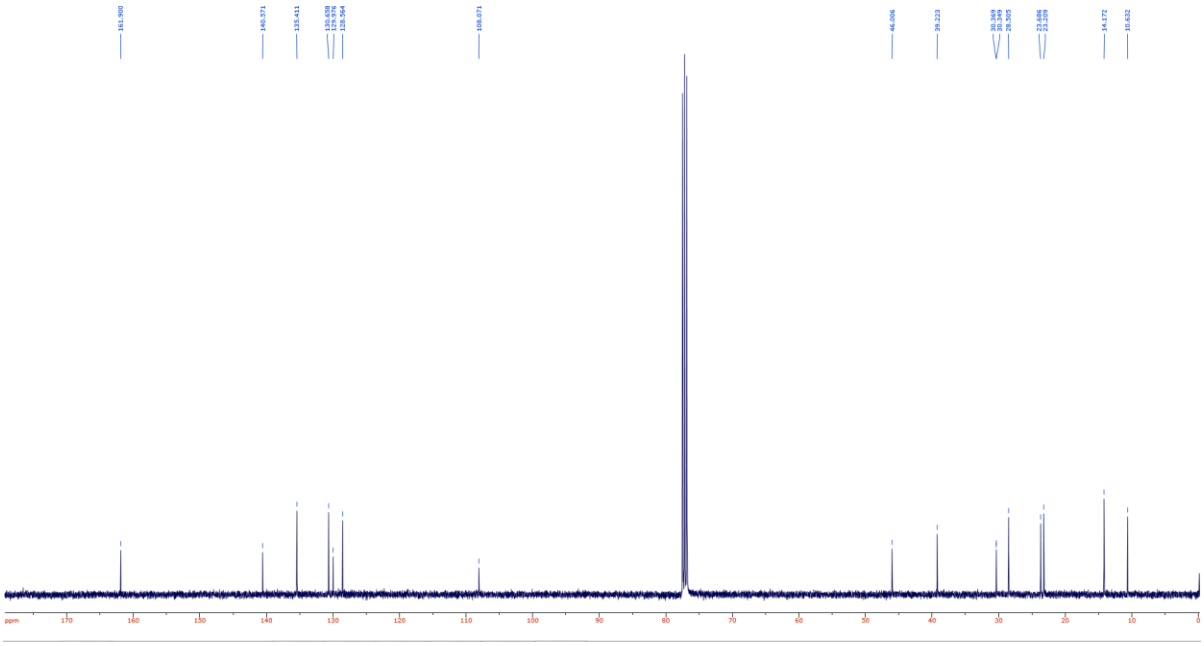

^{13}C NMR of **71** in $CDCl_3$ (calibrated against $CDCl_3$ 77.16 ppm)

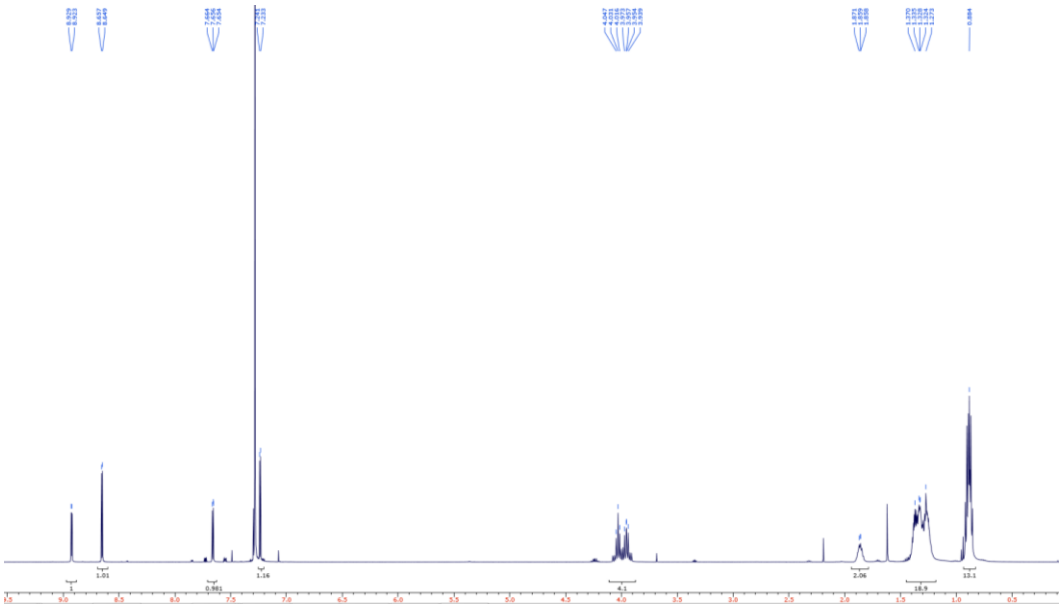

^{1}H NMR of **72** in $CDCl_3$ (calibrated against residual $CHCl_3$ in the $CDCl_3$ 7.26 ppm)

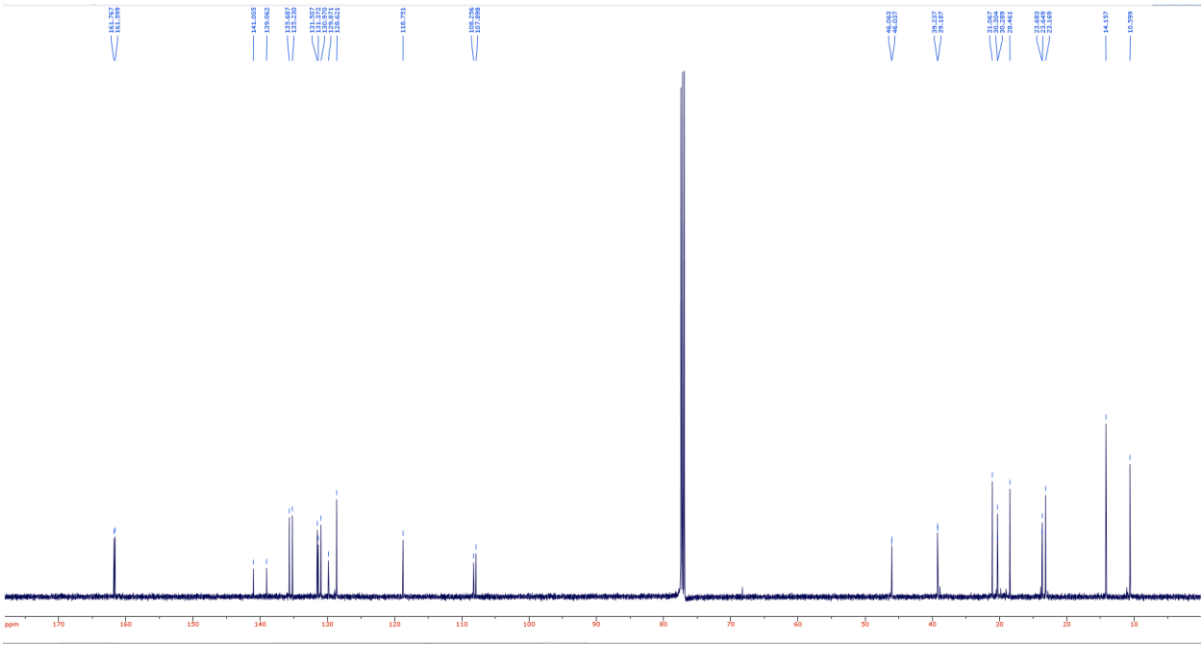

^{13}C NMR of **72** in $CDCl_3$ (calibrated against $CDCl_3$ 77.16 ppm)

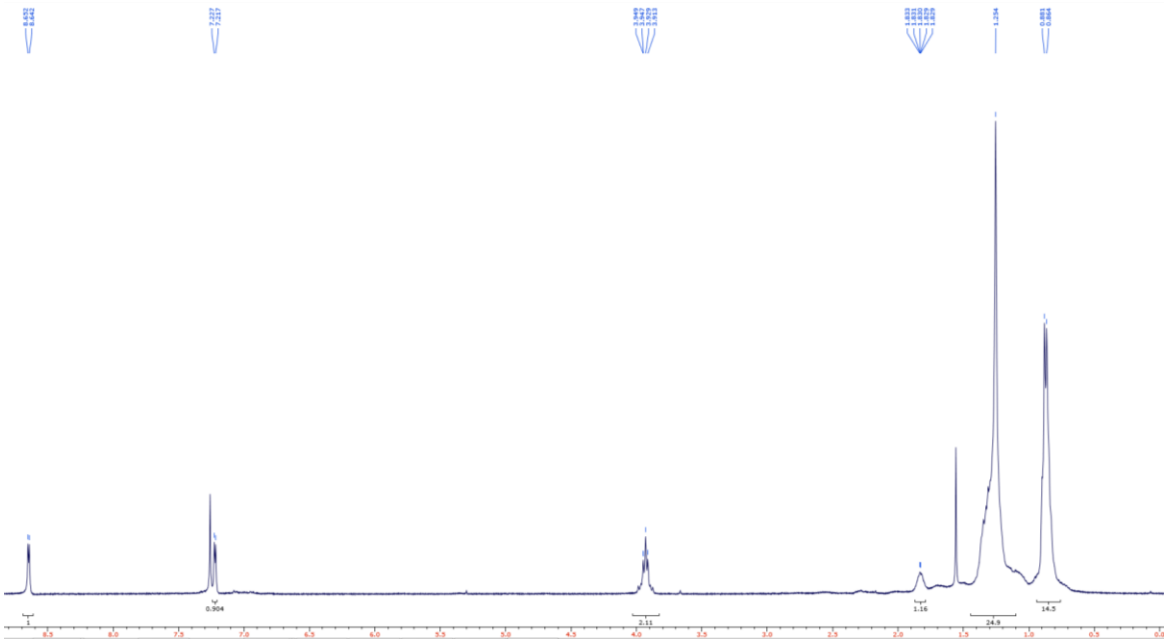

^{1}H NMR of **73** in $CDCl_3$ (calibrated against residual $CHCl_3$ in the $CDCl_3$ 7.26 ppm)

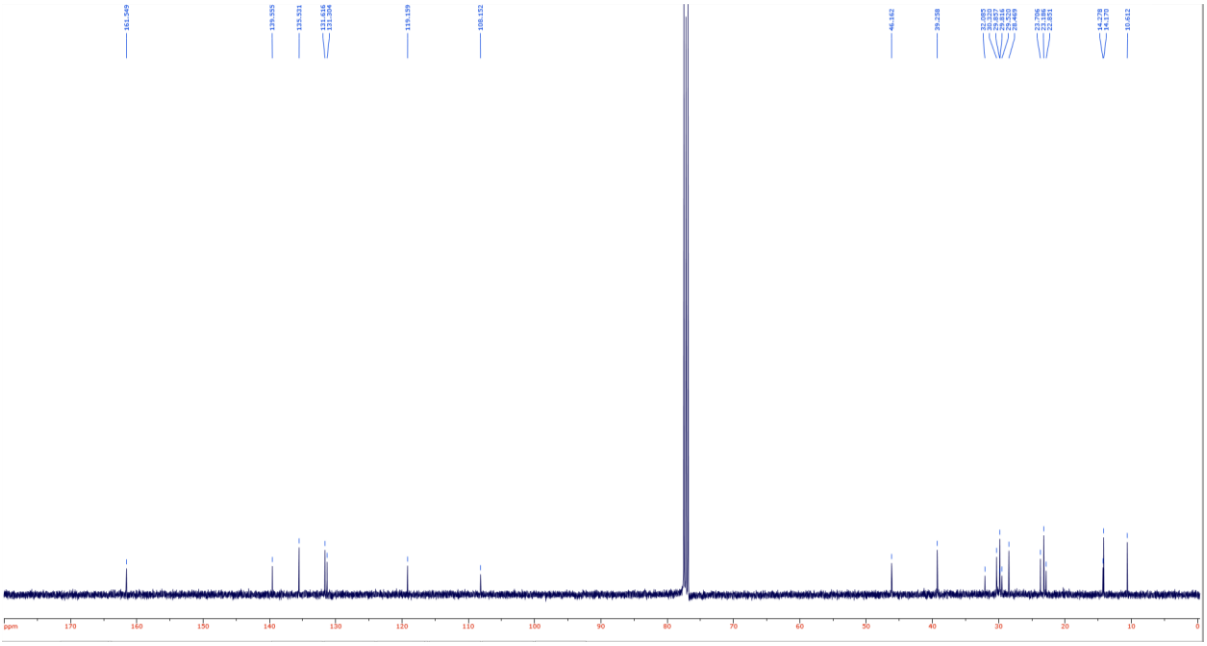

^{13}C NMR of **73** in $CDCl_3$ (calibrated against $CDCl_3$ 77.16 ppm)

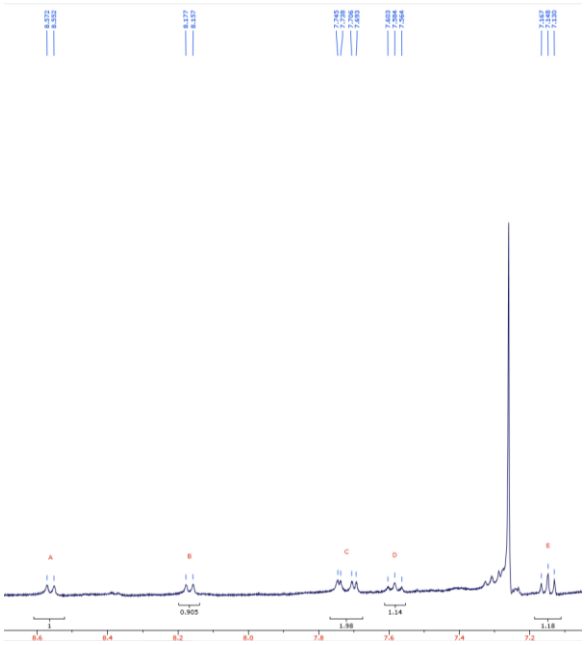

^{1}H NMR of **75** in $CDCl_3$ (calibrated against residual $CHCl_3$ in the $CDCl_3$ 7.26 ppm)

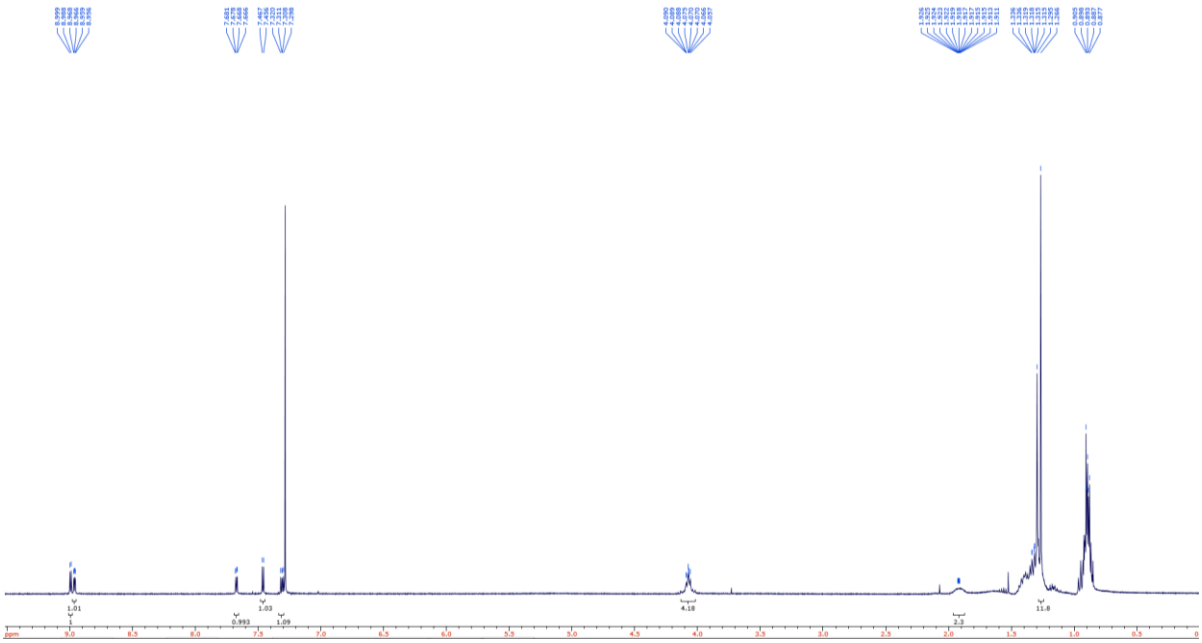

^{1}H NMR of **78** in $CDCl_3$ (calibrated against residual $CHCl_3$ in the $CDCl_3$ 7.26 ppm)

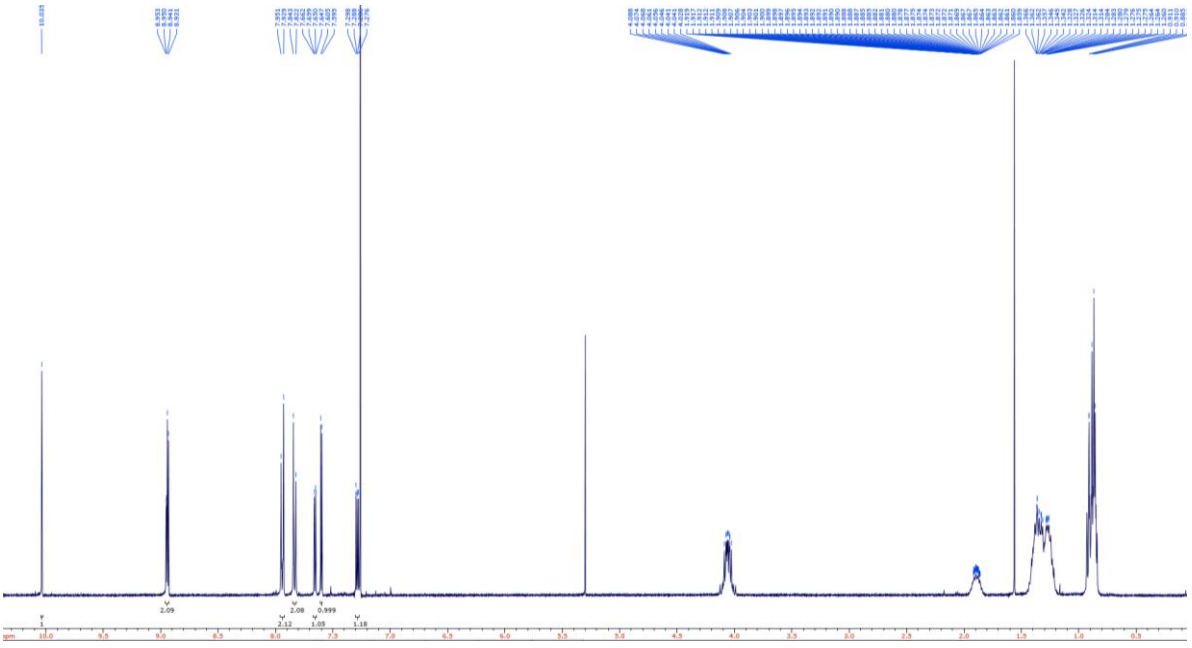

^{1}H NMR of **88** in $CDCl_3$ (calibrated against residual $CHCl_3$ in the $CDCl_3$ 7.26 ppm)

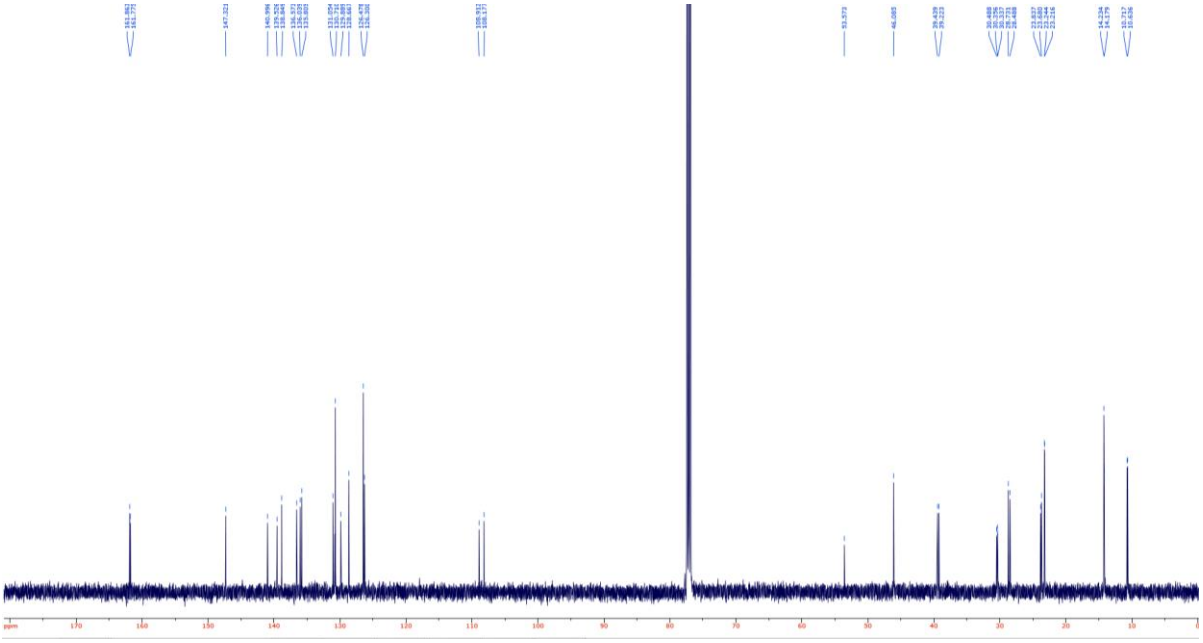

^{13}C NMR of **88** in $CDCl_3$ (calibrated against $CDCl_3$ 77.16 ppm)

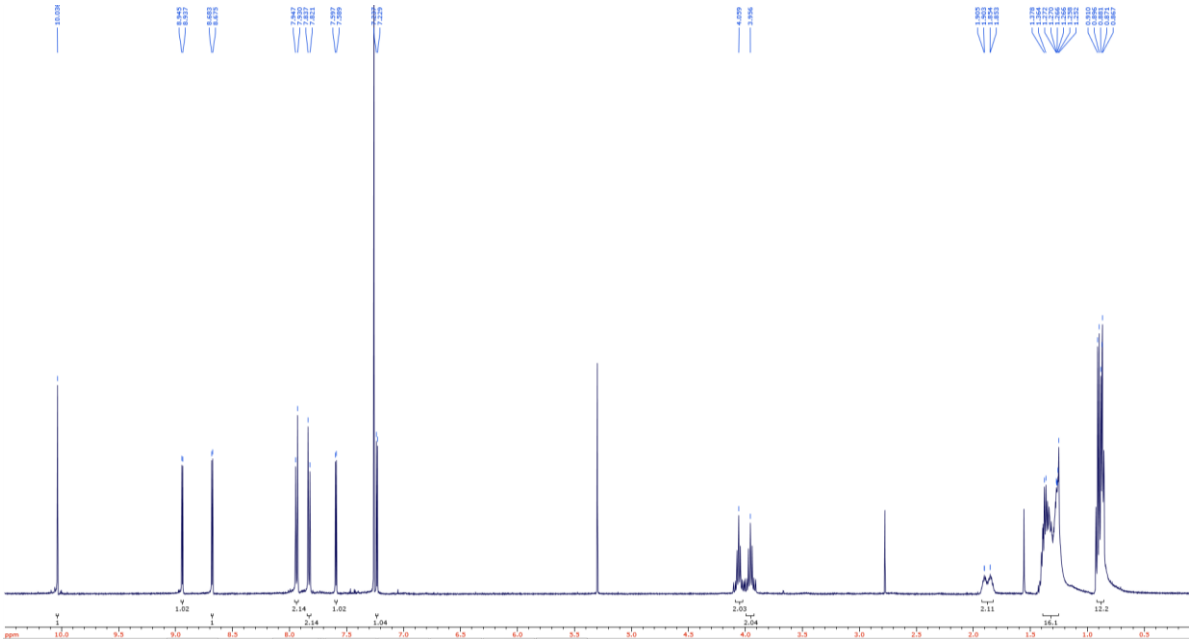

^{1}H NMR of **89** in $CDCl_3$ (calibrated against residual $CHCl_3$ in the $CDCl_3$ 7.26 ppm)

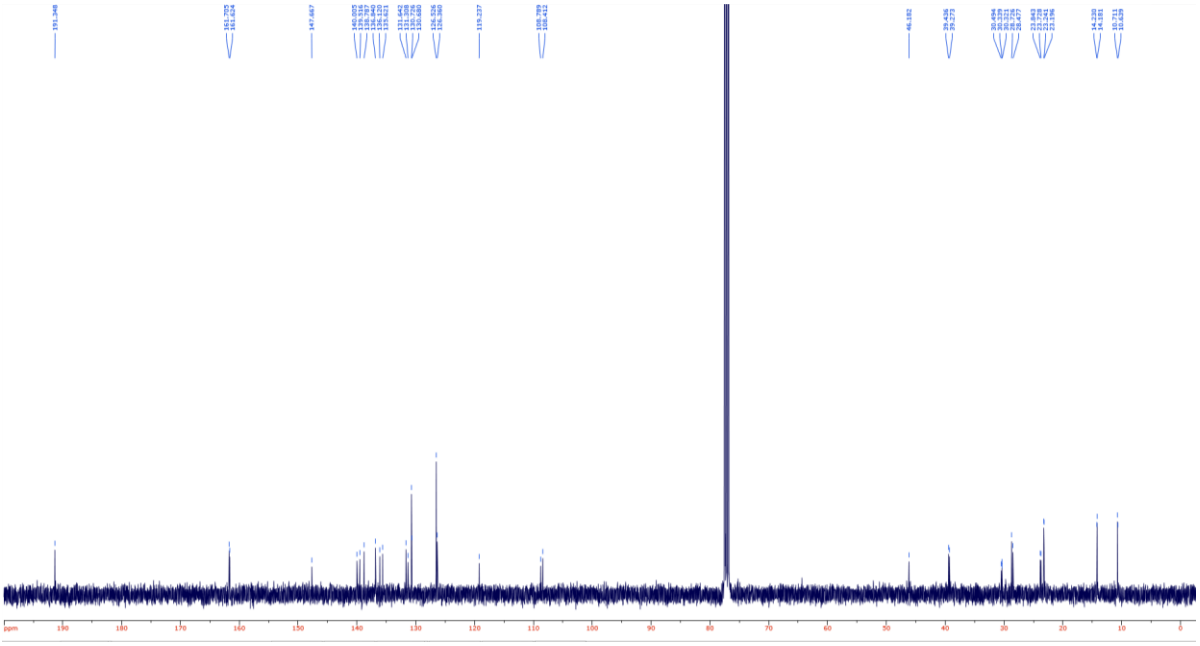

^{13}C NMR of **89** in $CDCl_3$ (calibrated against $CDCl_3$ 77.16 ppm)

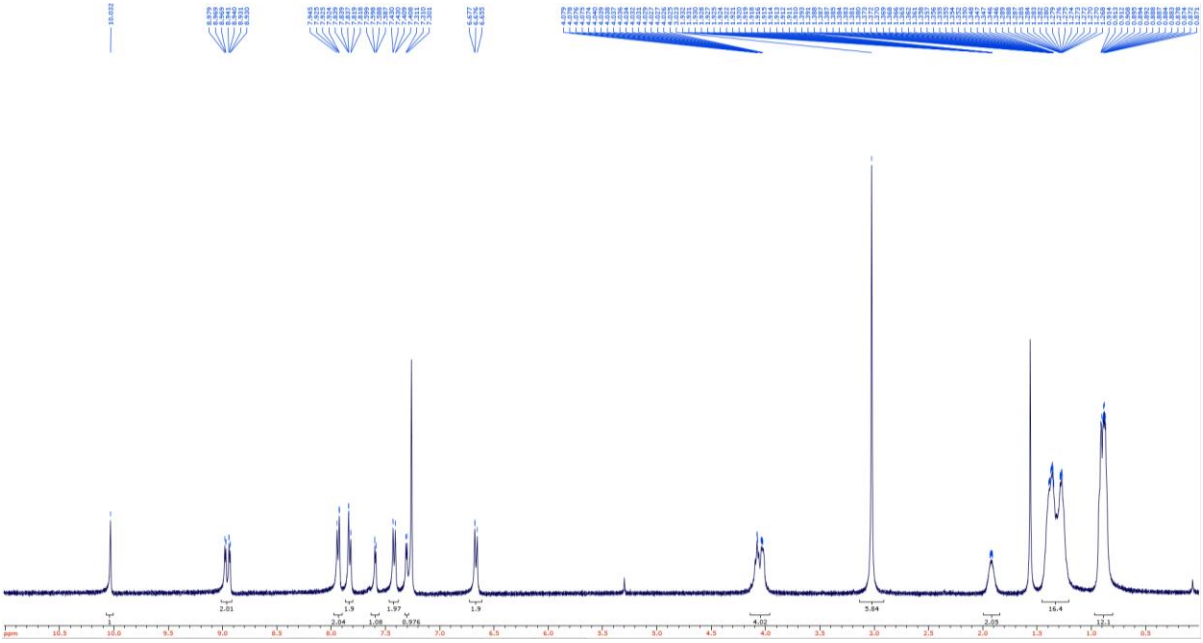

^{1}H NMR of **90** in $CDCl_3$ (calibrated against residual $CHCl_3$ in the $CDCl_3$ 7.26 ppm)

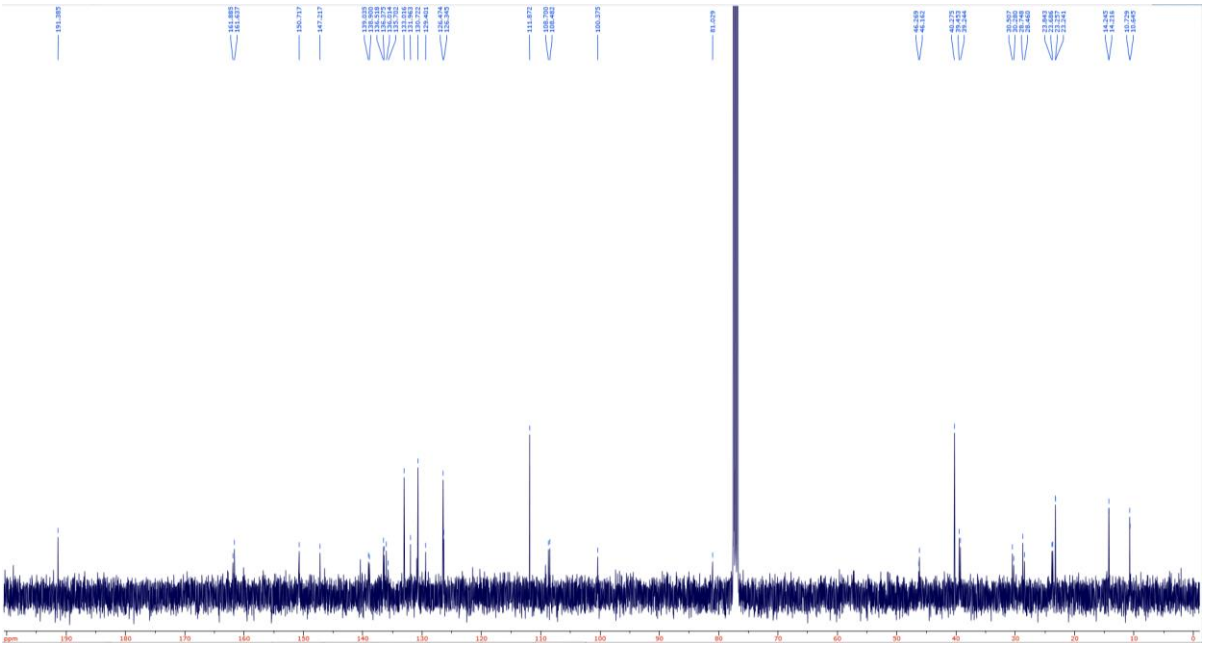

^{13}C NMR of **90** in $CDCl_3$ (calibrated against $CDCl_3$ 77.16 ppm)